The role of acid ceramidase in host defense against enteropathogenic bacterial infection

Inaugural-Dissertation

zur

Erlangung des Doktorgrades

Dr. rer. nat.

der Fakultät für

Biologie

an der

Universität Duisburg-Essen

vorgelegt von

Jana-Fabienne Ebel

aus Arnsberg

Februar 2023

DOI: 10.17185/duepublico/78540
URN: urn:nbn:de:hbz:465-20230615-125223-1

Die der vorliegenden Arbeit zugrundeliegenden Experimente wurden am Institut für Medizinische Mikrobiologie der Universität Duisburg-Essen durchgeführt.

1. Gutachter: Prof. Dr. Astrid M. Westendorf
2. Gutachter: Prof. Dr. Utta Berchner-Pfannschmidt

Vorsitzender des Prüfungsausschusses: Prof. Dr. Matthias Gunzer

Tag der mündlichen Prüfung: 13. Juni 2023

Table of Contents

Summary

The sphingolipid family comprises important components of the cellular membrane and its members ceramide (Cer), sphingosine (Sph) and sphingosine-1-phosphate (S1P) are involved in various cellular processes. Ceramide is the central hub of the sphingolipid metabolism and is hydrolysed by acid ceramidase (Ac) to form Sph, which gives rise to S1P. The functions of sphingolipid enzymes have been investigated in infections or gut inflammation, however studies on the role of Ac in intestinal inflammation are limited and are lacking in the context of gut infection.

In the present study, the impact of Ac on the host response against attaching and effacing bacterial infection of the gut was investigated using the natural murine enteropathogen *Citrobacter* (*C.*) *rodentium*. Mouse strains with systemic and cell type specific Ac depletion were implemented to unravel the contribution of Ac to the distinct cellular responses in gut infection. Global Ac deficiency enhanced susceptibility to *C. rodentium* induced colitis, with influx of inflammatory immune cells into the colonic mucosa. Acid ceramidase depletion in intestinal organoids, a 3D *ex vivo* model of the epithelium, and *C. rodentium* infection of mice with epithelial specific deletion revealed that Ac does not impair epithelial function under homeostasis nor during disease. Macrophage and granulocyte specific Ac ablation showed modest effects in colonic histopathology and cytokine milieu, indicating that Ac is of minor importance in these cells to combat bacterial infection. Acid ceramidase deficiency in T cells aggravated bacterial-induced colitis, with a pro-inflammatory cytokine release in the colon originating from overshooting T helper (T_h)1 and T_h17 responses. $CD4^+$ and $CD8^+$ cytotoxic T lymphocytes further contributed to intestinal inflammation. These hyperactive, pro-inflammatory T cell responses were also systemically evident. Finally, RNA sequencing of $CD4^+$ T cells revealed that Ac may influence T cell activation and differentiation through alternative splicing, oxidative phosphorylation and signaling proteins such as D-aspartate methyltransferase and the interferon alpha/beta receptor.

In conclusion, Ac seems to function as a checkpoint controlling effector T cell function. Thus, Ac expression in T cells, but not in epithelial cells, macrophages and granulocytes, is an important factor for host protection in intestinal infection.

Zusammenfassung

Die Familie der Sphingolipide umfasst wichtige Komponenten der Zellmembran, darüber hinaus sind ihre Vertreter Ceramid (Cer), Sphingosin (Sph) und Sphingosin-1-phosphat (S1P) an diversen zellulären Prozessen beteiligt. Ceramid ist der zentrale Knotenpunkt des Sphingolipid-Stoffwechsels und wird durch die saure Ceramidase (Ac) zu Sph hydrolysiert, aus dem wiederum S1P entsteht. Die Funktion von Enzymen des Sphingolipidsystems wurde in Bezug auf Infektionen oder entzündliche Darmerkrankungen untersucht, jedoch ist die Studienlage zur Rolle von Ac bei Darmentzündungen begrenzt und Studien zu seiner Rolle in der Darminfektion sind nicht vorhanden.

In der vorliegenden Arbeit wurde die Auswirkung von Ac auf die zelluläre Wirtsreaktion gegenüber einer bakteriellen Darminfektion unter Verwendung des natürlichen murinen Enteropathogens *Citrobacter* (*C.*) *rodentium* untersucht. Um den Einfluss dieses Enzyms auf die Funktion der verschiedenen Zellen zur Abwehr des Pathogens zu untersuchen, wurden Mauslinien mit systemischer und Zelltyp-spezifischer Depletion von Ac eingesetzt. Die globale Ac-Defizienz führte zu einer verstärkten Kolitis in der *C. rodentium* Infektion, wobei entzündliche Immunzellen vermehrt in die Darmschleimhaut einwanderten. Die Deletion von Ac in Darmorganoiden, einem *ex vivo* 3D Epithelmodell, und die *in vivo* Infektion von Mäusen mit *C. rodentium* bei Epithelzell-spezifischer Defizienz von Ac ergaben, dass Ac unter Homoöstase und in der Infektion keinen Einfluss auf die Epithelfunktion hat. Eine Makrophagen- und Granulozyten-spezifische Ac-Ablation führte zu moderaten Auswirkungen auf die Histopathologie und das Zytokinmilieu im Kolon während der Infektion. Dies zeigt, dass Ac in diesen Zellen von geringer Bedeutung für die Bekämpfung der Bakterien ist. Der Ac-Mangel in T-Zellen verstärkte jedoch die bakterielle Kolitis, in der durch überschießende T-Helfer (T_h)1- und T_h17-Reaktionen ein pro-inflammatorisches Mikromilieu im Kolon verursacht wurde. Die Ac-Defizienz förderte zudem die Generierung von $CD4^+$ und $CD8^+$ zytotoxischen T-Lymphozyten, die zur Darmentzündung beitrugen. Darüber hinaus konnten die hyperaktiven, entzündlichen Reaktionen der T-Zellen auch systemisch nachgewiesen werden. Schließlich ergab eine RNA-Sequenzierung von $CD4^+$ T-Zellen, dass Ac möglicherweise die T-Zellfunktion durch alternatives Spleißen, oxidative Phosphorylierung und Signalproteine wie die D-Aspartat-Methyltransferase und den Interferon alpha/beta Rezeptor beeinflussen kann.

Zusammenfassend konnte gezeigt werden, dass Ac die Aktivität von Effektor T-Zellen reguliert. Damit ist die Expression von Ac in T-Zellen, jedoch nicht in Epithelzellen, Makrophagen und Granulozyten, ein wichtiger Faktor zum Schutz des Wirtes während einer Darminfektion.

1 Introduction

1.1 The gut and mucosal immunity

The gut, comprising the small intestine (SI) and large intestine (LI) or colon, is structured in several layers: The mucosa is the most inner layer, consisting of a muscle layer (muscularis mucosa), a connective tissue layer (lamina propria) and the epithelium lining the gut lumen [1]. The most external part, is a fibrous layer (serosa), under which lies smooth muscle tissue (muscularis propria), followed by the submucosa, a connective tissue layer with blood vessels, lymphatics and nerves [1].

An essential function of the intestine is the digestion of food and nutrient resorption resulting in close contact to environmental factors [2]. The gut is steadily confronted with a plethora of antigens, originating from food, residing commensal bacteria as well as pathogens including parasites, bacteria, viruses and fungi [2, 3]. Commensal bacteria are most abundant in the colon, where they metabolize non-digestible carbohydrates from fibers, generating short-chain fatty acids (SCFA), which were shown to influence intestinal immunity [2-4]. The intestinal mucosal immune system evolved into a complex network of coordinated cellular, structural and biochemical factors to tolerate harmless dietary and commensal antigens, while also ensuring protection against invading pathogens, as summarized in Fig. 1 [2, 5].

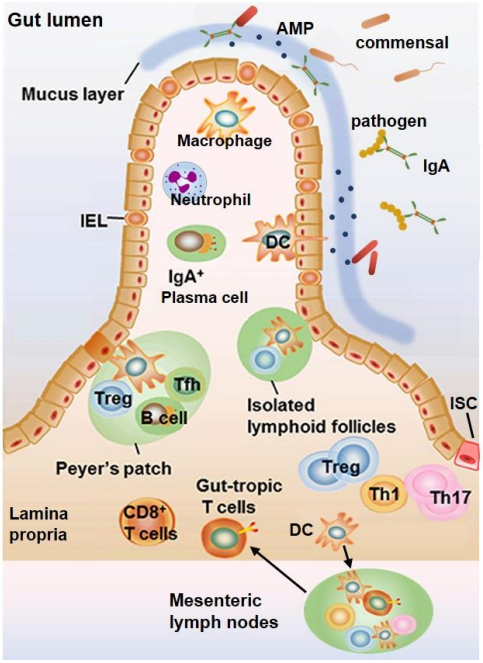

Fig. 1: The mucosal immune system.
The epithelium is constantly renewed by intestinal stem cells (ISCs) and is covered by a mucus layer containing antimicrobial peptides (AMPs) and plasma cell derived immunoglobulin A (IgA), which binds pathogens. Immune cells reside in the lamina propria, epithelium [intraepithelial lymphocytes (IEL)], Peyer's patches, isolated lymphoid follicles and mesenteric lymph nodes (mLN). Neutrophils eliminate invading pathogens. Macrophages and DCs migrate to the mLN and recruit $CD8^+$, T helper (T_h)17, T_h1, regulatory T cells (T_{regs}) and B cells to the lamina propria. (Adapted from [6])

The tight epithelial cell layer covered by mucus, forms a physical and biochemical barrier [7]. Homeostasis is further maintained by the immune cells in the gut, which are located in the lamina propria (LP), epithelium, draining mesenteric lymph nodes (mLN) and the gut associated lymphoid tissue (GALT), including isolated lymphoid follicles and Peyer's patches in the small intestine [2]. The multifactorial innate and adaptive immune responses exert their function by helper, cytotoxic and regulatory immune cells of the myeloid and lymphoid lineage, as well as cytokines, chemokines and immunoglobulins [8]. A balance of this system is key for the host's health, preventing overshooting immune responses or immunosuppression, which ultimately lead to inflammatory tissue destruction, cancer or autoimmune disease [9, 10].

1.1.1 The intestinal epithelial barrier

The epithelium is a tight layer of simple columnar epithelial cells with finger-like protrusions, microvilli, forming the brush border on the apical membrane [1, 11]. Nutrients are taken up via the brush border, which have been further digested by the numerous enzymes located within the microvilli membrane [11]. The epithelium is organized in villi, which are only found in the SI, and invaginations, called crypts [1]. The crypt base harbors intestinal stem cells (ISCs), marked by leucine-rich repeat-containing G-protein-coupled receptor 5 (Lgr5) expression, which are constantly replenishing a pool of intestinal progenitor cells, the transit-amplifying (TA) cells [12]. These TA cells further differentiate into enterocytes and into the secretory enteroendocrine, goblet and Paneth cells (only SI). During differentiation, IECs migrate up the crypt towards the lumen, except for the Paneth cells, which are located next to the ISCs at the crypt bottom. Differentiated enterocytes, the most abundant cell type in the epithelium, absorb and metabolize nutrients and can also generate antimicrobial peptides (AMPs), such as the C-type lectin regenerating islet-derived protein 3γ (Reg3γ) [7, 13]. Enteroendocrine and Paneth cells produce hormones and antimicrobial defensins and lysozyme, respectively [7]. Goblet cells are important for secretion of mucins, highly glycosylated proteins making up the mucus layer covering the epithelium, also referred to as glycocalyx [14, 15]. The colonic glycocalyx is thicker compared to SI, consisting of two layers, a dense layer bound to the epithelial membrane and a second, loose layer on top of it, harboring commensal bacteria [14]. The thick covering is a necessity to separate the trillions of bacteria from the epithelium [7]. The inner mucus layer further protects by antimicrobial peptides that directly destroy invading microbes, and contains immunoglobulin A (IgA) that binds bacteria and holds them in the lumen until they are excreted by peristalsis [16, 17]. Immunoglobulin A is secreted by plasma cells and transported by IECs into the luminal mucus [18].

Intestinal epithelial cells are connected by tight junctions, adherens junctions and desmosomes to form a selective physical barrier, as depicted in Fig. 2 [19].

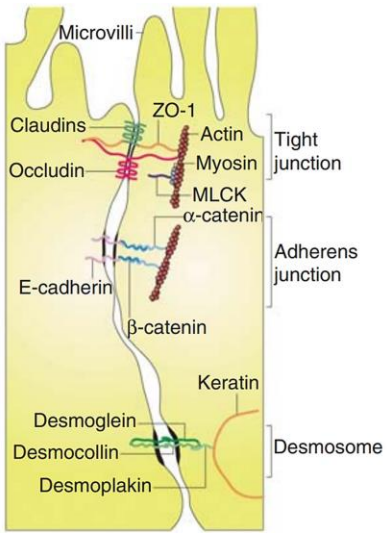

Fig. 2: The junctional complex.
Tight junctions consisting of claudins, zonula occludens 1 (ZO-1) and occludin, connected to the actin-myosin cytoskeleton, are located close to the apical membrane of intestinal epithelial cells (IECs). Underneath lie adherens junctions, consisting of α- and β-catenin and E-cadherin, similarly anchored to the cytoskeleton. Closest to the lamina propria, desmoglein, -collin and –plakin constitute the desmosomes bound to keratin filaments. (Adapted from [20])

Tight junctions are located near the apical membrane of IECs [19]. Their components claudin, occludin and zonula occludens 1 (ZO-1) are bound to intracellular actin and myosin [21]. Similarly, in the subjacent adherens junctions, α- and β-catenins interact with the actin-myosin cytoskeleton of one cell and E-cadherin of the adjacent cell [21]. Desmoglein, desmocollin and desmoplakin forming the desmosomes are located at the basolateral side of the cell, where desmoplakin links the complex to keratin filaments [21]. As the term tight junction implies, these complexes form the closest connection between IECs, controlling paracellular transport of soluble factors and bacterial antigens between the gut lumen and immune cells residing in the underlying lamina propria [22, 23]. Tight junctions and in turn intestinal epithelial barrier function can be negatively modulated by cytokines including tumor necrosis factor α (TNFα) and interferon γ (IFNγ) secreted by pro-inflammatory immune cells [23, 24].

1.1.2 The immune system

Hematopoietic stem cells reside in the bone marrow and give rise to stem cells of the lymphoid and myeloid lineage [25]. Myeloid stem cells differentiate into granulocyte-macrophage progenitors (GMPs) and further into granulocytes and monocyte-dendritic precursor cells (MDPs) [25]. Monocytes in turn, derived from MDPs or GMPs of the myeloid lineage, further mature into macrophages [25]. The development of dendritic cells (DCs) is dichotomous, as these cells differentiate from common dendritic precursors originating from

either the lymphoid lineage or the MDPs of myeloid lineage. As for the lymphoid lineage, innate lymphoid cells (ILCs), Natural Killer (NK), NK-T, B and T cells develop via precursor stages from the lymphoid stem cells [8, 25, 26].

1.1.2.1 The innate immune system

Innate immune cells are located close to the epithelium, in the lamina propria and provide a rapid response to incoming antigens, which are distinguished into danger signals and tolerable commensal or dietary factors [8].

Danger signals include pathogen-associated or damage-associated molecular patterns, PAMPs and DAMPs, respectively, which are sensed with the innate immune cells' pattern recognition receptors (PRRs) [27, 28]. Those molecular patterns are stable signals like mitochondrial DNA for tissue damage or factors that are vital for the pathogenic organism and hence remain unchanged, as for example lipopolysaccharide (LPS), which mainly constitutes the protective membrane of gram-negative bacteria [27-29]. Different types of PRRs have been identified, for instance toll-like receptors (TLRs) and nucleotide-binding oligomerisation domain (NOD)-like leucine-rich repeat receptors (NLRs) [28, 30]. Toll-like receptors are predominantly expressed by typical antigen-presenting cells (APCs) as macrophages and DCs, although also other cells like neutrophils and eosinophils express TLRs [8]. The different TLRs can be located intracellularly or on the cell surface depending on which molecules they bind [28]. One of the best known is the surface receptor TLR4, which characteristically recognizes LPS, but also fungal mannan [28].

Innate immune cells exert their function via cytokine production and recruitment of T cells, as well as direct pathogen killing [8]. Phagocytes, commonly neutrophils, macrophages and monocytes, ingest bacteria or infected cells marked by immunoglobulins or complement factors, followed by destruction via reactive oxygen species (ROS) and proteases [8]. Another pathogen defense mechanism is the destruction by cytotoxic granules of granulocytes, typically neutrophils and eosinophils, with the latter more specifically targeting parasites [31]. Eosinophils attack pathogens extracellularly, by extruding granules containing cytotoxic basic and cationic proteins, as well as peroxidase [31]. Neutrophils developed two mechanisms against pathogens: Granules containing ROS, myeloperoxidases and lysozyme to kill bacteria intracellularly in the phagolysosome and neutrophil extracellular traps (NETs), DNA networks which are additionally supplied with toxic enzymes and pattern recognition molecules to bind and degrade bacteria outside the cell [31, 32]. Additionally, neutrophils are capable of recruiting T helper (T_h)1 and T_h17 cells with CC-chemokine ligands 2 and 20, and CXC-chemokine ligands 9 and 10, while T_h1 cells and T_h17 cells especially, promote neutrophil responses [32]. Basophils function differently

by secretion of platelet activating factor, leukotrienes and prostaglandins with pro-inflammatory and vasomodulatory properties [31].

Specific T cell recruitment is facilitated by the aforementioned APCs, which uniquely express major histocompatibility complex (MHC) class II molecules additionally to ubiquitously expressed MHC class I [31]. APCs migrate to draining lymph nodes and activate T cells by presenting antigens via their MHC molecules [31]. T cells differentiate in response to the cytokine milieu at the site of infection or inflammation, generated among others, by innate immune cells [32-34]. Innate immune cell function in turn is also modulated by cytokines of the adaptive immunity [32-34].

Macrophages polarize, depending on the surrounding cytokines, into distinct subtypes, which are classically divided in M1 and M2 macrophages [33]. The cytokines IFNγ and TNFα as well as PRR encounter with LPS triggers M1 polarization and concomitant pro-inflammatory IL-1, IL-12 and IL-23, but also ROS and nitric oxide (NO) production by these macrophages [33]. M2 macrophages present a rather regulatory phenotype, induced by IL-4, IL-13 and IL-10, in presence of immune complexes and upon TLR or IL-1 receptor binding [33]. This macrophage phenotype characteristically produces IL-10, TGFβ and IL-6 acting immunoregulatory and tissue regenerating, although M2 macrophages were also shown to be antiparasitic [33]. Macrophages are in interdependent relationship with T cells, as M1 derived IL-12 induces T_h1 differentiation and T_h1 derived IFNγ in turn mediates M1 polarization. Similarly M2 cytokines promote a regulatory T cell (T_{reg}) response and T_{reg} derived IL-10 facilitates the M2 phenotype [33, 34]. Additionally, the macrophage cytokine IL-1 was shown to support $CD4^+$ T cell activation upon antigen presentation and its subtype IL-1β induces IL-12 production in DCs [35, 36].

Other innate immune cells, like NK cells and ILCs, are important players in mucosal immunity [26]. NK cells are cytotoxic with IFNy, granzyme and perforin production acting against intracellular bacteria [26, 37]. ILCs are classified into ILC1, ILC2 and ILC3, analogous to T_h1, T_h2 and T_h17 cells, respectively, sharing a similar cytokine secretion profile and antibacterial properties [26, 37].

1.1.2.2 Adaptive immune system

In the adaptive immune system specific responses are directed by T and B cells bearing antigen receptors, the T and B cell receptors (TCR and BCR) [31]. B cells mature and obtain the BCR in the bone marrow, while T lymphocyte progenitors migrate and further develop in the thymus, giving rise to a large population of T cells carrying TCRs with αβ chains and a smaller subset of γδ TCR T cells [8, 31]. Cluster of differentiation (CD)4^+ $CD8^+$ double positive αβ TCR T cells undergo positive selection for T cells carrying a TCR recognizing self-MHC and mature into single positive $CD4^+$ or $CD8^+$ T cells, binding MHC class II and I,

respectively [31, 38]. A wide repertoire of antigen-specific BCRs and TCRs is generated by recombination events and rearrangement of the receptors, while auto-reactive B and T cells undergo apoptosis [31]. After thymic development, T cells circulate through peripheral tissues [8, 31].

Antigen experienced T cells mediate B cell differentiation into plasma cells, producing antibodies, such as the aforementioned IgA, as well as memory B cells [2, 17, 31]. Activation of T cells occurs via the TCR:CD3 complex interacting with an antigen presented by MHC on APCs and concomitant co-stimulation through binding of CD28 on T cells to CD80/CD86 receptors on the APCs [8]. Different cytokines mediate T cell differentiation into distinct subpopulations including $CD4^+$ helper, cytotoxic and $CD4^+$ regulatory T cells [35, 39, 40]. An overview of the different $CD4^+$ T cell lineages is depicted in Fig. 3.

IL-12 and IFNγ originating from DC and macrophages typically induce the T helper 1 (T_h1) lineage during bacterial and viral infections [33, 39, 41]. T_h1 cells express T-box transcription factor (T-bet) and secrete pro-inflammatory cytokines, such as IFNγ, TNFα and IL-2 [39, 42]. The T_h1 cytokines IFNγ and TNFα were shown to enhance pathogen clearance by macrophages and to modulate intestinal epithelial function, by inducing apoptosis in IECs [33, 43]. T_h2 responses are elicited against parasitic infections and allergens [39, 44]. T_h2 cells are characterized by expression of the transcription factor GATA binding protein 3 (GATA3) and differentiation is mediated by IL-4 and IL-2, which in turn leads to secretion of a variety of cytokines, including IL-4, IL-5, IL-10 and IL-13 [39]. T_h2 cytokines promote the formation of IgE producing B cells, eosinophil responses, but also anti-inflammatory responses and tissue regeneration by M2 macrophage polarization and inhibitory functions of IL-10 [39, 45, 46]. Upon infections with extracellular bacteria, but also in fungal infections, T_h17 cells are characteristically induced by the cytokines IL-1β, IL-6, IL-21, IL-23 and transforming growth factor β (TGFβ) via the transcription factor retinoic acid receptor-related orphan γt (RORγt) [39]. T_h17 cells typically produce IL-17A, IL-17F, IL-21 and IL-22, which trigger protective AMP production and attract neutrophils to eliminate bacteria [32, 39, 46].

$CD8^+$ and $CD4^+$ cytotoxic T cells (CTLs) are usually induced in response to tumor growth and viral, but also bacterial infections [35, 40, 47]. These cells execute cytotoxicity to other infected or aberrant (tumor) cells by release of granules containing granzymes through pores formed by perforin [48, 49]. Effector $CD8^+$ CTLs are induced by IL-2, IL-12 and type I interferons involving the transcription factors Id2 (Inhibitor of DNA binding), IRF4 (Interferon regulator factor 4) and T-bet [35, 48]. The cytokine milieu and molecules favoring induction of the $CD4^+$ cytotoxic T cell lineage is not entirely clarified, however similar to $CD8^+$ CTLs, the cytokines IL-2 and IL-12 were shown to promote cytotoxicity of $CD4^+$ T cells [50, 51].

T helper and cytotoxic T cells are important effectors in infections; however, their immune responses carry the risk for tissue damage from persistent inflammation or aberrant reactivity, if these are not controlled to restore homeostasis. This is where regulatory T cells come into action, being able to dampen pro-inflammatory immune responses [52]. T_{regs} typically express the transcription factor FoxP3 (Forkhead box P3) and CD25, also known as IL-2 receptor [39]. Two T_{reg} lineages are described, the natural T_{regs} (nT_{regs}), which develop in the thymus, and induced T_{regs} (iT_{regs}), which mature in secondary lymphoid organs [52, 53]. Differentiation of T_{regs} occurs in the presence of IL-2 and TGFβ, but also IL-10 was shown to contribute to T_{reg} development [52, 53]. T_{regs} promote immune suppression via several mechanisms, such as secretion of inhibitory TGFβ, IL-10 and IL-35, as well as direct cell lysis with intrinsically produced granzymes and perforin, and IL-2 consumption, which is needed for activation and survival of non-T_{regs} [52]. Furthermore, T_{regs} can occupy the APC receptors CD80/86 and MHC II, by binding with cytotoxic T-Lymphocyte-associated protein 4 (CTLA4) and lymphocyte-activation gene 3 (LAG-3), respectively and thereby affecting the activation of cytotoxic and helper T cells [52]. However, a well-balanced T_{reg} response is also an indispensable necessity, as excessive suppression supports pathogen expansion, chronic infections or tumor formation [54, 55].

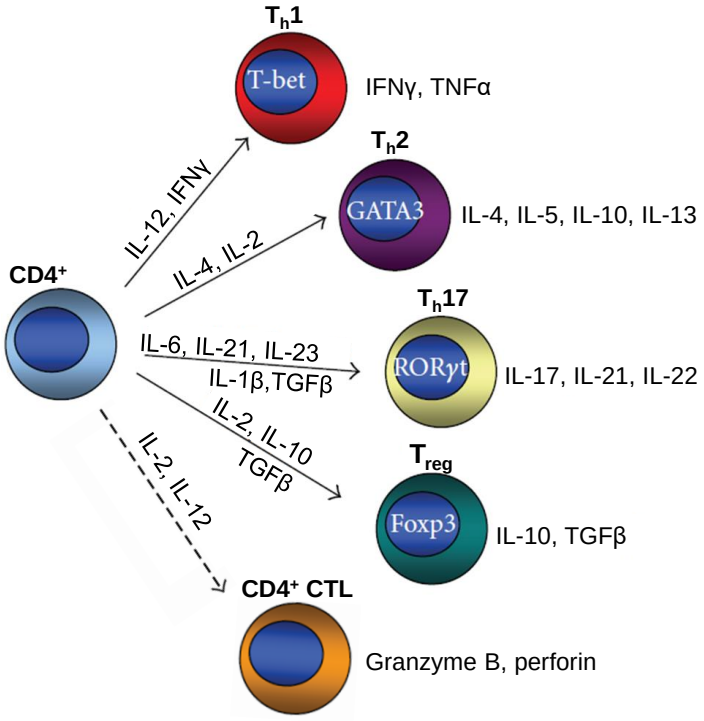

Fig. 3: Differentiation of CD4⁺ T cells.
CD4⁺ T cells are activated after antigen encounter via crosstalk of their TCR and the MHC II:peptide complex on APCs, along with co-stimulation. Different cytokine milieus trigger differentiation into distinct CD4⁺ T cell subsets including helper, cytotoxic and regulatory CD4⁺ T cells. (Adapted from [50])

1.2 Gut infection and inflammation

The immune system, as described above, is multilayered and acts with its various components to protect the host from invading pathogens [2]. A balanced immune response is an important pillar for maintaining homeostasis and health, as uncontrolled and misdirected immune responses foster acute and chronic inflammation or cancer [2]. The intestine is an organ at risk for infection with enteropathogenic bacteria as *Escherichia* (*E.*) *coli* strains, which lead to acute inflammation and diarrhea, with even fatal outcomes in developing countries [56]. Disturbance of the homeostatic balance due to aberrant pro-inflammatory immune responses, unhealthy lifestyle, genetic predisposition or an imbalance of the microbiota, mediate inflammatory bowel disease (IBD) [57].

1.2.1 Inflammatory Bowel Disease

Inflammatory bowel disease comprises mainly two subtypes of relapsing intestinal disorders, Crohn's disease (CD) and ulcerative colitis (UC), which cause (bloody) diarrhea and abdominal pain [57]. In Crohn's disease, the entire gastrointestinal tract can be involved, although the ileocecal and colonic areas are most commonly affected and inflammation can occur in all layers of the intestinal wall [58]. In ulcerative colitis, the inflammation is confined to mucosa and as the term suggests, UC affects the LI, typically propagating from the rectum [59].

The exact etiology of IBD is not understood, but a variety of interdependent risk factors have been identified, including genetic variants as for example in the IL-23 receptor gene, which are associated with the occurrence of IBD [57]. A Western diet, antibiotic intake, infections, low exercise and smoking (only in CD) can increase the risk of developing IBD [57, 60]. A balanced diet, on the other hand, promotes a diverse intestinal flora and positively influences intestinal health [60]. Immunologically, IBD involves recruitment of neutrophils and macrophages mediating a pro-inflammatory microenvironment and tissue damage [57]. CD and UC are characterized by excessive T_h1 and T_h2 reactivity, respectively, with accordingly elevated levels of IFNγ as well as IL-5 and IL-13 [57]. An enhanced or insufficient response of T_h17 and T_{reg} cells, respectively, is observed in both CD and UC [57]. Furthermore, a strong IL-12 and IL-23 expression by macrophages was detected in IBD patients, which may further fuel the pro-inflammatory T_h1 and T_h17 response [57]. Overall, genetic factors as well as the pro-inflammatory cytokine milieu lead to breakdown of the intestinal epithelial barrier function, which opens the door for bacterial entry [57].

IBD affects many people worldwide, with the incidence remaining constant or declining in industrialized countries, while emerging economies are experiencing a rising incidence, as was previously the case with the industrialization of Western countries [61, 62]. In industrialized nations, however, the prevalence is still increasing, with IBD being diagnosed

at an increasingly younger age [62]. In Western Europe, Germany is facing the highest burden of CD and UC [61].

1.2.2 Enteric EPEC and EHEC infection

Many pathogenic germs, such as rotavirus, or bacterial *Shigella*, *Salmonella* and *Escherichia* (*E.*) *coli*, invade the gut and are often accompanied by diarrhea [56]. *E. coli* are in general gram-negative, facultative anaerobe bacteria, which also belong to the commensal microbiota in humans [63, 64]. Intestinal pathogenic *E. coli* (InPEC) strains however, are well-known causative agents of diarrheal disease that can lead to death, especially in the context of poor drinking water availability, inadequate hygiene and insufficient protection through vaccination against pathogenic *E. coli* [63, 64]. InPECs include the extracellular enteropathogenic (EPEC) and enterohaemorraghic *E. coli* (EHEC) strains [65, 66]. EPEC infections are a major problem in developing and emerging countries, where children under 5 years of age are particularly at risk for lethal courses [64]. Infections with EHEC can occur worldwide and are most abundant in developed countries [64, 65].

EHEC typically generates shiga toxin leading to hemolysis, kidney damage and life-threatening kidney failure [64, 65]. Shiga toxin also mediates local apoptosis of epithelial cells and tissue damage in the colon resulting in bloody diarrhea [65]. Both, EPEC and EHEC characteristically colonize the intestine through a type III secretion system (T3SS) including the translocated intimin receptor (Tir) and intimin expressed via the locus of enterocyte effacement (LEE) [65, 67]. After initial binding of EPEC or EHEC to the epithelium, Tir is released into the host cell by T3SS, migrates through the cytoplasm and is presented at the surface of the epithelial cell and the bacteria in turn bind tightly to the host cell via intimin:Tir crosstalk [68]. Starting from Tir, a cascade is initiated that induces the actin-related protein 2/3 complex (ARP2/3) causing the host cell to construct platform-like structures for bacterial adhesion by reorganizing actin [68]. At EPEC/EHEC binding sites the microvilli of the epithelial cells are erased, hence these sites are also referred to as attaching and effacing (A/E) lesions [65].
T3SS also introduces other factors, including Map (mitochondrial-associated protein) and various *E. coli* secreted proteins (Esp), which act, in not fully elucidated mechanisms, to inhibit phagocytosis, destroy tight junctions and modulate hormone, electrolyte and fluid transport, ultimately leading to diarrhea [68]. Flagella and LPS of *E. coli* elicit an immune response in the host through the PRRs, TLR5 and TLR4, respectively [65]. In addition, EPEC/EHEC derived intimin has been shown to specifically trigger T_h1 reactivity in the host [65].

1.2.3 *Citrobacter rodentium* mouse model

EHEC and EPEC show weak pathogenicity in mice, yet the bacterium *Citrobacter* (*C.*) *rodentium* is a gram-negative, naturally occurring intestinal pathogen in mice, which is the murine counterpart to human pathogenic EHEC and EPEC [67, 69]. *C. rodentium* also utilizes the T3SS, leading to A/E lesions and has therefore been used to study this system *in vivo* [66]. A/E bacteria characteristically induce hyperproliferation of intestinal stem cells (crypt hyperplasia), generating immature epithelial cells that do not metabolize oxygen, resulting in a more aerobic lumen, which in turn supports bacterial growth [66]. *C. rodentium* itself does not penetrate the host' cells and is non-invasive, therefore does not actively lead to systemic infection [67, 70]. Host immune responses to A/E enteropathogens including *C. rodentium*, EHEC and EPEC have largely been studied *in vivo* in the *C. rodentium* mouse model [66].

Infection with *C. rodentium* occurs via fecal-oral transmission and subsequent colonization of the LI starting from the cecum, with *C. rodentium* being detectable in the colonic mucosa and feces 3 days after infection [71, 72]. Infection reaches a plateau at approximately 7-12 days after inoculation, where the *C. rodentium* load is the highest [71-74]. As in most mouse strains, *C. rodentium* infection in wild type C57BL/6 mice is not lethal with complete elimination of the pathogen after 3 to 4 weeks [67, 71, 72]. *C. rodentium* colonization typically mediates dysbiosis of the microbiota and colitis, particularly in the distal colon [75, 76]. During the course of infection, the epithelial barrier is damaged, allowing bacteria to invade the lamina propria [76]. This induces hyperproliferation of the crypts, resulting in colonic hyperplasia and thickening of the colon, accompanied by a reduction in goblet cells and colon shortening [67, 75, 77]. Because of the transferability of the infection and in turn the hyperplasia, this hallmark is also referred to as transmissible murine colonic hyperplasia [67, 78].

The host innate immune cells sense *C. rodentium* via TLR2 and TLR4, with TLR2-mediated signaling exerting protective effects on the mucosa, while TLR4 signaling was linked to inflammatory tissue damage due to the recruitment of macrophages and neutrophils [69, 79, 80]. Furthermore, myeloid differentiation primary response protein 88 (MyD88) signaling acting downstream of TLR2 but also TLR4, is important to keep the pathogen in check, via inducible nitric oxide synthase (iNOS) and by macrophage secreted IL-6 and TNFα [76, 79]. The lamina propria is heavily infiltrated by T cells during *C. rodentium* infection [81, 82]. There is a strong influx of $CD4^+$ T_h1 and T_h17 cells, which are vital for bacterial eradication, such that during peak infection the colonic frequencies of immunosuppressive T_{regs} may be even lower than under homeostasis [81-83]. It has been shown that in TNFα-, IFNγ- and IL-12-deficient mice bacterial expansion is less effectively controlled and infection is accompanied with more severe pathological changes in the colon, such as enhanced

thickening of the mucosa, and even lethal courses in IL-12-deficient animals [70, 84]. In this context, macrophage production of IL-12 mediated T_h1 differentiation and subsequent IFNγ release [85]. Bacterial attachment to the epithelium and secretion of IL-6 and TGFβ by DCs in response to apoptotic IECs, mediates T_h17 maturation [86, 87]. T_h17 cytokines IL-17 and IL-22 are important players in the elimination of pathogens, by recruiting neutrophils and stimulating epithelial cells to produce antimicrobial Reg3β and Reg3γ, respectively [88, 89]. In addition, at the beginning of infection, ILC3 cells have been identified as important producers of IL-17 and IL-22, a role subsequently fulfilled by T helper cells [76, 87, 90]. Finally, B cells and specific IgG antibodies have been shown to be essential for the elimination of *C. rodentium* [91]. Apart from pathogen clearance, protective mediators as T_{regs}, are also important in *C. rodentium* induced colitis to reduce colon pathology and initiate tissue healing at later stages of the infection [87, 92]. Cellular signaling and mechanisms in *C. rodentium* induced colitis are summarized in Fig. 4.

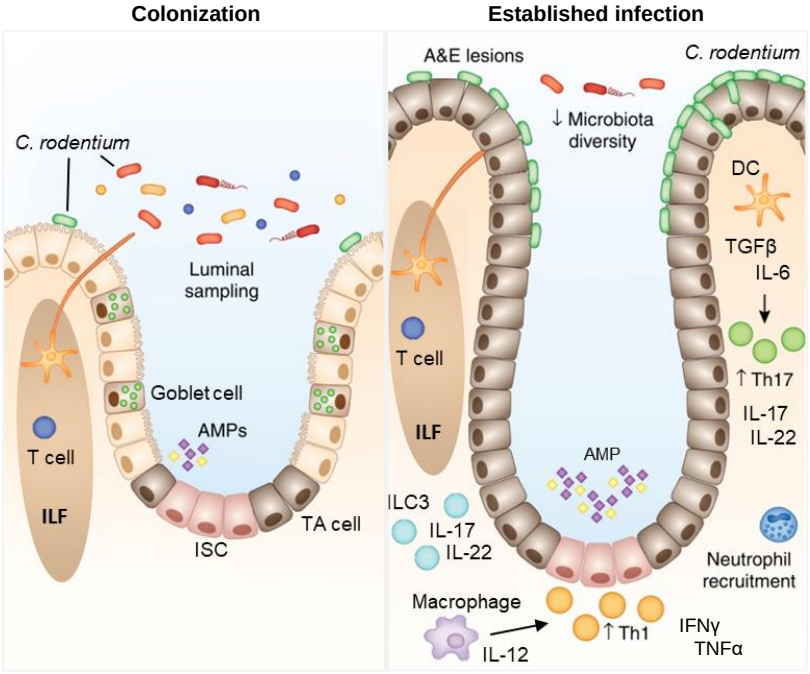

Fig. 4: *Citrobacter rodentium* induced colitis.
In the healthy colon, intestinal stem cells (ISCs) give rise to transit-amplifying cells (TA), which mature into differentiated epithelial cells such as goblet cells. Dendritic cells (DCs) monitor the lumen by sampling antigens. *Citrobacter* (*C.*) *rodentium* colonizes the gut by binding to the epithelium leading to attaching and effacing (A&E) lesions, elongation of the transit-amplifying zone and in turn epithelial hyperplasia. Infection with *C. rodentium* results in microbial dysbiosis with concomitant influx of neutrophils and type 3 innate lymphoid cells (ILC3). Macrophages and DCs mediate T_h1 and T_h17 responses, increasing antimicrobial peptide (AMP) production and attracting neutrophils. (Adapted from [93])

C. rodentium infection provides a valuable model to investigate complex host defense mechanisms in the intestinal mucosa in a natural host-pathogen combination [67, 69]. Furthermore, it is used as a model for IBD, as infectious colitis shares many features with IBD such as epithelial barrier disruption and healing processes, hyperplastic thickening of

the mucosa and the cellular immune response such as T_h1/T_h17 cells and their cytokines [57, 76, 94].

1.3 The sphingolipid network and acid ceramidase

Sphingolipids were initially identified by J. L. Thudichum in 1884 and were named after the sphinx due to their puzzling properties at that time [95]. This lipid class is composed of a sphingoid backbone, which consists of the hydrophobic molecule sphingosine and a hydrophobic fatty acid coupled to it via an amide bond (Fig. 5) [95]. In addition, sphingolipids contain a polar head group, making them amphiphatic molecules, which corresponds to their nature as membrane building blocks (Fig. 5) [95, 96]. Sphingolipids are distinguished based on the length, saturation and hydroxylation of their fatty acid chains, as well as by the different polar moieties [95]. Ceramide (Cer) has a hydrogen at the position of the residue, but ceramides are further differentiated according to the fatty acid chain length, as in C16-Cer, based on its 16 carbon fatty acyl group [97].

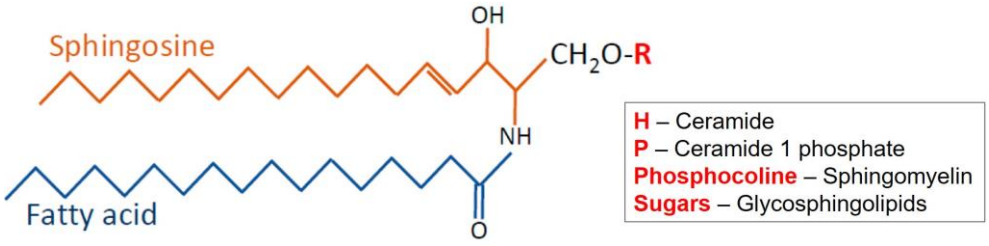

Fig. 5: Structure of sphingolipids.
Sphingolipids consist of a sphingosine base (orange) connected to a fatty acid of varying chain length (blue) as well as a polar head group, which can differ in its structure (red R). The box shows examples of different residues at the polar moiety, with the name of the corresponding sphingolipid. (Adapted from [98])

In response to certain stimuli, sphingolipids can accumulate in distinct regions of the cell membrane, forming lipid rafts in which receptors and signaling molecules cluster [99]. For example, it has been shown that upon stimulation of CD95, Cer accumulates in lipid rafts, so-called ceramide enriched platforms, in which CD95 in turn becomes increasingly incorporated leading to apoptosis [99]. In the past decades, the bioactive properties of sphingolipids have been characterized, in particular of Cer, sphingosine (Sph) and their phosphorylated forms ceramide-1-phosphate (C1P) and sphingosine-1-phosphate (S1P), which are involved in cellular growth, maturation and cell death [96]. Thereby, S1P and Cer have been identified as opposing regulators, with S1P mediating cell cycle progression and proliferation and Cer leading to cell cycle arrest and apoptosis [100].

1.3.1 Sphingolipid metabolism

The sphingolipid metabolism is complex and its distinct pathways, connected via Cer as central nexus, are distributed throughout the cellular compartments [97]. The pathways and enzymatic reactions described in the following are summarized in Fig. 6.

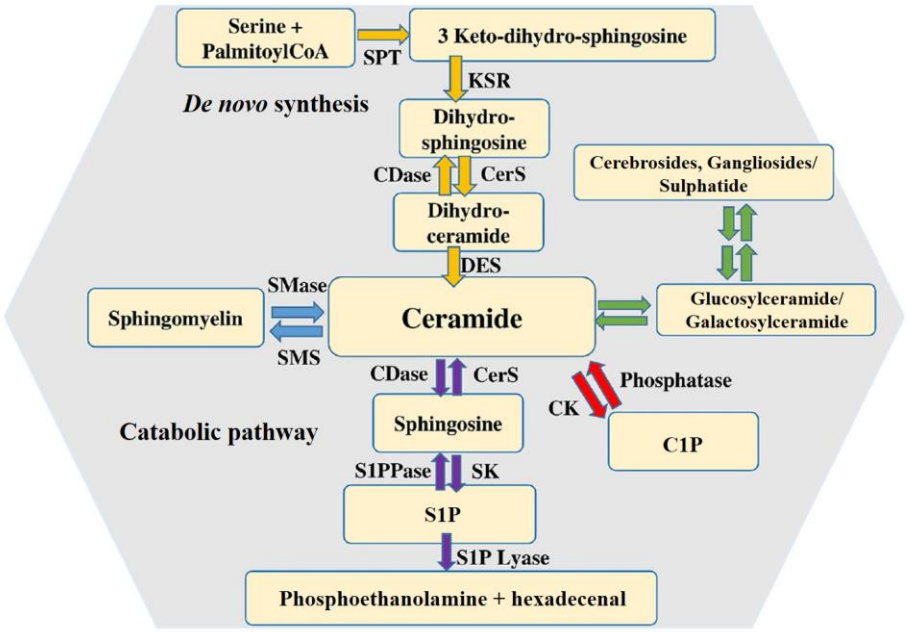

Fig. 6: The sphingolipid metabolism.
De novo synthesis is mediated by serine palmitoyl transferase (SPT), 3-ketosphinganine reductase (KSR), (dihydro)ceramide synthase (CerS) and dihydroceramide desaturase (DES). Ceramide is the central hub, which is converted by sphingomyelin synthase (SMS) to sphingomyelin or vice versa by sphingomyelinases (SMase). Ceramide kinase (CK) phosphorylates ceramide to ceramide-1-phosphate (C1P), which can be reverted by ceramide phosphatase. Ceramide can also enter the glycosphingolipid pathway, by either conversion to glucosyl- or galactosylceramide, which are further metabolized to cerebrosides and gangliosides or sulphatide, respectively. In the catabolic pathway, ceramide is degraded by ceramidases (CDase) to sphingosine, which is further phosphorylated to sphingosine-1-phosphate (S1P) by sphingosine kinases (SK). These reactions can be reverted by CerS and S1P phosphatase (S1PPase). The final exit of the sphingolipid pathway, from S1P to phosphoethanolamine and hexadecenal is catalyzed by S1P lyase and is not reversible. (Adapted from [101])

The *de novo* synthesis takes place in the endoplasmic reticulum (ER), conversion of sphingolipids such as phosphoryl-, glycosyl- and acetylation mainly occur in the Golgi apparatus, and the catabolic pathway, via which sphingolipids are recycled, is located in the lysosome and later in the cytosol or ER [97, 100]. At the beginning of the synthesis, serine palmitoyl transferase mediates condensation of serine and palmitoyl-CoA to 3-keto-dihydrosphingosine, which in turn is converted by a reduction reaction to dihydrosphingosine (sphinganine) [96]. Dihydrosphingosine is conjugated with fatty acids to form dihydroceramide (dhCer) by ceramide synthases through N-acetylation [96]. Dihydroceramide desaturases, as the name implies, convert dhCer into Cer by generating a double bond in the sphingosine base [102].

Ceramide is then transported from the ER to the Golgi via four-phosphate adaptor protein (FAPP2) or ceramide transfer protein (CERT) [100]. In the Golgi apparatus, Cer can be converted to sphingomyelin through linkage with phosphocoline by sphingomyelin synthases [102]. Furthermore, glycosphingolipids are produced from Cer, by ceramide galactosyltransferases in the ER or glucosylceramide synthases in the Golgi, which catalyze the reaction of Cer to galactosyl- or glucosylceramide, respectively [102]. C1P is generated via phosphorylation of Cer by ceramide kinases in the Golgi body [102]. Ceramide can in

turn be recovered from membrane sphingomyelin or glucosylceramide by the action of acid sphingomyelinase (Asm) or glucosidases in the lysosome [96]. Acid ceramidase (Ac) deacetylates Cer to Sph, which is released from the lysosome [100, 102]. Sphingosine can then be further converted to S1P by sphingosine kinases in the cytosol and eventually to phosphoethanolamine and hexadecanal by S1P lyase at the ER [102].
Under the influence of various stimuli, sphingosine kinases and Asm can also translocate and generate S1P and Cer at the plasma membrane [96]. Furthermore, alkaline and neutral ceramidases as well as neutral sphingomyelinase were identified apart from lysosomal Ac and Asm, which accordingly act at different pH values, in the ER, Golgi or plasma membrane [102].

1.3.2 Acid ceramidase

N-acylsphingosine amidohydrolase 1 (ASAH1), more commonly known as acid ceramidase (Ac), is encoded by the human *ASAH1* gene, which encompasses 14 exons [103]. *ASAH1* transcripts are translated into an approximately 55 kDa precursor protein of 395 amino acids [103, 104]. Likewise, Ac is encoded by the *Asah1* gene in mice, spanning 14 exons [105]. Murine *Asah1* also gives rise to the Ac pro-protein, which shares 90% identity with the human equivalent [105]. Precursor Ac is transferred from Golgi to lysosomes via mannose-6-phosphate, where proteolysis to functional Ac is facilitated by the acidic environment [104]. This active form of Ac consists of two subunits, a smaller α-monomer of 13 kDa and a larger β-monomer of 40 kDa [106]. In 1963, Shimon Gatt already demonstrated that this enzyme catalyzes the hydrolytic cleavage of the amide bond in Cer between the Sph moiety and the acyl group [107, 108]. Furthermore, Ac has been shown to bind with saposin D (acronym for sphingolipid activator protein), which enhances Ac mediated degradation of Cer, especially in the additional presence of anionic phospholipids [109, 110].

1.3.3 Acid ceramidase and associated sphingolipids in immunity and disease

The importance of Ac becomes apparent upon Ac deficiency as in Farber disease (FD), also called Farber lipogranulomatosis, and in spinal muscular atrophy with progressive myoclonic epilepsy (SMA-PME) [111, 112]. Distinct mutations in the *ASAH1* gene, often affecting the enzymes β-subunit in FD and the α-subunit in SMA-PME, lead to impaired activity of Ac of under 10% in FD and under 33% in SMA-PME with concomitant accumulation of Cer in various tissues [112, 113]. SMA-PME and FD are very rare autosomal recessive inherited diseases [112, 113]. SMA-PME onset can occur from 3 years of age, with muscle weakness progressing to atrophy as well as myoclonic epileptic seizures, due to the nerve loss [113]. The disease also affects the respiratory muscles and

leads to death by the age of 12 to 20 years [113]. FD onset is much earlier with classic symptoms such as subcutaneous nodules, hoarse voice, joint contractures and often hepatosplenomegaly, and further respiratory and neurological impairments [112]. Frequently, FD is severe and leads to early death by the age of 3 years [112]. Several cases of severe FD also manifested with diarrhea and severe tissue damage in the gastrointestinal tract [112, 114].

Apart from acid ceramidase deficiencies, Ac also plays important roles in other diseases [115]. It has been reported in type 2 diabetes that increased expression of the enzyme has a beneficial effect as it prevents Cer from blocking insulin induction [115]. In contrast, overexpression of Ac is negatively associated with Alzheimer's disease, where high abundance and activity of the enzyme was detected in the brain of Alzheimer's disease patients [115]. In viral infections, expression of Ac was protective, for example in herpes simplex virus infection, where Ac prevents viral propagation in macrophages by trapping the virus in sphingosine rich multivesicular bodies [116]. Acid ceramidase is also an essential mediator to control measles virus infection, as blocking Ac activity resulted in increased infection of human lymphocytes *in vitro* [117]. Regarding cancer, reduced Ac expression was shown in tumors of the gastrointestinal tract, however, increased Ac expression was found in many other cancers, including prostate and skin cancer [115]. In this context, depletion of Ac in T cells was beneficial, as it reduced tumor growth in a melanoma mouse model by promoting cytotoxic activity of $CD8^+$ T cells [118]. In fibrosarcoma and melanoma, inhibition of Ac and accordingly increased Cer levels, enhanced apoptosis of DCs [119].

The effect of sphingolipids in immune cells varies with disease context. However, in general S1P is known to affect lymphocyte and neutrophil migration and function [120]. CC-chemokine ligand 5 (CCL5), which is produced by plethora of immune cells, including NK cells, DCs, macrophages, monocytes, T cells but also epithelial cells, was found to be regulated by sphingolipids [121, 122]. In fibroblasts and breast cancer cells, Ac and Asm potently induced CCL5 production potentially via their downstream metabolite Sph [121]. In neutrophils, ceramides were found, to block superoxide production and modulate their phagocytic and migratory properties [123]. As mentioned above Cer mediates apoptosis of DCs, as absence of ceramidase activity enhanced DC death, but on the other hand it is also important in DC differentiation in response to LPS, IL-1β or TNFα [123, 124]. In macrophages, Cer accumulation enhanced TNFα and IL-1β production [123]. Ceramide and ceramide enriched platforms in T cells, were similar to the melanoma study described earlier, involved in T cell cytotoxicity in models of graft versus host disease [123].

1.3.3.1 Sphingolipids and acid ceramidase in bacterial infections

The role of sphingolipids, especially Cer due Cer enriched platform formation, was mostly studied in the context of Asm, converting sphingomyelin to Cer [125]. Ceramide enriched platforms often function as entry site for pathogenic bacteria such as *Neisseria gonorrhoeae* and *meningitidis* [126]. However, Asm activity and Cer formation can also be disadvantageous for bacteria, for example leading to cellular engulfment of *Pseudomonas* (*P.*) *aeruginosa* in lung infection and subsequent apoptosis to eradicate the bacteria [126]. Acid ceramidase derived Sph was also shown to be important to manage pulmonary infections in cystic fibrosis [127]. Accordingly, recombinant Ac conferred reduced inflammation in a cystic fibrosis mouse model and more resistance to *P. aeruginosa* and *Staphylococcus aureus* infection in human cystic fibrosis airway epithelial models [128]. Sph is known for its antimicrobial properties, but for *E. coli* divergent results were obtained [126]. Acid ceramidase was also reported to increase the survival of alveolar macrophages, via induction of extracellular signal-regulated kinase (ERK) and protein kinase B (AKT) signaling [129]. Upon blockade of Ac antigen processing and presentation via the human leukocyte antigen (HLA) class II of APCs to $CD4^+$ T cells is disrupted, which was however beneficial in an arthritis mouse model, resulting in reduced inflammation [130].

As for the role of Ac in intestinal infections and immunity, studies are lacking and the role of sphingolipids in *E. coli* infection remains incompletely defined. Glycosphingolipids, however were identified as receptors for *E. coli* (and *P. aeruginosa*) [126]. Similarly, complex gangliosides in the intestine were capable of binding cholera toxin of *Vibrio cholerae* [131]. The blockade of ceramide synthase in pigs led to reduced IL-8 levels and concomitant increased susceptibility to pathogenic *E. coli* infection in the gut and modulation of epithelial barrier function was observed [132, 133]. In line with that, TLR4 stimulation by the *E. coli* derived LPS or fimbriae in monocytes or epithelial cells, respectively, was reported to be mediated by Cer [134, 135]. Acid sphingomyelinase was also shown to be activated by *E. coli* or LPS in DCs, leading to Cer production and apoptosis [125].

1.3.3.2 Sphingolipids and acid ceramidase in intestinal inflammation

In the intestine, complex sphingolipids are commonly present in the brush border of epithelial cells and the gut typically degrades both, intrinsically produced and dietary sphingolipids [136]. IBD is associated with increased levels of sphingomyelin, Cer, C1P and S1P, while glucosylceramide and ganglioside GM3 levels are reduced [136]. Similarly, in a mouse model in which colitis is chemically induced by dextran sodium sulfate (DSS), sphingomyelin and Cer were elevated [136]. In the same direction, inhibition of Asm, which converts sphingomyelin to Cer, ameliorated DSS colitis and reduced pro-inflammatory cytokine production by macrophages [137, 138]. However, in *C. rodentium* induced colitis

deficiency of Asm activity enhanced colitis along with elevated pro-inflammatory T_h1/T_h17 responses and reduced T_{regs} [83]. In UC patients, the expression of neutral ceramidase was found to be elevated in the epithelium, consistent with that, epithelial neutral ceramidase expression was elevated during DSS colitis [139]. However, deletion of neutral ceramidase aggravated DSS colitis with increased levels of pro-inflammatory cyclooxygenase 2 (COX2) in the epithelium and enhanced systemic S1P together with higher neutrophil and lymphocyte abundance [139]. Ceramide synthases, catalyzing the reverse reaction compared to Ac, the synthesis of Cer from Sph, have been studied in IBD mouse models as well with divergent results. In T cell transfer colitis, Cer synthase 6 deficiency attenuated colitis, while in DSS colitis with Cer synthase 6 and 2 deficient mice an aggravation of was observed [140-142]. Ceramide synthase 2 deficiency was accompanied with upregulation of T_h17 cells and T_{regs} during DSS colitis, whereas Cer synthase 6 knockout was associated with increased neutrophil influx along with increased S1P levels [141, 143]. In naïve Cer synthase 2 knockout mice, also enhanced intestinal permeability was observed, mediated by the loss of ZO-1 expression [140]. Production of pro-inflammatory prostaglandin E2 (PEG_2), which is highly abundant in the gut, is induced by C1P and S1P, via phospholipase A2 (PLA2) and COX2, respectively [120]. In fibroblasts, Ac was found to be a driver of PGE_2 production via TNFα/COX2 signaling induced by its downstream molecules Sph and S1P [144]. Sphingosine kinase inhibitors have been shown to attenuate DSS colitis [145]. S1P exerts anti-apoptotic functions on macrophages, while Sph, which is also downstream of Ac, acts pro-apoptotically on macrophages [120].

Finally, Espaillat *et al.* conferred a study specifically about Ac function in intestinal inflammation, reporting that Ac protein is increased in the lamina propria of IBD patients and Ac deficiency in myeloid cells in turn leads to decreased neutrophil infiltration, overall attenuated DSS induced colitis and decreased colitis-associated carcinogenesis in mice [146].

Collectively, the functions of the individual sphingolipids in the gut are complex and their effects are highly dependent on the pathological context, in which cell type they are located and how they are synthesized. While the influence of distinct sphingolipids and corresponding enzymes have been studied in intestinal inflammation and to very limited extent in intestinal infection, their contribution to intestinal diseases and immunity is still incompletely understood. More importantly, studies about the function of Ac in gut inflammation and especially in gut infection are completely lacking.

2 Objective

Intestinal diseases, including *E. coli* infections, and intestinal inflammation, as seen in IBD are a global burden on health and welfare. *E. coli* infections remain a major concern in developing countries, whereas IBD is predominantly encountered in developed nations, with increasing incidence in emerging countries. In order to develop effective vaccines or therapies to combat gut infections and inflammation, an understanding of the pathomechanisms is highly valuable. Sphingolipids are important membrane components that also function as signaling molecules in inflammation, cell survival and cell death. The enzyme Ac has pivotal functions, which becomes evident upon Ac deficiency as in Farber disease. Acid ceramidase importantly catabolizes the central sphingolipid mediator Cer to Sph and in turn fuels the S1P pool. Different enzymes of the sphingolipid system and corresponding sphingolipids have been studied in intestinal diseases, mainly in the context of IBD and scarcely in intestinal infections. The role of Ac however, is poorly defined in intestinal inflammation and remains completely elusive in intestinal infections with pathogenic A/E bacteria such as *E. coli* or *C. rodentium*.

Therefore, the present study investigated the role of Ac in intestinal infection with the natural mouse enteropathogen *C. rodentium*. More specifically, the function of Ac in the different cellular elements of the host defense against invading pathogens, which include epithelial cells and innate and adaptive immune cells, was studied. The results of this study shed light on the functions of Ac in intestinal inflammation in general and in infections in particular, and therefore contribute to potential preventive and therapeutic measures against *E. coli* infections and IBD in the future.

3 Material

Consumables, reagents, equipment and software used in this study are listed in the following tables.

3.1 Consumables

Tab. 1: Consumables

Consumables	Manufacturer
96-well PCR plate (0.1 mL)	BIOplastics, Landgraaf, Netherlands
Acella 50 slides	Anvajo GmbH, Dresden, Germany
Cell strainer (40, 70 and 100 µm)	Falcon, Durham, USA
Chromatography paper (3 x 100 cm)	Whatman GmbH, GE Healthcare Life Sciences, Dassel, Germany
Cover slips (0,4 x 20 x 26 mm)	Assistent, Sondheim vor der Röhn, Germany
Culture plates (6-, 12-, 24-, 48- and 96- well)	Greiner BioOne, Frickenhausen, Germany
Histology cassettes	Kartell Spa, Noviglio, Italy
Inoculum tubes MicroScan (3mL water)	Beckman Coulter Inc., Brea, USA
MacConkey selection plates	Oxoid, Wesel, Germany
Micro reaction tubes (0.6 mL)	Biozyme Scientific GmbH, Oldendorf, Germany
Micro reaction tubes (1.5 mL)	Sarstedt, Nümbrecht, Germany
Micro reaction tubes (2 mL)	Greiner BioOne, Frickenhausen, Germany
Needle (26G x 13 mm)	BD Biosciences, Heidelberg, Germany
Opti-Seal Optical sealing sheet	BIOplastics, Landgraaf, Netherlands
Petri dish, 92 x 16 mm	Sarstedt, Nümbrecht, Germany
Pipettes (5, 10, 25 mL)	Greiner BioOne, Frickenhausen, Germany
Pipettes tips (10, 200, 1000 µL)	Sarstedt, Nümbrecht, Germany
Round bottom plates (96-well)	Greiner BioOne, Frickenhausen, Germany
Safety-Multifly (21G, tube 200 mm)	Sarstedt, Nümbrecht, Germany
Scalpel disposable	Mediware, Servoprax GmbH, Wesel, Germany
Syringe sterile (1 mL, 2 mL, 10 mL)	BD Biosciences, Heidelberg, Germany
Syringe Filcons (30 µm)	BD Biosciences, Heidelberg, Germany
Strips 8 PCR tubes with cap strips (0.2 mL)	Bio-Budget technologies GmbH, Krefeld, Germany
Tubes conical (15 and 50 mL)	Greiner BioOne, Frickenhausen, Germany
Tubes round bottom (1.3 mL) FACS-tubes	Greiner BioOne, Frickenhausen, Germany
Tubes round bottom (12 x75 mm) FACS-tubes	Falcon, Durham, USA

3.2 Chemicals

Tab. 2: Chemicals

Chemicals	Manufacturer
Agar-Agar	Merck, Darmstadt, Germany
Ammonium chloride [NH_4Cl]	Carl Roth GmbH & Co. KG, Karlsruhe, Germany
AutoMACS Pro Washing Solution	Miltenyi Biotec, Bergisch Gladbach, Germany

Chemicals	Manufacturer
AutoMACS Running Buffer	Miltenyi Biotec, Bergisch Gladbach, Germany
Boric acid [H_3BO_3]	Carl Roth GmbH & Co. KG, Karlsruhe, Germany
Bovine serum albumin (BSA), Fraction V	BIOMOL GmbH, Hamburg, Germany
Brefeldin A (BFA)	Sigma-Aldrich, St. Louis, USA
C17 ceramide	Avanti Polar Lipids, Alabaster, USA
Chloroform	AppliChem GmbH, Darmstadt, Germany
Corn oil	Sigma-Aldrich, St. Louis, USA
Dimethyl sulfoxide (DMSO)	Carl Roth GmbH & Co. KG, Karlsruhe, Germany
Di-sodium hydrogen phosphate dihydrate [Na_2HPO_4 x 2 H_2O]	Carl Roth GmbH & Co. KG, Karlsruhe, Germany
Ethanol, absolute	Carl Roth GmbH & Co. KG, Karlsruhe, Germany
Ethylene glycol tetraacetic acid (EGTA)	Carl Roth GmbH & Co. KG, Karlsruhe, Germany
Ethylenediaminetetraacetic acid (EDTA)	Carl Roth GmbH & Co. KG, Karlsruhe, Germany
FACS Clean Solution	BD Biosciences, Heidelberg, Germany
FACS Flow Sheath Fluid	BD Biosciences, Heidelberg, Germany
FACS Rinse Solution	BD Biosciences, Heidelberg, Germany
Fetal calf serum (FCS)	Sigma-Aldrich, St. Louis, USA
Fixable viability dye eFluor780 (FvD)	eBioscience, San Diego, USA
Gentamicin solution 10 mg/mL	Sigma-Aldrich, St. Louis, USA
Glycerin ≤ 86 %	Carl Roth GmbH & Co. KG, Karlsruhe, Germany
Heparin-Natrium-25000-ratiopharm	Merckle GmbH, Blaubeuren, Germany
Hydrochloric acid [HCl]	Merck, Darmstadt, Germany
IGEPAL CA-630 (NP-40)	Sigma-Aldrich, St. Louis, USA
Ionomycin calcium salt	Sigma-Aldrich, St. Louis, USA
LE Agarose	Biozyme Scientific GmbH, Oldendorf, Germany
Magnesium chloride [$MgCl_2$]	Carl Roth GmbH & Co. KG, Karlsruhe, Germany
Magnesium chloride solution 25 mM	Promega, Mannheim, Germany
Matrigel Growth Factor Reduced Basement Membrane Matrix	Corning, Bedford, USA
Methanol	Carl Roth GmbH & Co. KG, Karlsruhe, Germany
Midori Green Advance	Nippon Genetics Europe, Düren, Germany
Paraformaldehyde (PFA)	Carl Roth GmbH & Co. KG, Karlsruhe, Germany
Penicillin-Streptomycin (10.000 U/mL)	Gibco, Life Technologies, Carlsbad, USA
Phorbol 12-myristate 13-acetate (PMA)	Sigma-Aldrich, St. Louis, USA
Potassium bicarbonate [$KHCO_3$]	Carl Roth GmbH & Co. KG, Karlsruhe, Germany
Potassium chloride [KCl]	Carl Roth GmbH & Co. KG, Karlsruhe, Germany
Potassium dihydrogen phosphate [KH_2PO_4]	Carl Roth GmbH & Co. KG, Karlsruhe, Germany
Sodium chloride [NaCl]	Carl Roth GmbH & Co. KG, Karlsruhe, Germany and Merck, Darmstadt, Germany

Chemicals	Manufacturer
Sodium dodecyl sulfate (SDS) Ultra pure	Carl Roth GmbH & Co. KG, Karlsruhe, Germany
Streptomycin	Sigma-Aldrich, St. Louis, USA
Tamoxifen	Sigma-Aldrich, St. Louis, USA
Tris(hydroxymethyl)aminomethane (TRIS)	Carl Roth GmbH & Co. KG, Karlsruhe, Germany
Trypan blue stain (0.4 %)	Gibco, Life Technologies, Carlsbad, USA
Tryptone (Bacto)	Gibco, Life Technologies, Carlsbad, USA
Yeast extract (Bacto)	Gibco, Life Technologies, Carlsbad, USA
β-Mercaptoethanol	Promega, Mannheim, Germany

3.3 Enzymes, primers and nucleic acids

Tab. 3: Enzymes and nucleic acids

Enzymes and nucleic acids	Manufacturer
Collagenase Type IV	Merck, Darmstadt, Germany
RNase-Free DNase Set	Qiagen, Hilden, Germany
Deoxynucleotide Triphosphate (dNTP)	Bio-Budget technologies GmbH, Krefeld, Germany
Gene Ruler 100 bp Plus DNA ladder	Thermo Fisher Scientific, Braunschweig, Germany
GoTaq Hot Start Polymerase	Promega, Mannheim, Germany
Maxima SYBR Green/ROX qPCR Master Mix (2x)	Thermo Fisher Scientific, Braunschweig, Germany
M-MLV Reverse Transcriptase (H-) Point Mutant	Promega, Mannheim, Germany
Oligo (dT) 12-18 Primer	Invitrogen, Karlsruhe, Germany
Proteinase K	Merck, Darmstadt, Germany
Random Primer	Invitrogen, Karlsruhe, Germany

Tab. 4: Primers for genotyping of transgenic mouse strains

Transgene	Primer sequence	Annealing temperature
Asah1$^{flox/flox}$	ACAACTGTGTAGGATTCACGCATTCTCC	58°C
	TCGATCTATGAAATGTCGCTGTCGG	
Cre	ACGACCAAGTGACAGCAATG	60°C
	CTCGACCAGTTTAGTTACCC	
creER	TCCAATTTACTGACCGTACACCAA	62°C
	CCTGATCCTGGCAATTTCGGCTA	
LysMcre	CTTGGGCTGCCAGAATTTCTC	58°C
	TTACAGTCGGCCAGGCTGAC	
	TTAGCTGGCCCAAATGTTGCTG	
Vilcre	ACGACCAAGTGACAGCAATG	60°C
	CTCGACCAGTTTAGTTACCC	

Tab. 5: Primers used in semi-quantitative PCR and RT-qPCR

Gene	Primer sequence	Annealing temperature
Asah1	TTCTCACCTGGGTCCTAGCC	60°C
	TATGGTGTGCCACGGAACTG	
Lgr5	ACCCGCCAGTCTCCTACATC	58°C
	GCATCTAGGCGCAGGGATTG	
Occludin	GCCCTGGCTGACCTAGAACTTAC	55°C
	AGACTTAGCCAAAACTGCCTTAGC	
Rps9	CTGGACGAGGGCAAGATGAAGC	58°C
	TGACGTTGGCGGATGAGCACA	

3.4 Buffer and Media

Tab. 6: Buffer

Buffer	Ingredients or Manufacturer
AutoMACS Running Buffer	Commercial buffer, Miltenyi Biotec, Bergisch Gladbach, Germany
ACK buffer (Erythrocyte-Lysis buffer)	In demineralized water 8.29 g/L Ammonium chloride 1 g/L Potassium bicarbonate 0.1 mM EDTA adjust to pH 7.2-7.4
FACS buffer (Fluorescence-activated cell sorting buffer)	In PBS buffer 2 % v/v heat inactivated FCS 2 mM EDTA
Green GoTaq 5x Flexi buffer	Commercial buffer, Promega, Mannheim, Germany
Roti-CELL HEPES solution 1 M	Commercial solution, Carl Roth GmbH & Co. KG, Karlsruhe, Germany
MML V-RT 5x buffer	Commercial buffer, Promega, Mannheim, Germany
PBS buffer (Phosphate-Buffered-Saline buffer)	In demineralized water 8 g/L Sodium chloride 0.2 g/L Potassium chloride 1.44 g/L Di-sodium hydrogen phosphate dihydrate 0.2 g/L Potassium dihydrogen phosphate
PBS/EDTA	In PBS buffer 3 mM EDTA
PBS PSG (Penicillin-Streptomycin-Gentamycin)	In PBS buffer 100 U/mL penicillin 100 µg/mL streptomycin 50 µg/mL gentamycin
Rapid tail buffer	In demineralized water 100 mM TRIS/HCl (pH 8.5) 11,69 g/L Sodium chloride 5 mM EDTA 0.2 % w/v SDS

Buffer	Ingredients or Manufacturer
TBE buffer (TRIS-borate-EDTA-buffer)	In demineralized water 89 mM TRIS 89 mM Boric acid 2 mM EDTA
TE buffer (TRIS-EDTA-buffer)	In demineralized water 10 mM TRIS/HCl (pH 8.0) 1 mM EDTA

Tab. 7: Media

Media	Ingredients or Manufacturer
Advanced DMEM	Commercial advanced Dulbecco's modified eagle medium/ Ham's F-12 (DMEM/F12) with reduced Serum medium (1:1), non-essential amino acids, 110 mg/L Sodium Pyruvate Gibco, Life Technologies, Carlsbad, USA
DMEM	Commercial Dulbecco's modified eagle medium (DMEM) with 4.5 g/L D-Glucose, 580 mg/L L-Glutamine, 110 mg/L Pyruvate Gibco, Life Technologies, Carlsbad, USA
DMEM complete	In DMEM with 4.5 g/L D-Glucose, 580 mg/L L-Glutamine, 110 mg/L Pyruvate 1 % v/v heat inactivated FCS 100 U/mL penicillin 100 µg/mL streptomycin 50 µg/mL gentamycin
IMDM	Commercial Iscove's modified Dulbecco's medium (IMDM) with GlutaMax -I and 25 mM HEPES Gibco, Life Technologies, Carlsbad, USA
IMDM complete	In IMDM with GlutaMax -I and 25mM HEPES 10% v/v heat inactivated FCS 100 µg/mL Streptomycin 100 U/mL Penicillin 25 µM ß-Mercaptoethanol
IntestiCult OGM	Commercial IntestiCult organoid growth medium (OGM) STEMCELL Technologies, Cologne, Germany
LB medium (Lysogeny broth-medium)	In demineralized water 10 g/L Tryptone 5 g/L Yeast extract 10 g/L Sodium chloride adjust to pH = 7.5
LB Agar	In LB-medium with 15 g/L Agar-Agar
RPMI medium	Commercial Roswell Park Memorial Institute (RPMI) 1640 medium with GlutaMax -I and 25 mM HEPES Gibco, Life Technologies, Carlsbad, USA
RPMI/FCS	In RPMI 1640 with GlutaMax -I and 25 mM HEPES 20 % v/v heat inactivated FCS
RPMI/FCS/EGTA/ $MgCl_2$	In RPMI 1640 with GlutaMax -I and 25 mM HEPES 1 % v/v heat inactivated FCS 1 mM EGTA 1.5 mM Magnesium chloride

3.5 Kits

Tab. 8: Kits

Kit	Manufacturer
$CD4^+$ T cell Isolation Kit, mouse	Miltenyi Biotec, Bergisch Gladbach, Germany
Anti-F4/80 MicroBeads UltraPure, mouse	Miltenyi Biotec, Bergisch Gladbach, Germany
FoxP3/Transcription Factor Staining Buffer Set	eBioscience, San Diego, USA
Luminex Discovery Assay Mouse Multi-Analyte	R&D Systems, Minneapolis, USA
NucleoSpin RNA XS	Macherey-Nagel, Düren, Germany
RNeasy Fibrous Tissue Mini Kit	Qiagen, Hilden, Germany
RNeasy Mini Kit	Qiagen, Hilden, Germany
QuantSeq 3' mRNA-Seq Library Prep Kit FWD	Lexogen, Vienna, Austria
NextSeq High Output (75 cycles)	Illumina Inc., San Diego, USA

3.6 Antibodies, cytokines and fluorophores

Tab. 9: FACS and MACS antibodies

Epitope	Fluorochrome	Clone	Manufacturer
CD4	APC	RM4-5	BD Biosciences, Heidelberg, Germany
	PB	RM4-5	BD Biosciences, Heidelberg, Germany
	PE	H129.19	BD Biosciences, Heidelberg, Germany
	PE-Cy7	RM4-5	BioLegend, San Diego, USA
	PerCP	RM4-5	BD Biosciences, Heidelberg, Germany
CD8a	APC	53-6.7	BD Biosciences, Heidelberg, Germany
	PB	53-6.7	BD Biosciences, Heidelberg, Germany
	PE-Cy7	53-6.7	eBioscience, San Diego, USA
CD11c	APC	HL3	BD Biosciences, Heidelberg, Germany
CD25	APC	PC61	BD Biosciences, Heidelberg, Germany
	Biotin	7D4	BD Biosciences, Heidelberg, Germany
	PE	PC61	BD Biosciences, Heidelberg, Germany
CD44	eFluor450	IM7	eBioscience, San Diego, USA
CD45	PE-Cy7	30-F11	BioLegend, San Diego, USA
F4/80	FITC	BM8	Invitrogen, Karlsruhe, Germany
Foxp3	eFluor450	FJK-16s	eBioscience, San Diego, USA
	FITC	FJK-16s	eBioscience, San Diego, USA
	PE	FJK-16s	eBioscience, San Diego, USA
GrzB	APC	GB12	Invitrogen, Karlsruhe, Germany
IFNγ	FITC	XMG1.2	BD Biosciences, Heidelberg, Germany
	PE	XMG1.2	BD Biosciences, Heidelberg, Germany
IL-17A	BV421	TC11-18H10.1	BioLegend, San Diego, USA
Ly-6G	BV421	1A8	BD Biosciences, Heidelberg, Germany
T-Bet	PE	4B10	eBioscience, San Diego, USA
	PE-Cy7	4B10	BioLegend, San Diego, USA

Tab. 10: Fluorochromes

Fluorochrome	Abbreviation	Excitation	Emission
Allophycocyanine	APC	650 nm	660 nm
Brilliant Violet 421	BV421	407 nm	421 nm
eFluor 450	eFluor450	405 nm	445 nm
eFluor 780	eFluor780	753 nm	785 nm
Fluorescein isothiocynate	FITC	494 nm	520 nm
Pacific Blue	PB	404 nm	455 nm
Peridinin-Chlorophyll-Protein	PerCP	477 nm	678 nm
R-Phycoerythrin	PE	496 nm	578 nm
R-Phycoerythrin-Cyanine dye 7	PE-Cy7	496 nm	785 nm

Tab. 11: Purified antibodies for *in vitro* assays

Epitope	Clone	Manufacturer
CD3ε	145-2C11	BD Biosciences, Heidelberg, Germany
CD28	37.51	BD Biosciences, Heidelberg, Germany
IFNy	XMG1.2	Affymetrix eBioscience, San Diego, USA
IL-2	JES6-1A12	R&D Systems, Minneapolis, USA
IL-4	11B11	eBioscience, San Diego, USA

Tab. 12: Cytokines used for *in vitro* assays [recombinant (r), mouse (m), human (h)]

Cytokine	Manufacturer	Reconstitution buffer
rh TGFβ1	R&D Systems, Minneapolis, USA	4 mM HCl containing 1 mg/mL BSA in demineralized water
rm IL-6	R&D Systems, Minneapolis, USA	PBS containing 0.1 % BSA
rm IL-1β	Gibco, Life Technologies, Carlsbad, USA	Demineralized water
rm IL-21	R&D Systems, Minneapolis, USA	PBS containing 0.1 % BSA
rm IL-23	R&D Systems, Minneapolis, USA	PBS
rm IL-12	R&D Systems, Minneapolis, USA	PBS containing 0.1 % BSA

3.7 Equipment

Tab. 13: Equipment

Equipment	Manufacturer
7500 Fast Real-Time PCR System	Thermo Scientific, Darmstadt, Germany
autoMACS Pro Separator	Miltenyi Biotec, Bergisch Gladbach, Germany
BD FACS Aria II cell sorter	BD Biosciences, Heidelberg, Germany
Centrifuge 5417R	Eppendorf AG, Hamburg, Germany
Centrifuge MULTIFUGE 3SR+	Thermo Fisher Scientific, Waltham, USA
Electrophoresis Apparatus Horizon 11.14	Analytik Jena, Jena, Germany
Flow cytometer BD LSRII	BD Biosciences, Heidelberg, Germany
Fluidlab R-300	Anvajo GmbH, Dresden, Germany
Gel electrophoresis station PowerPac universal	Bio-Rad, Feldkirchen, Germany
Gel Documentation System QUANTUM CX5 Edge	VILBER LOURMAT Deutschland GmbH, Eberhardzell, Germany
Heracell 150i CO_2-Incubator	Thermo Scientific, Darmstadt, Germany
Heraeus Multifuge 3SR+	Thermo Scientific, Darmstadt, Germany
HPLC 1290 Infinity II with Poroshell 120 EC-C8 column (3,0 × 150 mm, 2,7 µm)	Agilent Technologies, Waldbronn, Germany

Equipment	Manufacturer
Luminex MAGPIX Analyzer	Luminex Corporation, Austin, Texas, USA
Magnetic stirrer Variomag	Thermo Scientific, Darmstadt, Germany
Mass spectrometer Q-TOF 6530	Agilent Technologies, Waldbronn, Germany
Microscope Binokular Axiovert Z1	Carl Zeiss Microscopy GmbH, Jena, Germany
Leica DMIL LED microscope with Leica DFC450 C camera	Leica Microsystems GmbH, Wetzlar, Germany
Microscan turbidity meter	Siemens Healthcare Diagnostics, Erlangen, Germany
Microwave	Sharp, Hamburg, Germany
Minitron Incubator Shaker	Infors AG, Bottmingen, Switzerland
NanoDrop 1000 spectrophotometer	PeqLab, Erlangen, Germany
Neubauer counting chamber (0.0025mm^2)	Superior, Marienfeld, Germany
NextSeq 500 Sequencing System	Illumina Inc., San Diego, USA
Scale AX 120	Shimadzu, Duisburg, Germany
Scale Sartorius CP2202 S	Sartorius AG, Göttingen, Germany
Thermocycler T3000	Biometra, Göttingen, Germany
Thermomixer (comfort)	Eppendorf AG, Hamburg, Germany
Vortexer D-6013	Neo Lab, Heidelberg, Germany
Vortexer IKA MS 3 basic	IKA-Werke GmbH & Co. KG, Staufen, Germany
Water bath	GFL, Burgwedel, Germany
Work Bench MSC-Advantage	Thermo Scientific, Darmstadt, Germany

3.8 Software and scripts

Tab. 14: Software

Software	Supplier or Source
7500 Fast System Software v2.3	Thermo Scientific, Darmstadt, Germany
BD FACSDiva Software v8.0.1	BD Biosciences, Heidelberg, Germany
Endnote X9 v9.3.3	PDFNet SDK from PDF Tron Systems Inc., Vancouver, Canada
Graph Pad Prism v8.4.3	GraphPad Software, La Jolla, USA
BioVision	VILBER LOURMAT Deutschland GmbH, Eberhardzell, Germany
LAS Software v4.0	Leica Microsystems GmbH, Wetzlar, Germany
Luminex xPONENT Software v4.2	Luminex Corporation, Austin, USA
MassHunter Software B.07.00	Agilent Technologies, Waldbronn, Germany
Microsoft Office 2016	Microsoft Corporation, Redmond, USA
NanoDrop Software ND-1000 v3.7.1	Thermo Scientific, Darmstadt, Germany
R Software v4.2.2	https://www.R-project.org/ R Core Team (2022) R: A language and environment for statistical computing R Foundation for Statistical Computing, Vienna, Austria

Tab. 15: Scripts used for RNA sequencing analysis

Script/Package	Source
DESeq2 v3.16	https://bioconductor.org/packages/release/bioc/html/DESeq2.html [147]
FastQC v0.11.7	https://qubeshub.org/resources/fastqc Andrews, S. (2010). FastQC: A Quality Control Tool for High Throughput Sequence Data http://www.bioinformatics.babraham.ac.uk/projects/fastqc/
Genomic Alignments v1.34.0	https://bioconductor.org/packages/release/bioc/html/GenomicAlignments.html [148]
HISAT2 v2.2.1	http://daehwankimlab.github.io/hisat2/main/; [149, 150]
TrimGalore v0.6.0	http://www.bioinformatics.babraham.ac.uk/projects/trim_galore/ GitHub. 2021 https://github. com/FelixKrueger

4 Methods

4.1 Experimental animals and husbandry

Mice were kept under specific pathogen-free (SPF) conditions at the central animal laboratory of the University Hospital Essen. Mice were housed in individually ventilated (ICV2) cages, with a 12 h – 12 h light – dark cycle, at ~23°C and with food and water *ad libitum*. All mouse strains were on C57BL/6 background.

4.1.1 *Asah1*$^{flox/flox}$ mice

Asah1$^{flox/flox}$ mice (Asah1^{tmJhkh}), abbreviated as Ac^{flox}, possess two *loxP* sites, which flank the Exon 1 of the *Asah1* gene expressing acid ceramidase protein (Ac).

4.1.2 *Asah1*$^{flox/flox}$ x creER mice

Asah1$^{flox/flox}$ x creER mice (Asah1^{tmJhkh}/Gt(Rosa)26Sor$^{tm9(cre/ESR)Arte}$), abbreviated as Ac^{flox} creER KO, were obtained by crossing Ac^{flox} mice with Gt(Rosa)26Sor$^{tm9(cre/ESR)Arte}$ mice. In Gt(Rosa)26Sor$^{tm9(cre/ESR)Arte}$ mice a cre recombinase (cre) fused with a mutated ligand binding domain (LBD) of the estrogen receptor is inserted (knockin, ki) at the *Rosa26* locus [151]. The mutations in the LBD of the estrogen receptor lead to specific binding of tamoxifen, but not of the natural ligand 17β-estradiol [152]. In absence of tamoxifen the cre recombinase estrogen receptor fusion protein (creER) is sterically hindered by a complex containing heat shock protein 90 (Hsp90) and therefore the cytoplasmic chimeric creER protein remains inactive [153, 154]. Tamoxifen binding terminates Hsp90 mediated blockade and allows the creER to translocate into the nucleus and exert its cre activity [152]. Mice were bred heterozygously for creER to obtain Ac^{flox} creER wild type (WT, controls) and Ac^{flox} creER knockout (KO) mice.

4.1.3 *Asah1*$^{flox/flox}$ x Villin cre mice

To achieve specific knockout of Ac in enterocytes *Asah1*$^{flox/flox}$ x Villin cre (Asah1^{tmJhkh}/Tg(Vil-cre)20Syr), abbreviated as Ac^{flox} Vilcre KO, were bred. In Villin cre mice cre recombinase is expressed under the villin promoter, which results in cre activity along the crypt-villus axis [155]. Accordingly, Ac is excised in the intestinal epithelium of Ac^{flox} Vilcre KO mice, but not in Ac^{flox} Vilcre WT mice.

4.1.4 *Asah1*$^{flox/flox}$ x LysMcre mice

To obtain Ac depletion in myeloid cells *Asah1*$^{flox/flox}$ x LysMcre mice (Asah1^{tmJhkh}/ Lyz2$^{tm1(Cre)Ifo}$), hereafter referred to as Ac^{flox} LysMcre KO mice, were generated. In LysMcre mice a cre recombinase with nuclear localization is expressed under control of the

lysozyme 2 promoter/enhancer elements [156]. Accordingly, Ac^{flox} LysMcre transgenic mice are depleted of Ac expression in cells of the myeloid lineage, in particular macrophages and granulocytes [156, 157]. This mouse strain was bred heterozygously for LysMcre to obtain Ac^{flox} LysMcre WT (controls) and Ac^{flox} LysMcre KO mice.

4.1.5 *Asah1*$^{flox/flox}$ x CD4cre mice

For a T cell specific Ac knockout, *Asah1*$^{flox/flox}$ x CD4cre mice ($Asah1^{tm1Jhkh}$/$Tg(CD4\text{-}cre)^{1Cwi}$) were bred, which are abbreviated as Ac^{flox} CD4cre KO mice. In CD4cre mice, CD4 enhancer, promoter and silencer direct the expression of the cre recombinase. Hence, in Ac^{flox} CD4cre KO mice this leads to a deletion of Ac expression in $CD4^+$ T cells and, given the $CD4^+$ $CD8^+$ double positive stage during T cell development, Ac expression is also deleted in $CD8^+$ T cells [158]. Ac^{flox} CD4cre WT mice without cre recombinase expression were used as controls.

4.2 Animal procedures

For all experiments, both female and male mice were used at an age of at least 8 weeks. All experiments were performed following the specifications of the German Animal Welfare Act and were authorized by the State Agency for Nature, Environment and Consumer Protection (LANUV), North Rhine-Westphalia, Germany.

4.2.1 Tamoxifen treatment

To induce Ac depletion *Asah1*$^{flox/flox}$ x $creER^{ki}$ mice received 4 mg tamoxifen in 100 µL corn oil intraperitoneally 8, 6 and 4 days before analysis or infection, resulting in global Ac deletion (Ac^{flox} creER KO). Ac^{flox} creER WT littermates received the same treatment.

4.2.2 *Citrobacter rodentium* culture and infection

In this study, mice were infected with the *Citrobacter* (*C.*) *rodentium* strain ICC169 leading to development of colitis. ICC169 is a derivative of ICC168 strain obtained from the original *C. rodentium* stocks (previously *C. freundii* (4280)) of S. Barthold [159-161]. The ICC169 strain has a spontaneous naladixic acid resistance but identical pathogenicity compared to the ICC168 strain as mentioned by Mundy *et al.* (based on unpublished data) [67]. The *C. rodentium* ICC169 strain was kindly provided by apl. Prof. Dr. Christian Riedel (Ulm University, Germany).

C. rodentium was cultured from cryo stocks stored at -80°C. Cryo stocks were obtained by a 1:1 (v/v) mixture of *C. rodentium* overnight culture and sterile glycerin solution (≤ 86 %). For *C. rodentium* cultivation 50 µL of *C. rodentium* cryo stock were streaked with an inoculation loop on a LB agar to obtain single colonies. The same inoculation tube was used

to streak on a MacConkey agar, which is selective for gram-negative bacteria, to confirm the purity of the *C. rodentium* suspension. For the overnight broth, 200 mL LB medium were inoculated with one colony of *C. rodentium* and cultivated in a shaking incubator at 37°C and 180 rpm constantly shaking. After 14 to 14.5 hours the optical density (OD) of the overnight broth was measured at 600 nm compared to LB medium using MicroScan turbidity meter and MicroScan inoculum tubes. In stationary growth phase, the OD ranged between 0.64 – 0.75. At this time point, 3 mL of the overnight broth per mouse, containing ~2 x 10^9 CFU *C. rodentium*, were centrifuged at 3450 g for 10 min and the bacterial pellet was suspended in 100 µL PBS buffer. Each mouse was orally gavaged with 100 µL of this suspension containing ~2 x 10^9 CFU *C. rodentium*. The exact infection dose and the purity of gavage suspension were determined as described in the next chapter 4.2.3.
At 3, 5, 7 and 10 days post infection the body weight of the mice was measured and feces were collected to determine the *C. rodentium* load (chapter 4.2.3). Mice were sacrificed 10 days post infection by cervical dislocation. Blood was drawn by cardiac puncture and organs including, spleen, mesenteric lymph nodes and the colon were collected and processed as described in the following chapters.

4.2.3 Determination of the *C. rodentium* load

To assess the exact infection dose and to analyze the course of infection the colony forming units (CFU) of the gavage suspension and of homogenized fecal samples, respectively, were determined. The gavage solution was serially diluted in 1:10 dilutions and 100 µL of the dilutions 10^{-5} to 10^{-9} were plated on MacConkey agar. Fecal pellets were weighted and suspended in 500 µL PBS and homogenized. Homogenized fecal suspensions were then subjected to serial 1:10 dilution in PBS and 100 µL of the dilutions 10^{-2} to 10^{-6} were plated on MacConkey agar. Inoculated agar plates were incubated over night at 37°C and 5 % CO_2 and colonies were counted. The *C. rodentium* load of 100 µL gavage broth was calculated as described in Formula 1.

$$\text{Bacterial load [CFU/100 µL]} = \text{mean (counted colonies} \times \text{dilution factor} \times 5)$$

Formula 1: Calculation of bacterial load in a bacterial suspension [CFU/100 µL].

The *C. rodentium* load in the feces was calculated with the following Formula 2:

$$\text{Bacterial load [CFU/g feces]} = \frac{\text{mean (counted colonies} \times \text{dilution factor} \times 5)\ \text{[CFU]}}{\text{feces weight [g]}}$$

Formula 2: Calculation of bacterial load in the feces [CFU/g feces].

4.2.4 Colonic macroscopic analysis and biopsies

Collected colons were rinsed with 10 mL ice-cold PBS to remove fecal content, fat and connective tissue was removed and subsequently colon length and weight were measured. Colonic biopsies of 10 – 20 mg were excised from the rectal part. Afterwards colon tissue was subjected to histological analysis (chapter 4.2.5) or lamina propria lymphocyte isolation (chapter 4.3.4).

To assess colonic cytokine secretion, colonic biopsies were incubated in 300 µL IMDM complete at 37°C and 5 % CO_2 in a 48-well plate for 6 h. Medium was collected and tissue remnants were eliminated by centrifuging at 6800 g for 10 min. Supernatant was collected and cytokine levels were determined using Luminex technology (see chapter 4.4.7).

For PCR analysis, colonic biopsies were lysed in RLT buffer and frozen at -20°C until RNA isolation (see chapter 4.4.2.1).

4.2.5 Histology

To assess the degree of inflammation colons were analyzed by histology. Colons were rolled as swiss rolls into histology cassettes covered by filter papers on both sides. Swiss rolls were fixed in 4% paraformaldehyde (PFA) and embedded in paraffin. From the embedded colonic tissue, 4 - 5 µM thick slices were cut from proximal, middle and distal parts of the colon and stained with hematoxylin and eosin (H&E). Tissue slices were assessed microscopically, in different magnifications for inflammatory cell infiltration of the lamina propria and tela submucosa, neutrophil infiltration, epithelial defects and crypt abscesses. These aspects were scored in a blinded manner from 0 (not present) to 3 (very pronounced) for each part of the colon. To determine the histopathological score all scores of a colon were summed. To investigate crypt hyperplasia, the length of 30 crypts per colon was measured and the mean was calculated.

Histological analysis from embedding to scoring, as well as crypt length measurement and imaging was kindly performed by Prof. Dr. Robert Klopfleisch (Freie Universität Berlin, Institute of Veterinary Pathology, Germany).

4.3 Cell biological procedures

4.3.1 Crypt isolation, organoid culture and morphology

To assess intestinal epithelial cell function, colonic crypts were isolated and cultured to form intestinal epithelial organoids. Colons were rinsed with ice-cold DMEM containing antibiotics and FCS (DMEM complete) to remove fecal contents. Fat and connective tissue was removed. Only the rectal half of the colon was used and was cut open longitudinally. Colonic tissue was cut in 2 mm pieces and washed two times at 4°C gently shaking with 20 mL PBS

supplemented with penicillin, streptomycin and gentamycin (PSG) to prevent contamination by fecal microbiota. Next, the tissue was digested with 10 mL DMEM complete containing 500 U/mL collagenase IV at 37°C and vigorously shaking every 5 min for 10 s. After 20 – 30 min first crypts were visible in the supernatant under the microscope and digestion was terminated by adding 10 mL DMEM complete. To further release crypts, tissue fragments were vigorously pipetted ten times and 10 mL supernatant was filtered through a 100 µM cell strainer into a 50 mL tube. Another 10 mL DMEM complete was added to the tissue pieces and three more fractions of crypts were collected by vigorously pipetting followed by filtering into the 50 mL tube. Crypt suspension was centrifuged at 300 g for 5 min and resuspended in 5 mL DMEM complete. Single cells were removed by centrifuging at 60 g for 3 min. The crypt pellet was resuspended in advanced DMEM and crypts were counted microscopically. Matrigel was added and ~200 crypts were plated in 40 µL advanced DMEM:Matrigel (1:2, v/v) onto a 24-well plate. After 15 min at 37°C and 5 % CO_2 the matrigel dome containing crypts was polymerized and 500 µL/well IntestiCult organoid growth medium (OGM) supplemented with 100 U/mL penicillin and 100 µg/mL streptomycin was added. Medium was changed every 2 – 3 days and formed organoids were passaged once a week in a 1:2 ratio.

For passage, organoids and matrigel dome were collected and washed in ice-cold PBS. Organoid suspension was centrifuged at 300 g for 5 min and the organoid pellet was resuspended in advanced DMEM. Organoids were mechanically disrupted by pipetting 20 times and organoid fragments were pelleted and plated as described above.

For RNA isolation, organoids were collected with the matrigel dome and matrigel was removed by washing in ice-cold PBS. Organoids were pelleted at 300 g for 5 min and lysed in RA1 buffer. RNA isolation is described in chapter 4.4.2.2.

To assess organoid morphology, organoids were classified in four categories: Intact organoids, forming crypt-like domains (intact & budding), intact, circular shaped organoids (intact w/o budding), partially intact organoids (partially intact) and completely disintegrated organoid structures (destroyed). For each mouse, organoid morphology was counted in triplicates with 80 – 230 organoids per replicate. Photos were taken with a 20x objective on a Leica DMIL LED microscope with Leica DFC450 C camera using LAS software.

4.3.2 Peritoneal lavage

Peritoneal lavage was performed to subsequently isolate peritoneal macrophages and assess Ac depletion. The fur of the mice was cut open, exposing the intact peritoneum. Next, 5 mL RPMI medium were injected with some air into the peritoneal cavity and mice were cautiously shaken to liberate cells into the medium. Next, the peritoneum was opened with a 3 mm cut and medium was collected with a pipette. Cells were pelleted at 450 g for

5 min at 4°C and resuspended in FACS buffer. Subsequent macrophage isolation is described in chapter 4.3.6.

4.3.3 Single cell suspension of spleen and mesenteric lymph nodes

To obtain single cells, spleens were rinsed with ACK buffer to lyse erythrocytes and release splenocytes. Spleens were further disrupted with a stamp through a 100 µm cell strainer to increase splenocyte yield. Next, ACK buffer was diluted with FACS buffer and the cell suspension was collected in a 15 mL tube. The splenocyte pellet was obtained by centrifuging at 300 g for 10 min. The cell pellet was suspended in appropriate amount of FACS buffer or IMDM complete and samples were kept on ice until further processing.
Mesenteric lymph nodes (mLN) were disrupted in FACS buffer using a stamp and passing single cells through a 100 µm cell strainer. Cells were collected, pelleted, resuspended and stored as described for the splenocytes above.

4.3.4 Colonic lamina propria lymphocyte isolation

Cleaned colons (chapter 4.2.4) were used for lamina propria lymphocyte (LPL) isolation. Colons were cut open longitudinally and sliced in 1 cm pieces. Tissue pieces were washed two times with 40 mL PBS/EDTA solution under constant agitation for 10 min at 37°C and 5 % CO_2 and detached epithelial cells were decanted. EDTA and further epithelial cells were removed by stirring the tissue pieces two times for 15 min in 20 mL RPMI medium containing FCS, EGTA and $MgCl_2$ at 37°C and 5 % CO_2. Additionally, tissue sections were vigorously mixed for 15 s in another 10 mL RPMI/FCS/EGTA/ $MgCl_2$. EGTA was cleared with PBS and tissue pieces were homogenized. The homogenized tissue was digested in 30 mL RPMI containing 20 % FCS and 100 U/mL collagenase IV for two times 30 min at 37°C and 5 % CO_2. After every half hour, the tissue was disintegrated further by pulling it up and down ten times with a syringe. Tissue was eliminated by filtering through a 40 µm cell strainer. The obtained cell suspension was centrifuged at 300 g for 10 min, followed by 450 g for 5 min and the cell pellet was resuspended in IMDM complete. Tissue remnants were removed by filtering the cell suspension through 30 µm cell strainer.

4.3.5 Flow cytometric analysis

The T cell phenotype was analyzed by flow cytometry using the antibodies listed in Tab. 9. Samples were measured on the flow cytometer BD LSR II and analyzed using the BD FACSDiva Software.

4.3.5.1 Staining of surface markers

For staining of cell surface proteins 100 µL cell suspension was transferred to a 96-well round bottom plate. Cells were centrifuged at 300 g for 5 min and washed with PBS. Cells

were stained with antibodies and fixable viability dye (FvD) in PBS for 10 min at 4°C in the dark. Staining was stopped by adding PBS. Residual antibodies were removed by centrifuging the cells at 300 g for 5 min and discarding the supernatant. Next, the cells were subjected to intracellular staining.

4.3.5.2 Staining of intracellular markers

For analysis of IFNy and IL-17A, cells were incubated for 4 h at 37°C and 5 % CO_2 in IMDM complete with 10 ng/mL phorbol 12-myristate 13-acetate (PMA) and 1 µg/mL ionomycin, stimulating cytokine production, and 5 µg/mL of brefeldin A (BFA), inhibiting cytokine secretion, before surface staining. After surface staining cells were fixed in 2 % PFA solution for 15 min at 4°C in the dark. Cells were washed by adding FACS buffer and supernatant was removed after centrifuging at 300 g for 5 min at 4°C. For permeabilization, cells were incubated in 0,1 % IGEPAL for 4 min at room temperature. Permeabilization was stopped by adding FACS buffer and centrifuging at 300 g for 5 min at 4°C. Supernatant was discarded and cells were stained with antibodies diluted in FACS buffer for 30 min at 4°C in the dark. Cells were washed by adding FACS buffer and centrifuging at 300 g for 5 min at 4°C. Supernatant was removed and the cell pellet was resuspended in FACS buffer and transferred into FACS tubes for flow cytometric analysis.

For staining of granzyme B (GrzB) and the nuclear transcription factors FoxP3 and T-bet the FoxP3/Transcription Factor Staining Buffer Set was used following the manufacturer's instructions. In brief, cells were fixed using fixation/ permeabilization solution for 1 h – 18 h at 4°C in the dark. Cells were washed with 1x permeabilization buffer, centrifuged at 300 g for 5 min at 4°C and supernatant was discarded. For intracellular and intranuclear staining cells were stained with antibodies diluted in 1x permeabilization buffer for 30 min at 4°C in the dark. Cells were washed with 1x permeabilization buffer and pelleted at 300 g for 5 min at 4°C. The supernatant was removed and cells were resuspended in FACS buffer. The cell suspension was pipetted into FACS tubes and subjected to flow cytometric analysis.

4.3.6 Magnetic-activated cell sorting

Naïve $CD4^+$ T cells from the spleen were enriched by magnetic-activated cell sorting (MACS) using the negative selection $CD4^+$ T cell Isolation Kit according to manufacturer's instructions. In brief, splenocytes were incubated with the provided antibody cocktail containing biotin-conjugated antibodies binding CD8a, CD11b, CD19, CD45R, CD49b, CD105, MHC class II, Ter-119 and TCRγ/δ. Additionally, biotin-conjugated CD25 antibody (Tab. 9) was added, to deplete activated $CD25^+$ T cells. Cells and antibodies were mixed and incubated for 5 min at 4°C. FACS buffer and anti-biotin MicroBeads were added, mixed and incubated for 10 min at 4°C. Afterwards, samples were sorted using AutoMACS Pro.

MicroBead-bound non-target cells were retained (positive fraction) and naïve $CD4^+$ $CD25^-$ T cells were in the negative fraction. Non-targeted cells bound by the MicroBeads were retained in the column surrounded by a magnetic field, while the unbound $CD4^+$ $CD25^-$ T cells passed through. Enriched T cells were subjected to fluorescence-activated cell sorting (chapter 4.3.6) to obtain highly pure T cells for the differentiation assays.

Macrophages from the peritoneal lavage were purified using the positive selection Anti-F4/80 MicroBeads UltraPure Kit following the manufacturer's protocol. In brief, $F4/80^+$ macrophages were labelled with anti-F4/80 MicroBeads for 15 min at 4°C. To remove excessive MicroBeads the cell suspension was washed with FACS buffer, centrifuged for 10 min at 300 g and 4°C and the supernatant was discarded. Cells were resuspended in FACS buffer and magnetically sorted. MicroBeads labelled peritoneal $F4/80^+$ macrophages were retained in the column and afterwards eluted in the positive fraction. Cells were centrifuged and the pellet was lysed in RLT buffer for RNA isolation (chapter 4.4.2.1)

4.3.7 Fluorescence-activated cell sorting

Fluorescence-activated cell sorting on BD FACS Aria II cell sorter was applied for isolation of immune cells populations from LPLs for subsequent PCR analysis and for further purification of magnetic-activated sorted $CD4^+$ T cells for T cell differentiation assays.

Cells were suspended in FACS buffer and appropriate antibodies were added. Sorted $CD4^+$ or $CD8^+$ T cells, $CD45^+$ $Ly\text{-}6G^+$ granulocytes, $CD45^+$ $F4/80^+$ macrophages and $CD45^+$ $F4/80^-$ $CD11c^+$ dendritic cells (DCs) were lysed in RA1 lysis buffer for RNA isolation (chapter 4.4.2.2) and subsequent PCR or RNA sequencing analysis. $CD4^+$ $CD25^-$ T cells were sorted from MACS-enriched $CD4^+$ $CD25^-$ T cells in FACS buffer for T cell differentiation assays (chapter 4.3.9).

4.3.8 Cell counting

Cells of single cell suspensions of spleen and lymph nodes, as well as sorted $CD4^+$ $CD25^-$ T cells were counted using the cell count feature for viable cells of Fluidlab R-300 with acella 50 slides. Resulting cell counts were given in cells/mL.

Absolute cell numbers of LPL suspensions were determined by diluting the sample 1:5 or 1:10 in trypan blue 0.4% solution, which stains dead cells, and counting unstained living cells in two quadrants of a Neubauer counting chamber ($0.0025 mm^2$). Total cell counts were calculated using the following Formula 3.

$$\text{cell count} = \text{mean (counted cells)} \times \text{dilution factor} \times \text{volume [mL]} \times 10^4$$

Formula 3: Cell count calculation using a Neubauer chamber

4.3.9 T cell differentiation assays

Naïve $CD4^+$ $CD25^-$ T cells purified via MACS and FACS were differentiated into T_h1 and T_h17 cells using appropriate antibodies (Tab. 11) and cytokines (Tab. 12) as described in the following chapters.

4.3.9.1 T_h1 differentiation

For T_h1 differentiation a 24-well plate was coated with 1 µg/mL anti-CD3ε antibody in PBS for 1 – 2 h at 37°C and 5 % CO_2. Excessive antibody was removed by washing with PBS. 5 x 10^5 $CD4^+$ $CD25^-$ naïve T cells were seeded in 2 mL IMDM complete supplemented with 1 µg/mL anti-CD28 antibody as control (T_h0) and additional 200 ng/mL anti-IL-4 and 20 ng/mL IL-12 for T_h1 differentiation. Medium was changed after 3 days with adding of IL-12 and anti-IL-4, but not anti-CD28. Cells were harvested after 5 days and subjected to flow cytometric analysis.

4.3.9.2 T_h17 differentiation

T_h17 differentiation was performed in a 48-well plate coated with anti-CD3ε as described above (chapter 4.3.9.1). 5 x 10^5 $CD4^+$ $CD25^-$ naïve T cells were cultured in 1 mL IMDM complete containing 1 µg/mL anti-CD28 antibody as control (T_h0) and additional cytokines and antibodies as listed in Tab. 16 for T_h17 differentiation.

Tab. 16: Cytokines and antibodies for T_h17 differentiation

Cytokine	Concentration	Antibody	Concentration
TGFβ	2 ng/mL	anit IL-4	200 ng/mL
IL-6	50 ng/mL	anti IFNγ	200 ng/mL
IL-1β1	20 ng/mL	anti IL-2	200 ng/mL
IL-21	100 ng/mL		
IL-23	20 ng/mL		

After 3 days cells were splitted 1:2 on uncoated plates and T_h17 conditioning medium without anti-CD28, and IMDM complete, for the T_h0 condition, was added. Cells were harvested after 5 days and analyzed via flow cytometry.

4.3.10 Sphingolipid quantification

The determination of ceramide content was kindly performed by Dr. Fabian Schumacher (University of Berlin, Germany). Lipids were extracted with 1.5 ml methanol:chloroform (2:1, v/v) from homogenized colon tissue, using C17-ceramide (C17-Cer) as internal standard, as previously described [162]. Samples were separated on the 1290 Infinity II High Performance Liquid Chromatography (HPLC) system on a Poroshell 120 EC-C8 column (both Agilent Technologies). Subsequently, samples were ionized by positive electrospray ionization (ESI), and ceramides were fragmented into *m/z* 264.3 productions by mass

spectrometry (MS)/MS on a Q-TOF 6530 mass spectrometer, as previously described [83, 163]. The precursor ions of the different ceramide species were as follows: C16-Cer *m/z* 520.5, C17-Cer *m/z* 534.5, C18-Cer *m/z* 548.5, C20-Cer *m/z* 576.6, C22-Cer *m/z* 604.6, C24-Cer *m/z* 632.6, and C24:1-Cer *m/z* 630.6.

For quantification, external calibration was performed from 1 fmol to 50 pmol, and the areas under the peaks of each ceramide were determined, followed by normalization to the internal standard C17-Cer. MassHunter software was used for the analyses. Ceramide amounts of all ceramide species were summed and normalized to the protein content of the colonic homogenate, quantified by Bradford assay.

4.4 Molecular biological procedures

4.4.1 Genotyping

Tail biopsies were collected from mice at least 4 weeks of age. Sample digestion was performed using rapid tail buffer with 10 mg/mL proteinase K constantly shaking for 3 h or overnight at 56°C. Proteinase K was inactivated by heating the samples to 95°C for 10 min. Samples were centrifuged at 10,000 g for 10 min. The supernatant with genomic DNA was collected and diluted 1:50 in water. Next, polymerase chain reaction (PCR) was performed with 1 µL diluted genomic DNA and 19 µL master mix (Tab. 17) containing specific primers (Tab. 4) under the conditions described in (Tab. 18). PCR products were analyzed using gel electrophoresis (chapter 4.4.5).

Tab. 17: PCR master mix for genotyping

Components	Dilution or Concentration
Green GoTaq Flexi Buffer	1:5
Magnesium chloride	1.5 mM
dNTPs	1 mM
Forward primer	5 µM
Reverse primer	5 µM
GoTaq Hot Start Polymerase	0,5 U
Water	64,7 % v/v (Fill up to 19 µL)

Tab. 18: PCR conditions for genotyping (AT = annealing temperature)

Repetitions		10 cycles			27 cycles			
Temperature	95°C	95°C	AT	72°C	95°C	AT	72°C	4°C
Time	10 min	30 s	90 s	90 s	15 s	45 s	45 s	∞

4.4.2 RNA isolation

4.4.2.1 RNeasy kits

For RNA isolation from colonic tissue the RNeasy Fibrous Tissue kit and for isolation from MACS enriched peritoneal macrophages, the RNeasy Mini Kit was used according to the manufacturer's protocols. In brief, lysed tissue was digested and proteins removed with Proteinase K. Digested tissue samples were centrifuged and supernatant without debris was mixed with ethanol. Lysed cellular samples were mixed with 70% (v/v) ethanol. These mixtures were transferred onto silica membrane columns where RNA was bound. Bound DNA was removed by digestion with 27 Kunitz units DNAse per sample. After several washing steps, RNA was eluted with RNase-free water and RNA concentration and purity was determined with a NanoDrop spectrophotometer and ND-1000 software. RNA samples were stored at -80°C until further analysis.

4.4.2.2 Nucleo spin XS kit

RNA isolation from small samples, organoids and immune cells sorted from LPLs was performed using the NucleoSpin RNA XS kit according to manufacturer's instructions. In brief, a reducing agent was added to the lysed samples to limit RNase activity. Next, carrier RNA was added to enhance RNA yield. Carrier RNA addition was omitted when samples would be sequenced afterwards. Samples were mixed with 70% (v/v) and loaded on a silica membrane column. RNA bound to the membrane and bound DNA was removed by DNase digestion. Samples were washed several times and RNA was eluted in RNase-free water. RNA samples were stored at -80°C until further analysis.

4.4.3 Complementary DNA synthesis

For subsequent PCR analysis, 0.1 – 1 µg isolated RNA was reverse transcribed into complementary DNA (cDNA). RNA in 13 µL was incubated with 0.5 µL OligodT Primer (0.5 µg/ µL) and 0.5 µL Random Primer (3 µg/µL) (both Invitrogen) using a Thermocycler at 70°C for 10 min for primer annealing. The master mix for cDNA synthesis was prepared as listed in Tab. 19 and 6 µL/sample were added.

Tab. 19: Master mix for cDNA synthesis

Components	Volume
MML V-RT 5x buffer	4 µL
M-MLV Reverse Transcriptase (H-) Point Mutant	1 µL
dNTPs	1 µL

Reverse transcription reaction was performed using a Thermocycler. Samples were incubated at 42°C for 1 h, followed by 95°C for 5 min. In case 1 µg RNA was reverse

transcribed resulting cDNA samples were diluted in TE buffer. Afterwards cDNA sample were subjected to PCR analysis (chapters 4.4.4 and 4.4.6).

4.4.4 Semi-quantitative PCR

Semi-quantitative PCR was applied to verify cDNA synthesis by amplification of the housekeeping gene *ribosomal protein 9* (*Rps9*) and to detect absence or presence of *Asah1* gene in colonic samples of Ac^{flox} Vilcre mice. For PCR 1 µL cDNA sample and 19 µL PCR master mix (Tab. 17) were used. Specific primers for *Rps9* and *Asah1* are listed in Tab. 5 and the PCR conditions are listed in Tab. 20. PCR products were analyzed using gel electrophoresis (chapter 4.4.5).

Tab. 20: Semi-quantitative PCR program

Repetitions		30 cycles				
Temperature	94°C	94°C	AT	72°C	72°C	4°C
Time	10 min	45 s	45 s	60 s	10 min	∞

4.4.5 Gel electrophoresis

PCR products and 5 µL Gene Ruler 100 bp Plus DNA ladder were loaded on a 1 % agarose gel in TBE buffer containing 5 µL DNA stain Midori Green per 100 mL gel. Gel electrophoresis was performed with 150 V constant for 25 min in a electrophoresis apparatus Horizon 11.14 using PowerPac universal power supply. DNA bands were visualized with the UV-light based gel documentation system QUANTUM CX5 Edge and BioVision software.

4.4.6 Real-time quantitative PCR

For quantification of gene expression cDNA was amplified with target gene and *Rps9* primers with Maxima SYBR Green/ROX qPCR Master Mix 2x using a 7500 Fast Real-Time PCR System following the manufacturer's protocols. The real-time quantitative PCR (RT-qPCR) reaction mixture is described in Tab. 21.

Tab. 21: Reaction mix for RT-qPCR

Components	**Concentration or Dilution**
Template	5 - 250 ng/µL
Maxima SYBR Green/ROX qPCR Master Mix 2x	1:2
Forward Primer (in water) *Rps9* *Asah1, Lgr5, Occludin*	 900 nM 300 nM
Reverse Primer (in water) *Rps9* *Asah1, Lgr5* *Occludin*	 50 nM 300 nM 900 nM
Water	4 µL in 20 µL reaction volume 3 µL for small samples

The quantity of a gene was calculated using a standard curve. Relative expression of target genes was determined using Formula 4.

$$\text{Relative expression} = \frac{\text{mean (quantity of target gene)}}{\text{mean (quantity of Rps9)}}$$

Formula 4: Calculation of relative gene expression.

4.4.7 Cytokine detection by Luminex technology

Secreted cytokines by colonic tissue were quantified using a Luminex Discovery Assay Mouse premixed Multi-Analyte Kit following manufacturer's instructions.
In brief, color-coded magnetic microspheres coupled with cytokine specific antibodies were used. These antibodies captured TNFα, IL-1β, IFNγ or IL-17 in the colon supernatant samples, giving each cytokine a unique color. In the next step biotin conjugated antibodies were added, which bound to cytokines previously captured by the microsphere. Streptavidin phycoerythrin (PE) labelled reporters were added, binding the biotin-antibodies. Samples were analyzed with Luminex xPONENT software on a Luminex MAGPIX Analyzer, which measurers the signals by keeping the microspheres in a monolayer with a magnetic field. One LED detects the code color, identifying the cytokine. A second LED measures the intensity of the PE signal, which is proportional to cytokine quantity.

4.4.8 RNA sequencing

Messenger RNA (mRNA) libraries were prepared from RNA extracted from sorted colonic $CD4^+$ T cells with QuantSeq 3' mRNA-Seq Library Prep Kit FWD synthesizing libraries only from the 3' end of the polyadenylated mRNA. Libraries were sequenced using NextSeq High Output (75 cycles) Kit and NextSeq 500 sequencer. The Genomics and Transcriptomics Facility (Essen University Hospital, Germany) performed library preparation and sequencing according to manufacturer's instructions.
Processing and analysis of the sequencing data was kindly performed by Dr. Bettina Budeus (Genomics and Transcriptomics Facility, Essen University Hospital, Germany). Data quality control was performed with FastQC and adapter trimming with TrimGalore. HISAT2 was used for read alignment to the GRCm38 *Mus musculus* genome. Read counting of mapped genes was conducted with the R/Bioconductor software package GenomicAlignments using the summarizeOverlaps feature.
Differential gene expression analysis was performed using the R/Bioconductor software package DESeq2. Genes with an adjusted p value less than 0.05 were defined as differentially expressed. Differentially expressed genes (DEGs) with a negative log2 fold

change (FC) greater 2 or less than -2 were considered as upregulated or downregulated, respectively. The volcano plot was generated using GraphPad Prism software.

4.5 Statistics

D'Agostino-Pearson and Shapiro-Wilk tests were applied to assess whether the data follow a normal distribution. F-test was used to compare variances between experimental groups. Statistical significance was assessed using Student's t-test for normally distributed data, Student's t-test with Welch's correction in case of significantly different variances and Mann-Whitney test for not normally distributed data. Statistical significance was shown as *$p < 0.05$, **$p < 0.01$, ***$p < 0.001$ and ****$p < 0.0001$. Except for RNA sequencing data, all data were analyzed with GraphPad Prism software. Statistics and analysis of RNA sequencing data are described in the previous chapter 4.4.8.

5 Results

5.1 Role of acid ceramidase in bacterial colitis

Several sphingolipid metabolizing enzymes have been studied in intestinal diseases such as IBD and colon cancer [164]. However, studies on intestinal infections and on the role of the ceramide-converting enzyme acid ceramidase (Ac) are lacking. Therefore, the role of Ac was investigated in intestinal infection with the natural mouse enteropathogen *Citrobacter (C.) rodentium* [165]. Similar to humans, the global knockout of Ac is lethal in early embryonic stage in mice [112, 166]. Therefore, mouse models with an inducible and cell type-specific deletion of Ac were used. Further, with cell type-specific knockouts, the role of Ac in different cell types can be distinguished, allowing its role in complex host defense to be clearly defined.

5.1.1 Acid ceramidase is essential to control bacterial colitis and is expressed in various cell types involved in host defense

As described above, the inducible Ac knockout model was used to assess the role of Ac in response to *C. rodentium* infection. For knockout induction, adult *Asah1*$^{flox/flox}$ x creER^{ki} (Ac^{flox} creER KO) and *Asah1*$^{flox/flox}$ x creER^{wt} (Ac^{flox} creER WT) mice received intraperitoneal (i.p.) injections of tamoxifen 8, 6 and 4 days before analysis or infection on day 0. Tamoxifen leads to activation of the cre recombinase estrogen receptor fusion protein (creER), which would result in excision of the *loxP*-flanked exon 1 in the *Asah1* gene in Ac^{flox} creER KO mice. To evaluate knockout induction, Ac^{flox} creER WT and KO mice were treated with tamoxifen and *Asah1* mRNA levels were analyzed in blood cells and colon tissue biopsies via RT-qPCR on day 0 (Fig. 7A). In fact, *Asah1* was expressed in blood and colonic tissue of Ac^{flox} creER WT mice, and expression was erased in Ac^{flox} creER KO mice (Fig. 7A). Of note, *Asah1* expression was 2-fold higher in colon tissue compared with blood (Fig. 7A). Next, ceramide (Cer) content on day 0 was determined using mass spectrometry to assess activity of the Cer converting enzyme Ac after *Asah1* exon 1 deletion (Fig. 7B). In line with the deletion of *Asah1* expression, Cer accumulated in colonic tissue of Ac^{flox} creER KO compared to WT mice, indicating reduced activity of Ac (Fig. 7B). Deletion of *Asah1* expression in spleen, liver and thymus and ceramide accumulation in the spleen of Ac^{flox} creER KO mice of the same breeding has been previously shown by others at this institute [167]. To investigate the impact of Ac deficiency in intestinal infection, Ac^{flox} creER WT and KO mice were infected with the natural murine enteropathogen *C. rodentium*, which induces colitis. Infection with *C. rodentium* is typically evident in the feces 3 days post infection (dpi) and reaches a peak spanning several days between 7 and 12 dpi [71-74]. Noteworthy, the experiments had to be terminated already 6 dpi due to the severe disease with high body

weight loss in Ac^{flox} creER KO mice during *C. rodentium* infection, as shown in previous work of this institute [168].

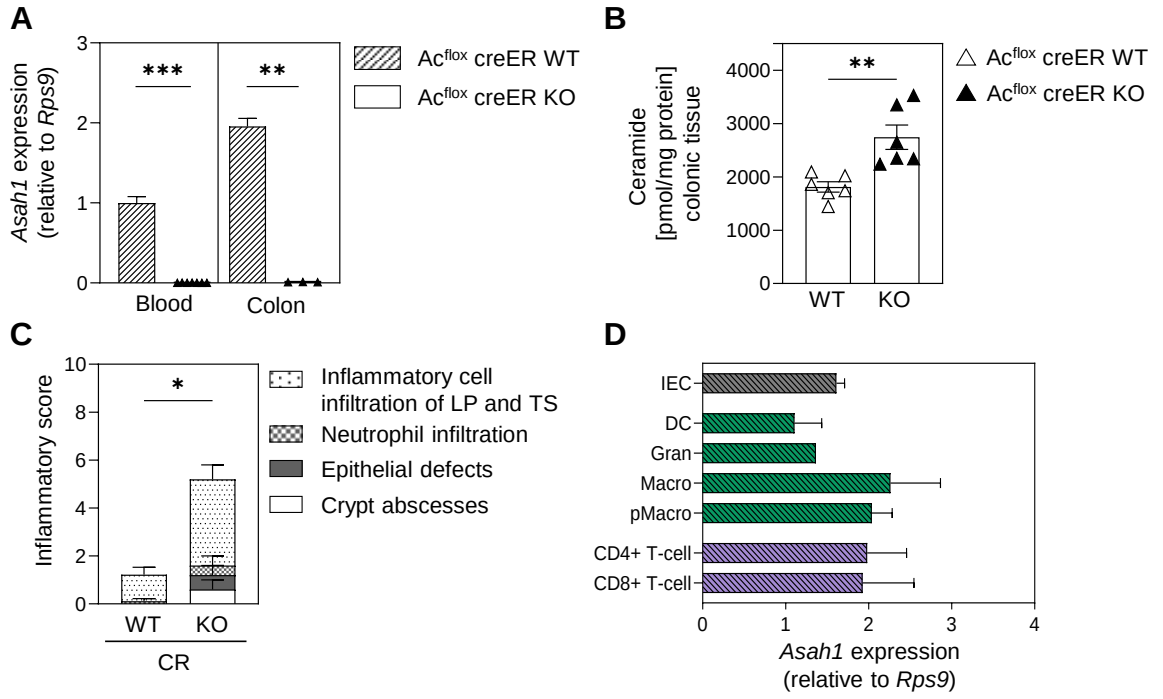

Fig. 7: Evaluation of Ac^{flox} creER mice and *Asah1* expression in cells involved in host defense.
(A-C) *Asah1*$^{flox/flox}$ x creER^{wt} and x creER^{ki} mice received 4 mg tamoxifen in 100 µL corn oil i.p. 8, 6 and 4 days before analysis or infection on day 0. These Ac^{flox} creER WT and KO mice were analyzed on day 0 for (**A**) *Asah1* mRNA levels relative to *Rps9* expression in blood and colon tissue determined via RT-qPCR (n = 3-7) and (**B**) ceramide levels in colon tissue via HPLC-MS/MS (n = 6). **(C**) Histopathological score from H&E stained colon sections of Ac^{flox} creER WT and KO mice, 6 days post infection (dpi) with ~2 x 10^9 CFU *C. rodentium* (n = 5-9). Lamina propria (LP), tela submucosa (TS). (**B, C**) Experiments were performed by Dr. Jana Meiners (University of Duisburg-Essen) and reanalyzed by Jana-Fabienne Ebel. (**D**) RT-qPCR analysis of *Asah1* mRNA levels in relation to *Rps9* expression in distinct cell populations of Ac^{flox} mice WT for cre recombinase. Intestinal epithelial cells (IEC) were harvested from colonic organoids (n = 7). Dendritic cells (DC, n = 4), granulocytes (Gran, n = 1), macrophages (Macro, n = 4), CD4$^+$ (n = 3) and CD8$^+$ T cells (n = 3) were FACS-sorted from the colonic lamina propria. Peritoneal macrophages (pMacro) were MACS-sorted from peritoneal lavage fluid (n = 9). Data are presented as mean ± SEM. Statistical analyses were performed using Mann-Whitney test (A), Student's t-test with Welch's correction (A, C) and Student's t-test (B) (*p < 0.05, **p < 0.01, ***p < 0.001).

Colons of *C. rodentium* infected (in figures abbreviated as CR) Ac^{flox} creER WT and KO mice were histologically examined for inflammation (Fig. 7C). Ac^{flox} creER KO mice developed a more severe colitis compared to WT mice as indicated by the significantly elevated inflammatory score (Fig. 7C). In detail, Ac^{flox} creER KO mice exhibited a massive inflammatory cell influx into the lamina propria (LP) and tela submucosa (TS) with concomitant with stronger epithelial defects, neutrophil infiltration and crypt abscesses (Fig. 7C).

Next, *Asah1* expression in the cellular components involved in the aforementioned histopathologies and in the host defense was assessed. As essential part of the intestinal barrier and first line of defense against invading pathogens, this includes intestinal epithelial cells (IEC), followed by cells of the early innate immune response such as macrophages, granulocytes and dendritic cells (DC), and T cells as part of the adaptive immune response. *Asah1* expression in colonic IECs, DCs, granulocytes, macrophages and T cells as well as

peritoneal macrophages was determined via RT-qPCR (Fig. 7D). *Asah1* was readily expressed in all cell types, although to a lesser extent in DCs and granulocytes (Fig. 7D).

Collectively, the severe *C. rodentium* induced colitis in absence of Ac suggests that the enzyme is important in the host defence to this pathogen. Interestingly, *Asah1* is highly expressed in the colon and on a cellular level expressed in various cell types of the host (immune) response. Therefore, the influence of Ac in *C. rodentium* induced colitis was studied in more detail by specifically investigating the effect of Ac deletion on the distinct cellular mediators.

5.1.2 Effect of acid ceramidase deficiency on intestinal epithelial cells under homeostasis and during *C. rodentium* induced colitis

To investigate the role of Ac in intestinal epithelial cells, colonic organoids as an *ex vivo* model of the gut epithelium were used. Organoids closely resemble the *in vivo* epithelium in structure, cell composition and barrier function [169, 170].

Epithelial crypts containing stem cells from colons of Ac^{flox} creER WT and KO mice were isolated and cultured to obtain organoids. *Asah1* mRNA expression was assessed by RT-qPCR analysis of differentiated colonic organoids derived from Ac^{flox} creER WT and KO mice (Fig. 8A). Ac^{flox} creER KO derived organoids showed a permanent depletion of *Asah1* (Fig. 8A).

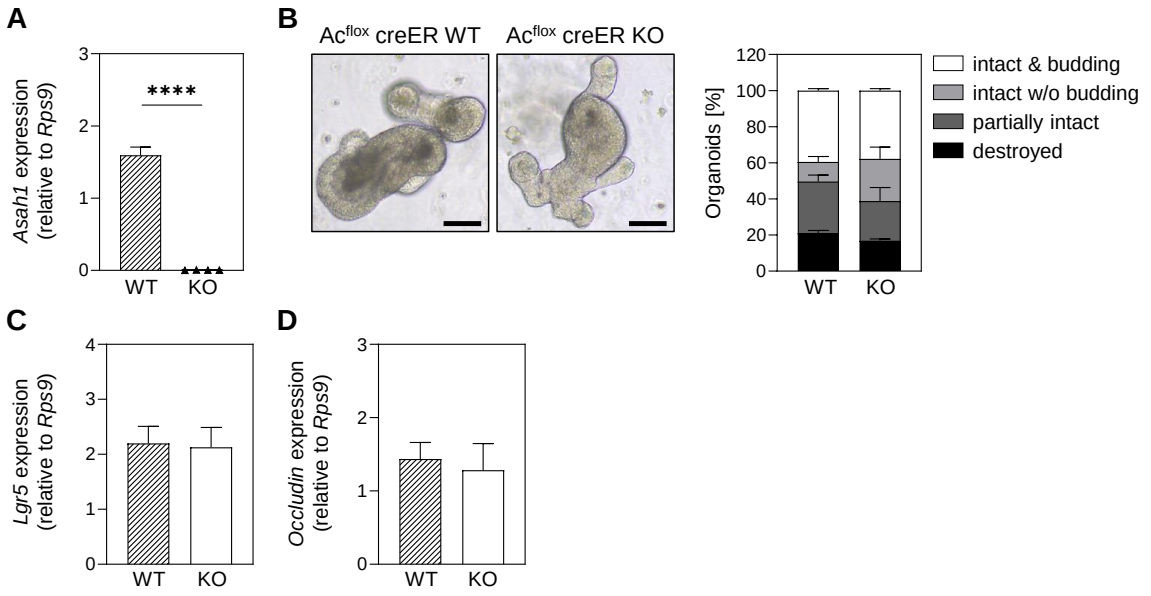

Fig. 8: Characterization of Ac deficient colonic epithelial organoids.
Ac knockout was induced in Ac^{flox} creER KO*Asah1*$^{flox/flox}$ x $creER^{ki}$ and x $creER^{wt}$ mice by three i.p. injections of 4 mg tamoxifen in 100 µL corn oil every other day. As control Ac^{flox} creER WT mice received tamoxifen in the same manner. Colonic crypts were isolated 11 days after the last injection and organoids were analyzed after 1-2 weeks of differentiation. (**A**) mRNA levels of *Asah1* were determined by RT-qPCR in relation to *Rps9* expression in colonic organoids to confirm *Asah1* deletion in Ac^{flox} creER KO organoids (n = 4-6). (**B**) Morphology of Ac^{flox} creER WT and KO organoids was analyzed (n = 3-4). (**C, D**) mRNA levels of stem cell marker *Lgr5* (**C**) and tight junction marker *Occludin* (**D**) in relation to *Rps9* expression were determined by RT-qPCR in colonic organoids (n = 4-6). Data are presented as mean ± SEM. Statistical analyses were performed using Student's t-test with Welch's correction (****p < 0.0001).

Next, organoid morphology, an indicator of epithelial growth and viability, was analyzed in absence and presence of Ac (Fig. 8B). Both WT and *Asah1* deprived colonic crypts showed the same ability to form differentiated organoids with crypt-like structures (intact & budding, Fig. 8B). The distribution of intact and partially or completely disintegrated organoids was also similar in the *Asah1* depleted organoids compared to WT (Fig. 8B). Further, epithelial stemness and tightness were determined in Ac WT and KO organoids using RT-qPCR (Fig. 8C, D). Epithelial stem cells and tight junctions were not affected by the knockout of Ac, as indicated by similar expression of the stem cell marker *Lgr5* and tight junction marker *Occludin* (Fig. 8C, D). These results indicate that deficiency of Ac does not alter the function of intestinal epithelial cells under homeostasis. However, it is unclear whether Ac is required in IECs in response to the enteropathogen *C. rodentium in vivo*. For this purpose, the Ac^{flox} Vilcre mouse model was applied, in which the cre recombinase is expressed under the Villin promoter and *Asah1* is specifically excised in the epithelial cells in *Asah1*$^{flox/flox}$ x Villin cre^{tg} mice (Ac^{flox} Vilcre KO).

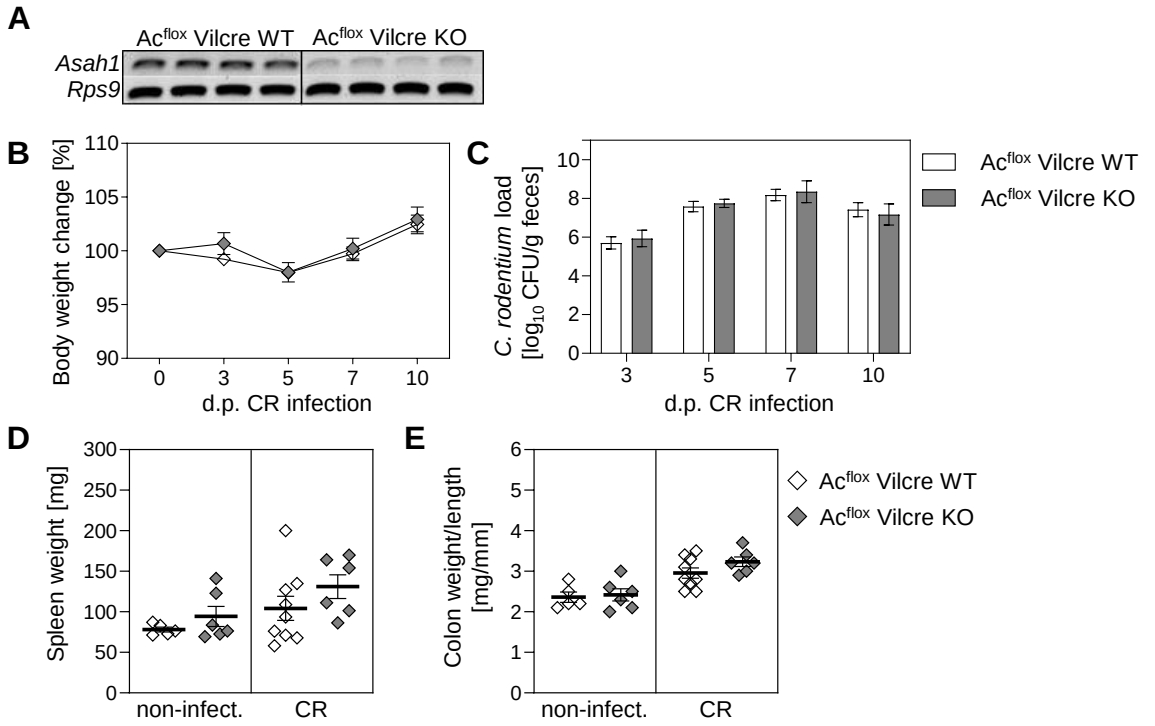

Fig. 9: Epithelial-specific deletion of Ac does not alter the course of *C. rodentium* induced colitis.
(**A-E**) Ac^{flox} Vilcre WT and KO animals were left untreated or orally gavaged with ~2 x 10^9 CFU *C. rodentium* in 100 µL PBS. (**A**) Semiquantitative PCR of colon tissue biopsies of Ac^{flox} Vilcre WT and KO animals. One representative experiment out of three is shown (n = 4). (**B**) Body weight change and (**C**) the load of *C. rodentium* in the feces of Ac^{flox} Vilcre WT and KO mice at indicated time points after infection (d.p. = days post, n = 6-9). (**D**) Spleen weight and (**E**) colon weight/length ratio of Ac^{flox} Vilcre WT and KO mice, non-infected and 10 days post infection (n = 5-9). Data are presented as mean ± SEM.

First, PCR analysis was performed on colonic tissue biopsies of Ac^{flox} Vilcre WT and KO mice to confirm *Asah1* depletion and in fact, *Asah1* expression was erased in the colon of Ac^{flox} Vilcre KO mice (Fig. 9A). Next, Ac^{flox} Vilcre WT and KO littermates were challenged

by infection with ~2 x 10^9 colony forming units (CFU) of *C. rodentium* (Fig. 9B-E). Since disease progression in the Ac^{flox} Vilcre KO mice was not as severe as in global Ac KO animals, the mice were examined during the peak at 10 dpi. *C. rodentium* infection led to a mild body weight loss in both Ac^{flox} Vilcre WT and KO mice, which peaked at 5 dpi (Fig. 9B). The load of *C. rodentium* in the feces peaks at 7 dpi and remains high at 10 dpi in both Ac^{flox} Vilcre WT and KO mice (Fig. 9C). To assess systemic involvement, spleen weight was measured and revealed in tendency larger spleens in infected Ac^{flox} Vilcre KO mice compared to WT (Fig. 9D). This was also observed in uninfected mice, however to a lesser extent. Colon weight/length ratio as indicator of colon pathology was slightly increased in infected Ac^{flox} Vilcre KO mice compared to infected WT mice (Fig. 9E). Colon weight/length ratios were comparable in the non-infected groups. For in detail investigations of the colon pathology, colonic tissue of non-infected and infected Ac^{flox} Vilcre mice were analyzed histologically (Fig. 10).

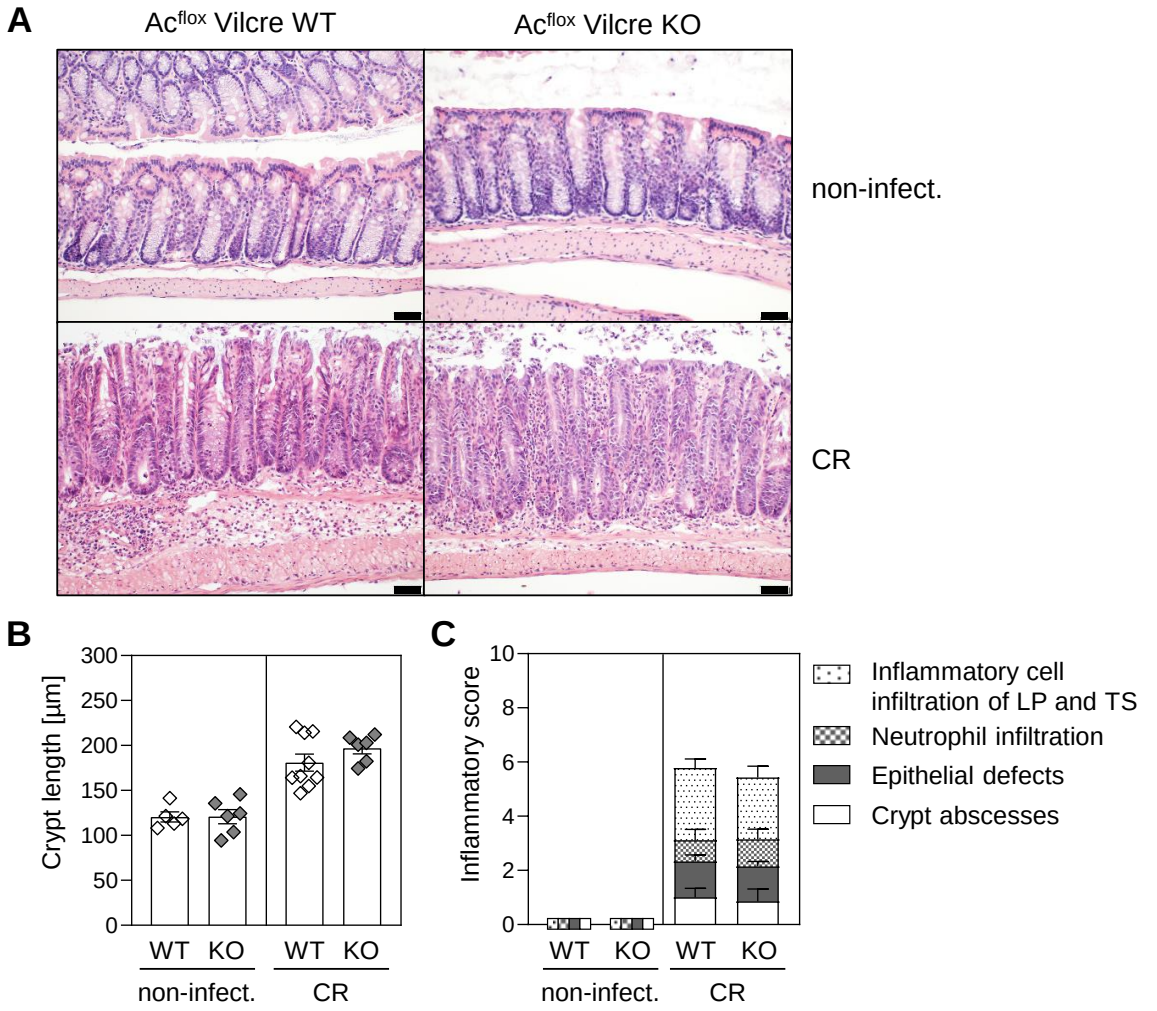

Fig. 10: Impact of Ac deficiency in epithelial cells on bacterial colitis.
(**A-C**) Ac^{flox} Vilcre WT and KO animals were left untreated or orally gavaged with ~2 x 10^9 CFU *C. rodentium* in 100 µL PBS and analyzed 10 days post infection. (**A**) Representative pictures of H&E stained colonic sections (n = 5-9). Scale bar 50 µm (**B**) Crypt hyperplasia determined by mean crypt length (n = 5-9). (**C**) Histopathological score from H&E stained colon sections (n = 5-9). Lamina propria (LP), tela submucosa (TS) Data are presented as mean ± SEM.

In line with the previous observations in colon organoids of Ac^{flox} creER mice, Ac^{flox} Vilcre KO mice did not differ from their WT littermates in crypt length and did not show any pathological alterations in the colon under homeostasis (Fig. 10A-C). In fact, colons of healthy Ac^{flox} Vilcre KO mice revealed an overall intact epithelium (Fig. 10A, C). After infection with *C. rodentium*, crypt abscesses and epithelial defects were induced in KO mice to the same extent as in WT mice, concomitant with similar levels of crypt hyperplasia, the pathological hallmark of *C. rodentium* induced colitis (Fig. 10A-C). Likewise, both infected groups exhibited comparable levels of neutrophil infiltration and infiltration of LP and TS by inflammatory immune cells (Fig. 10A, C).

Taken together, these results indicate that the function of Ac is dispensable for epithelial cell homeostasis and for the epithelial function in response to the intestinal pathogen *C. rodentium*.

5.1.3 Role of acid ceramidase in macrophages and granulocytes during bacterial induced colitis

As neutrophil infiltration and inflammatory immune cell infiltration in LP and TS was clearly enhanced in Ac^{flox} creER KO mice during *C. rodentium* infection, next the impact of Ac deficiency on innate immune cells was investigated. For this purpose, *Asah1*$^{flox/flox}$ mice (Ac^{flox}) were crossed with mice expressing the cre recombinase under lysozyme 2 promoter/enhancer elements (LysMcre), leading to Ac deletion in myeloid cells in transgenic offspring (Ac^{flox} LysMcre KO). Ac^{flox} LysMcre WT and KO mice were analyzed under homeostasis and after *C. rodentium* challenge. Similar to Ac^{flox} Vilcre KO animals, infected Ac^{flox} LysMcre KO mice were not macroscopically found to have extreme deviations from a normal course of infection, which allowed analysis during peak at 10 dpi (Fig. 11).

First, Ac deficiency was determined by RT-qPCR in peritoneal macrophages and colonic granulocytes, macrophages and DCs of Ac^{flox} LysMcre KO mice (Fig. 11A). Indeed, *Asah1* expression in macrophages of the peritoneal cavity and colonic granulocytes was clearly deleted in Ac^{flox} LysMcre KO mice, but not in WT mice (Fig. 11A). Expression of *Asah1* was profoundly reduced in colonic macrophages of Ac^{flox} LysMcre KO mice compared to Ac^{flox} LysMcre WT littermates (Fig. 11A). Colonic DCs were not targeted by *Asah1* deletion (Fig. 11A). As an aside, Ac deficiency of macrophages and neutrophils in the spleen and of neutrophils in the blood has been previously reported by others for the same Ac^{flox} LysMcre breeding at this institute [157, 167].

Next, the phenotype of Ac^{flox} LysMcre WT and KO mice was assessed (Fig. 11B-E). During *C. rodentium* infection the body weight of Ac^{flox} LysMcre WT and KO mice was similar 3 to 7 dpi, with the WT mice gaining slightly more body weight at 10 dpi (Fig. 11B). Both groups exhibited similar *C. rodentium* CFUs in the feces peaking 7 dpi and remaining high 10 dpi

(Fig. 11C). Systemically, spleens of non-infected Ac^{flox} LysMcre KO mice were of the same size compared to their WT littermates (Fig. 11D). During infection, KO mice showed a minor tendency of larger spleens (Fig. 11D). As first indicator of intestinal inflammation, the colon weight/length ratio was determined. The ratios were on the same level for naïve Ac^{flox} LysMcre WT and KO mice and ratios of both groups were equally elevated upon infection (Fig. 11E).

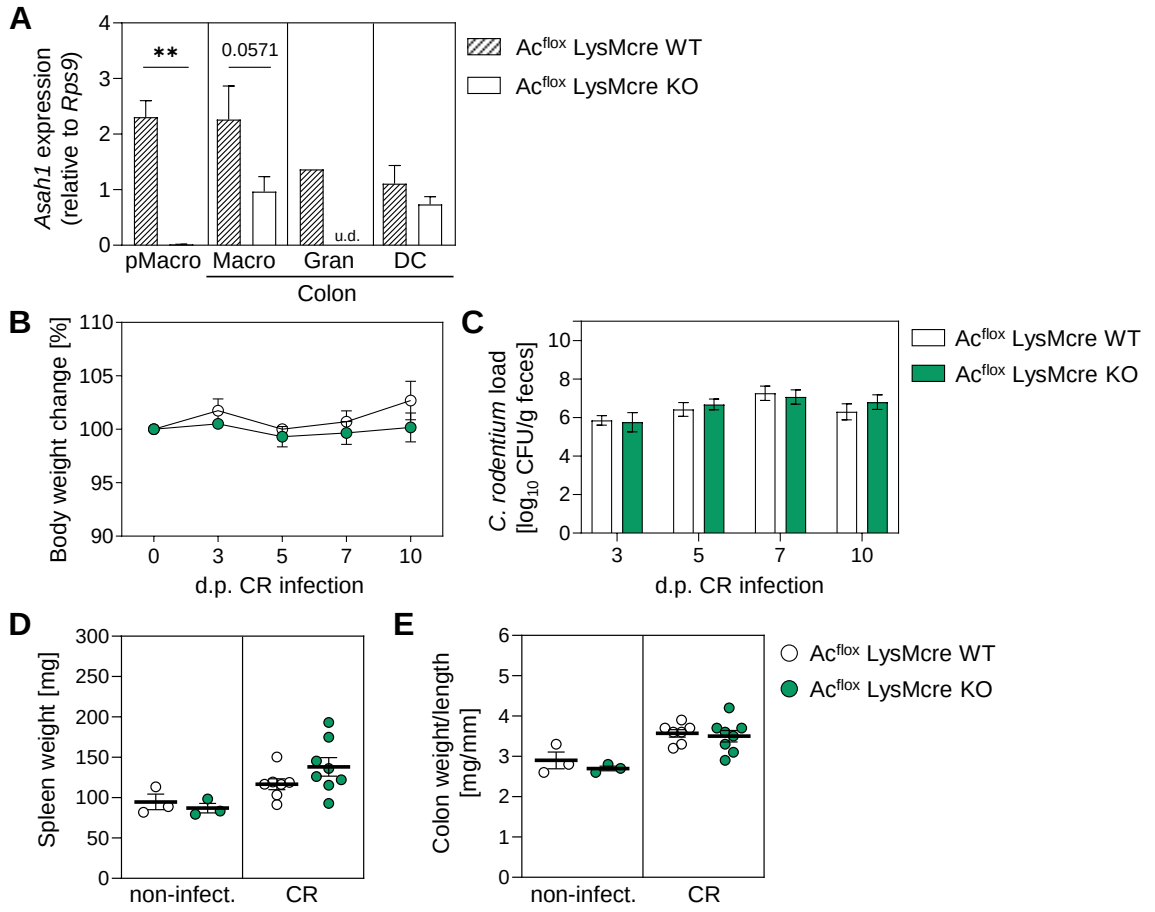

Fig. 11: Acid ceramidase deficiency in macrophages and granulocytes does not alter the course of bacterial colitis.
(**A-E**) Ac^{flox} LysMcre WT and KO animals were left untreated or orally gavaged with ~2 x 10^9 CFU *C. rodentium* in 100 µL PBS. (**A**) RT-qPCR for *Asah1* expression relative to *Rps9* expression of MACS-sorted peritoneal macrophages (pMacro, n = 5) and macrophages (Macro, n = 4), granulocytes (Gran, n = 1-2) and dendritic cells (DC, n = 4) FACS-sorted from colonic lamina propria of Ac^{flox} LysMcre WT and KO mice (u.d. = under detection limit). (**B**) Body weight change and (**C**) the load of *C. rodentium* in the feces of Ac^{flox} LysMcre WT and KO mice at indicated time points after infection (d.p. = days post, n = 7-8). (**D**) Spleen weight and (**E**) colon weight/length ratio of Ac^{flox} LysMcre WT and KO mice, non-infected and 10 days post infection (n = 3-8). Data are presented as mean ± SEM. Statistical analyses were performed using Student's t-test and Student's t-test with Welch's correction (**p < 0.01).

Subsequently, colons of naïve and *C. rodentium* infected Ac^{flox} LysMcre WT and KO mice were histopathologically examined (Fig. 12). Acid ceramidase deficiency in granulocytes and macrophages did not alter the crypt length in naïve mice (Fig. 12A, B). In addition, crypts were equally elongated in Ac^{flox} LysMcre WT and KO mice during *C. rodentium* infection (Fig. 12A, B). Histological scoring revealed an intact colonic tissue for non-infected

WT and KO mice (Fig. 12A, C). During *C. rodentium* colitis, the inflammatory score was slightly higher in Ac^{flox} LysMcre KO mice with a tendency of more crypt abscesses and epithelial defects (Fig. 12C). However, neutrophil infiltration and invasion of the LP and TS by inflammatory immune cells were not altered (Fig. 12C).

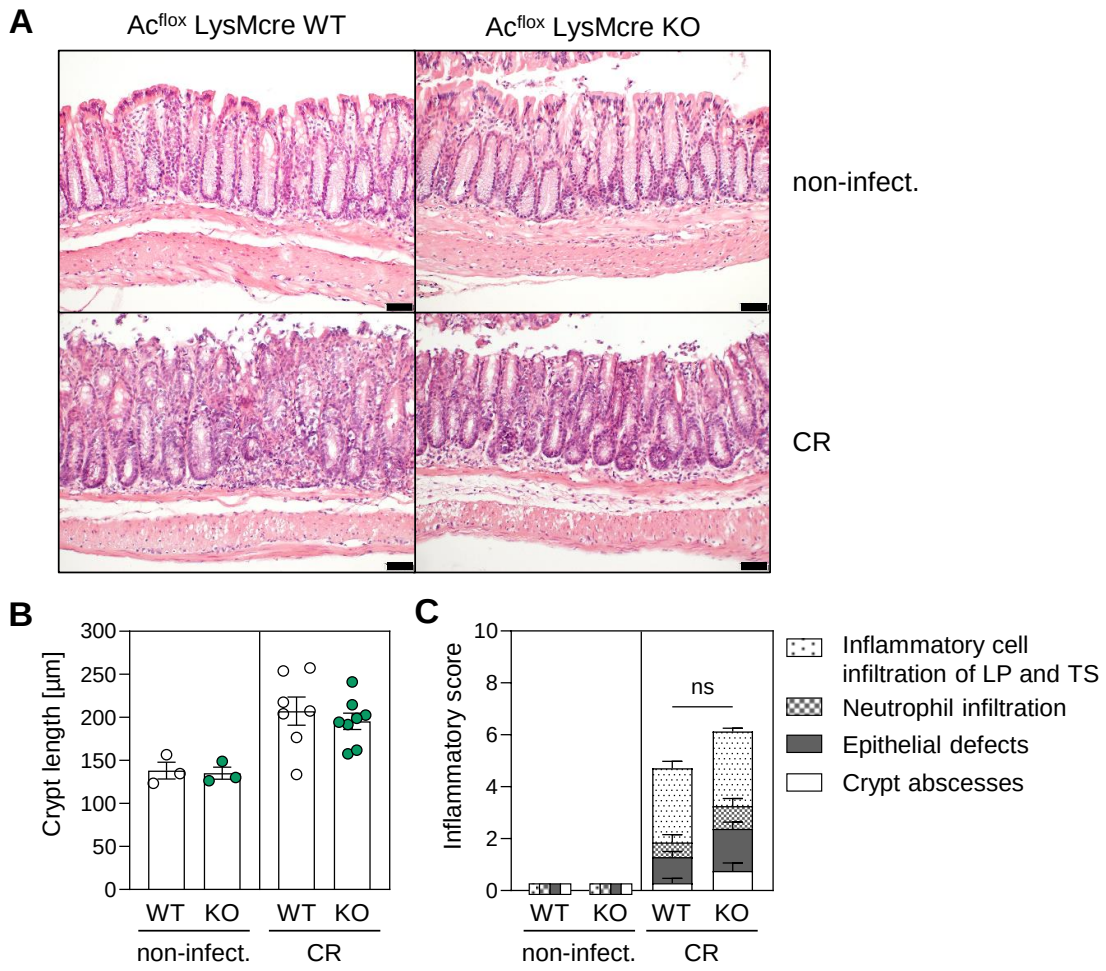

Fig. 12: Impact of Ac deficiency in macrophages and granulocytes on *C. rodentium* colitis.
(**A-C**) Ac^{flox} LysMcre WT and KO animals were left untreated or orally gavaged with ~2 x 10^9 CFU *C. rodentium* in 100 µL PBS and analyzed 10 days post infection. (**A**) Representative pictures of H&E stained colonic sections (n = 3-8). Scale bar 50 µm (**B**) Crypt hyperplasia determined by mean crypt length (n = 3-8). (**C**) Histopathological score from H&E stained colon sections (n = 3-8). Lamina propria (LP), tela submucosa (TS) Data are presented as mean ± SEM. Statistical analyses were performed using Mann-Whitney test (ns = not significant).

Next, the inflammatory milieu in the colon was assessed measuring cytokine secretion of colon explants from infected and non-infected Ac^{flox} LysMcre WT and KO mice. As in their WT littermates, colonic tissue of naïve Ac^{flox} LysMcre KO mice did not secrete any pro-inflammatory cytokines (Fig. 13A-D). After *C. rodentium* infection, pro-inflammatory cytokine secretion including IL-1β, TNFα, IL-17A and IFNγ was induced, however no differences became apparent between colonic explants of Ac^{flox} LysMcre WT and KO mice (Fig. 13A-D).

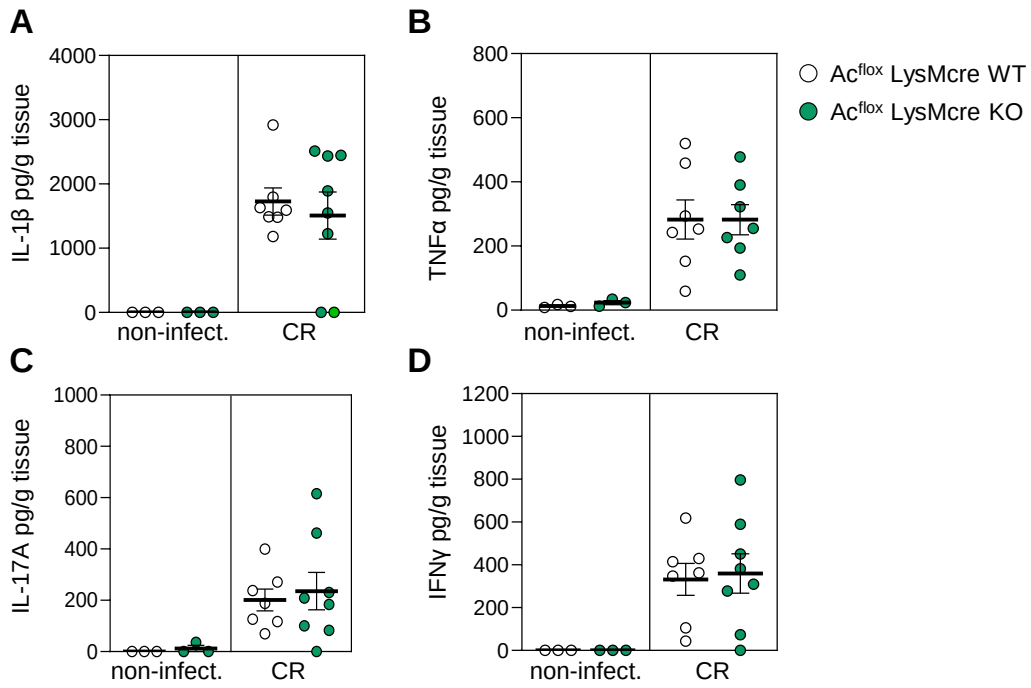

Fig. 13: Colonic cytokine secretion upon Ac deficiency of granulocytes and macrophages.
(**A-D**) Ac^{flox} LysMcre WT and KO animals were left untreated or orally gavaged with ~2 x 10^9 CFU *C. rodentium* in 100 µL PBS and analyzed 10 days post infection. Supernatants of colonic explants were analyzed for (**A**) IL-1β, (**B**) TNFα, (**C**) IL-17A and (**D**) IFNγ by Luminex technology (n = 3-8). Data are presented as mean ± SEM.

In summary, the results within the Ac^{flox} LysMcre model indicate that the function of Ac in granulocytes and macrophages plays a minor role in combating *C. rodentium* induced colitis.

5.1.4 Acid ceramidase expression in T cells protects from *C. rodentium* colitis

In global Ac deficient mice, a strong influx of inflammatory immune cells into the colonic mucosa and submucosa was observed during *C. rodentium* infection and Ac deficiency in epithelial cells, granulocytes and macrophages had little to no contribution to the observed phenotype. T lymphocytes are important players of the adaptive immune response, controlling the invasion of pathogens and mediate their elimination [5]. Therefore, the function of Ac in T cells was studied during *C. rodentium* infection. For this purpose, the Ac^{flox} CD4cre mouse model was employed, in which the cre recombinase is expressed under CD4 gene regulatory elements, resulting in deletion of *Asah1* expression in CD4$^+$ T cells and, due to the double positive stage in T cell development, also in CD8$^+$ T cells of *Asah1*$^{flox/flox}$ x CD4cre transgenic mice (Ac^{flox} CD4cre KO). The impact of Ac deficiency in T cells was assessed in naïve and *C. rodentium* infected Ac^{flox} CD4cre WT and KO animals, with peak infection at 10 days after inoculation (Fig. 14).

First, deletion of *Asah1* expression was confirmed via RT-qPCR in colonic CD4$^+$ and CD8$^+$ T lymphocytes of Ac^{flox} CD4cre KO mice (Fig. 14A). Of note, Cer accumulation in splenic Ac deficient CD4$^+$ and CD8$^+$ T cells was shown by others for the same Ac^{flox} CD4cre breeding at this institute [118, 167].

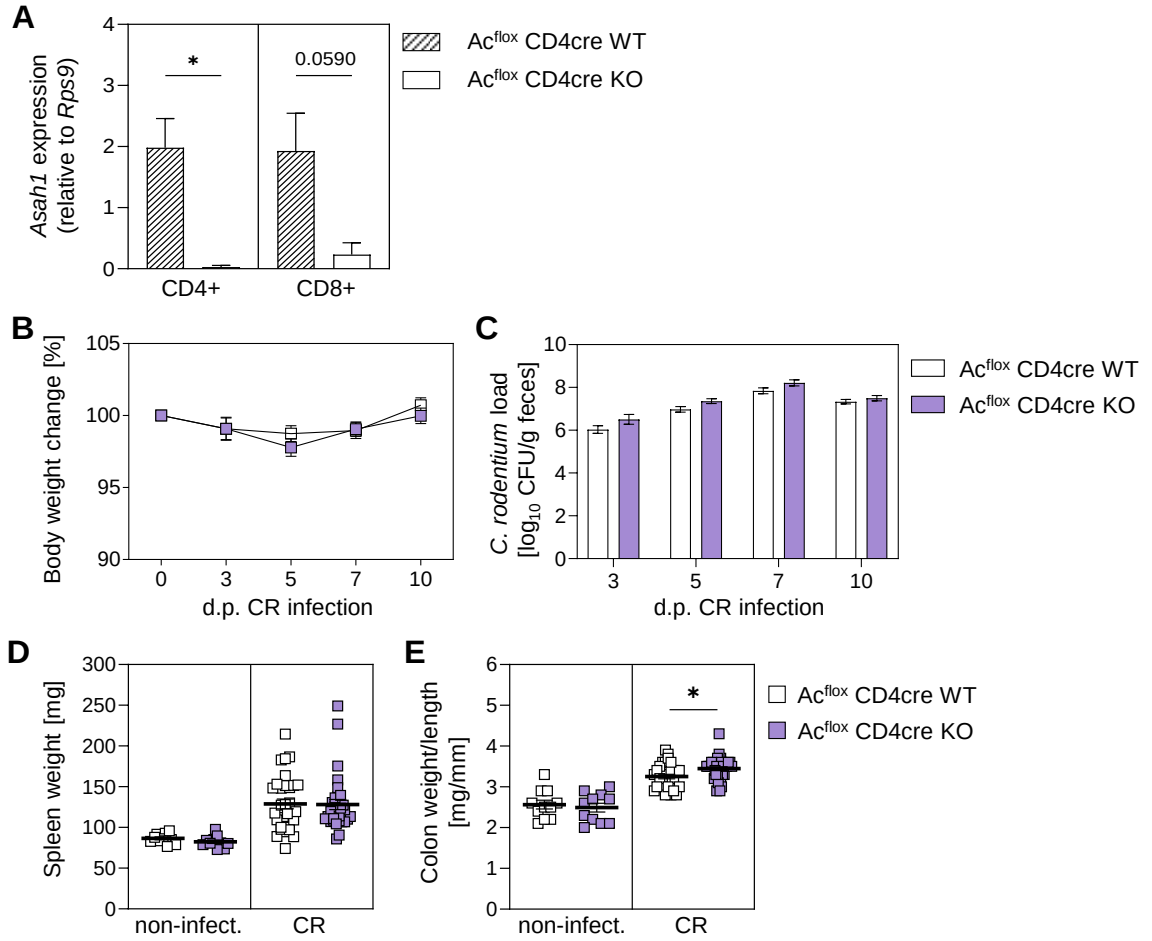

Fig. 14: Impact of Ac deficiency in T cells on *C. rodentium* induced colitis.
(**A-E**) Ac^{flox} CD4cre WT and KO animals were left untreated or orally gavaged with ~2 x 10^9 CFU *C. rodentium* in 100 µL PBS. (**A**) RT-qPCR for *Asah1* expression relative to *Rps9* expression of FACS-sorted colonic lamina propria T cells from Ac^{flox} CD4cre WT and KO mice (n = 3). (**B**) Body weight change and (**C**) the load of *C. rodentium* in the feces of Ac^{flox} CD4cre WT and KO mice at indicated time points after infection (d.p. = days post, n = 31-32). (**D**) Spleen weight and (**E**) colon weight/length ratio of Ac^{flox} CD4cre WT and KO mice, non-infected and 10 days post infection (n = 11-32). Data are presented as mean ± SEM. Statistical analyses were performed using Student's t-test (*p < 0.05).

Next Ac^{flox} CD4cre WT and KO animals were phenotypically analyzed (Fig. 14B-E). During *C. rodentium* infection, Ac deficiency in T cells led to slightly more body weight loss in mice at 5 dpi, but an overall comparable body weight was observed among Ac^{flox} CD4cre WT and KO littermates (Fig. 14B). The load of *C. rodentium* in the feces of Ac^{flox} CD4cre WT and KO animals was equal during the course of colitis (Fig. 14C). *C. rodentium* infected Ac^{flox} CD4cre KO mice had similarly enlarged spleens like their WT littermates, and both groups also showed normal spleen weights in the naïve state (Fig. 14D). The colon weight/length ratio was not altered in naïve Ac^{flox} CD4cre KO mice (Fig. 14E). During infection with *C. rodentium* however, the ratio was slightly, yet significantly enhanced in

Ac^{flox} CD4cre KO mice, which gives a first hint of a potentially altered course of colitis (Fig. 14E). Next, colonic inflammation of naïve and *C. rodentium* infected Ac^{flox} CD4cre WT and KO mice was analyzed in more detail by histopathology (Fig. 15).

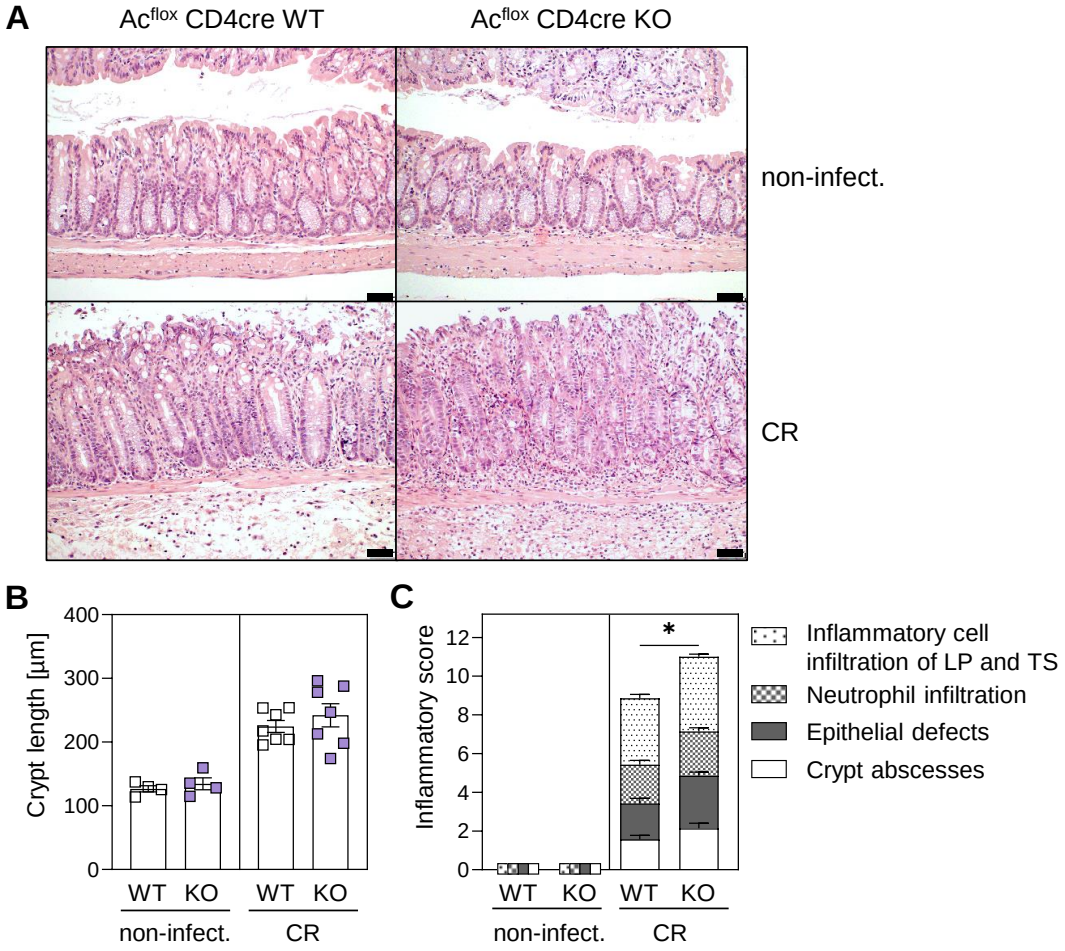

Fig. 15: Absence of Ac expression in T cells aggravates bacterial colitis.
(**A-C**) Ac^{flox} CD4cre WT and KO mice were left untreated or orally gavaged with ~2 x 10^9 CFU *C. rodentium* in 100 µL PBS and analyzed 10 days post infection. (**A**) Representative pictures of H&E stained colonic sections (n = 4-7). Scale bar 50 µm (**B**) Crypt hyperplasia determined by mean crypt length (n = 4-7). (**C**) Histopathological score from H&E stained colon sections (n = 4-7). Lamina propria (LP), tela submucosa (TS) Data are presented as mean ± SEM. Statistical analyses were performed using Student's t-test (*p < 0.05).

Non-infected Ac^{flox} CD4cre KO mice exhibited a normal crypt length and no signs of colitis like their WT littermates (Fig. 15A-C). Crypt hyperplasia during *C. rodentium* infection, characterized by enhanced crypt length, was in tendency more pronounced in mice carrying Ac KO in T cells (Fig. 15B). More importantly, Ac^{flox} CD4cre KO showed more crypt abscesses, epithelial defects, neutrophil infiltration and influx of inflammatory immune cells in mucosa and submucosa and thus a significantly aggravated inflammatory score compared to WT mice (Fig. 15C).

Subsequently, the cytokine milieu in the colon of Ac^{flox} CD4cre mice was assessed by Luminex technology. Like WT mice, mice lacking Ac expression in T cells did not produce substantial amounts of pro-inflammatory cytokines under homeostasis (Fig. 16A-D). During

C. rodentium infection IL-1β and TNFα levels were similar in Ac^{flox} CD4cre WT and KO mice (Fig. 16A, B). However, IL-17A secretion was enhanced and IFNγ production was significantly increased in colon explants of Ac^{flox} CD4cre KO mice in response to *C. rodentium* infection (Fig. 16C, D).

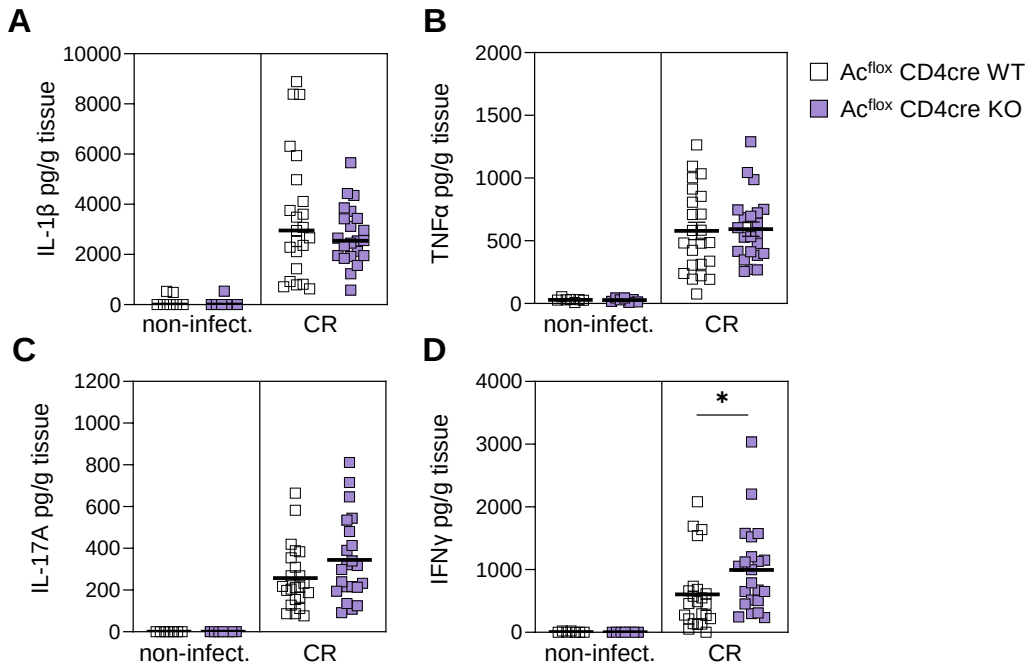

Fig. 16: Colonic pro-inflammatory cytokine production upon Ac deletion in T cells.
(**A-D**) Ac^{flox} CD4re WT and KO animals were left untreated or orally gavaged with ~2 x 10^9 CFU *C. rodentium* in 100 µL PBS and analyzed 10 days post infection. Supernatants of colonic explants were analyzed for (**A**) IL-1β, (**B**) TNFα, (**C**) IL-17A and (**D**) IFNγ by Luminex technology (n =7-23). Data are presented as mean ± SEM. Statistical analyses were performed using Mann-Whitney test (*p < 0.05).

Taken together, these results demonstrate an enhanced susceptibility to *C. rodentium* induced colitis of mice lacking Ac expression in T lymphocytes accompanied with accumulating ceramide levels.

5.2 Impact of acid ceramidase expression on CD4$^+$ and CD8$^+$ T cells and their activation in *C. rodentium* infection

The results obtained in the Ac^{flox} CD4cre mouse model revealed a protective effect of Ac expression in CD4$^+$ and CD8$^+$ T lymphocytes in *C. rodentium* induced colitis. Hence, we further investigated how the absence or presence of Ac influences the CD4$^+$ and CD8$^+$ T cell populations and their activation *in vivo* by flow cytometry.

5.2.1 Comparable T cell quantities in absence and presence of Ac

First, the amount of CD4$^+$ T cells in the colon at the site of infection, in draining mesenteric lymph nodes (mLN) and in the spleen, as representative organ of the systemic immune response, was analyzed in infected and naïve Ac^{flox} CD4cre WT and KO mice. The

lymphocyte population was identified by size (forward scatter, FSC) and granularity (side scatter, SSC) and dead cells characterized by positive fixable viability dye staining (FvD) were removed from the analysis (Fig. 17A). The $CD4^+$ T cell population was gated from viable lymphocytes and absolute cell numbers were determined (Fig. 17A-D).

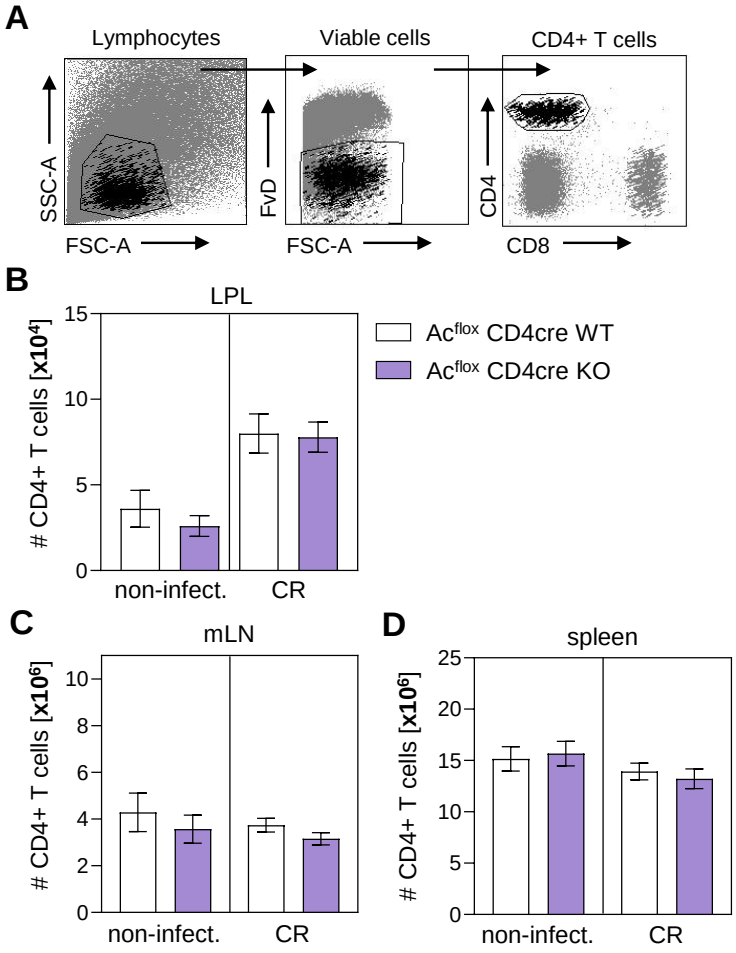

Fig. 17: $CD4^+$ T cell counts in colonic lamina propria, mLN and spleen of Ac^{flox} CD4cre WT and KO mice. (A-D) Ac^{flox} CD4cre WT and KO mice were left untreated or orally gavaged with ~2 x 10^9 CFU *C. rodentium* in 100 µL PBS and analyzed 10 days post infection. Colonic lamina propria lymphocytes (LPL) and single cell suspensions of spleen and mesenteric lymph node (mLN) were subjected to flow cytometric analysis and absolute cell counts of $CD4^+$ T cells were calculated. (**A**) Representative gating strategy to identify $CD4^+$ T cells. Forward scatter (FSC), side scatter (SSC), fixable viability dye (FvD). $CD4^+$ T cell counts in (**B**) LPLs (n = 9-27), (**C**) mLN (n = 6-23) and (**D**) spleen (n = 9-27). Data are presented as mean ± SEM.

Uninfected Ac^{flox} CD4cre KO mice show slightly less $CD4^+$ T cells in the colon, but *C. rodentium* infection led to similar $CD4^+$ T cell recruitment into the colonic lamina propria independent of Ac expression in T cells (Fig. 17B). In keeping with that, mLN and spleen did not reveal differential $CD4^+$ T cell amounts comparing Ac WT and KO mice, neither in naïve nor in infected mice (Fig. 17C, D). Generally, slightly fewer $CD4^+$ T cells were observed during *C. rodentium* infection in the mLN and spleen (Fig. 17C, D).

Next, the amount of CD8$^+$ T cells in colon, mLN and spleen was assessed in naïve and *C. rodentium* infected Ac^{flox} CD4cre WT and KO mice (Fig. 18A-D).

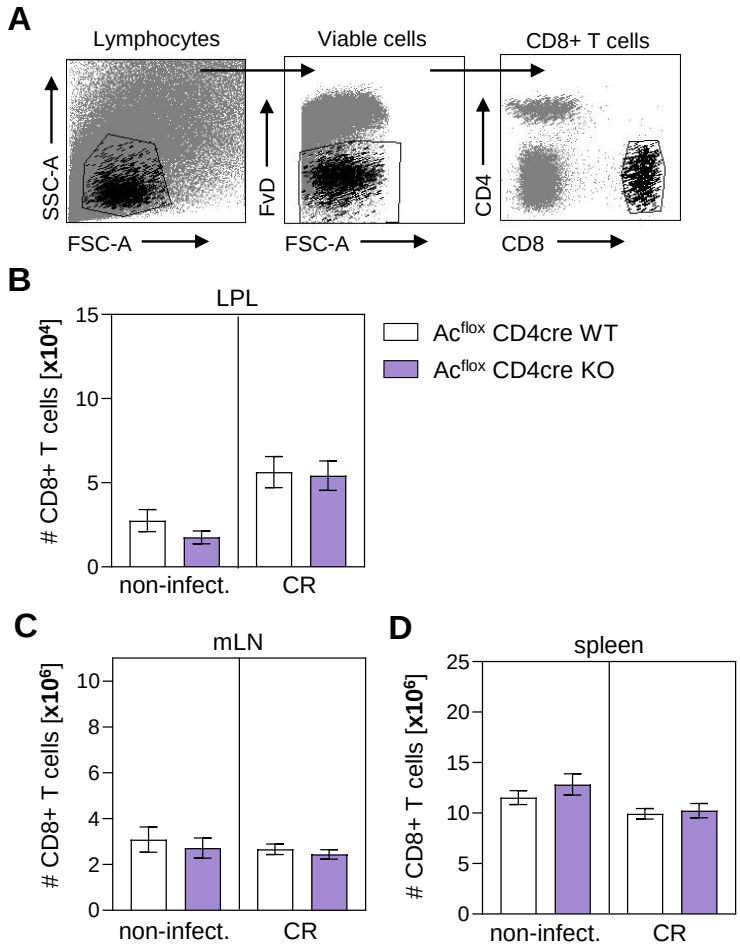

Fig. 18: CD8$^+$ T cell counts in colonic lamina propria, mLN and spleen of Ac^{flox} CD4cre WT and KO mice. (**A-D**) Ac^{flox} CD4cre WT and KO mice were non-infected or orally gavaged with ~2 x 10^9 CFU *C. rodentium* in 100 µL PBS and analyzed 10 days post infection. Colonic lamina propria lymphocytes (LPL) and single cell suspensions of spleen and mesenteric lymph node (mLN) were subjected to flow cytometric analysis and absolute cell counts of CD8$^+$ T cells were calculated. (**A**) Representative gating strategy to identify CD8$^+$ T cells. Forward scatter (FSC), side scatter (SSC), fixable viability dye (FvD). CD8$^+$ T cell counts in (**B**) LPLs (n = 9-27), (**C**) mLN (n = 6-23) and (**D**) spleen (n = 9-27). Data are presented as mean ± SEM.

Similar to the CD4$^+$ T cells, CD8$^+$ T cell counts were slightly lower in the colon of uninfected Ac^{flox} CD4cre KO mice compared to WT mice (Fig. 18B). During *C. rodentium* infection an influx of CD8$^+$ T cells into the colon was observed, with similar CD8$^+$ T cell counts in Ac^{flox} CD4cre WT and KO mice (Fig. 18B). In mLN CD8$^+$ T cells amounts were not modulated by Ac deficiency or *C. rodentium* infection (Fig. 18C). A modest increase of CD8$^+$ T cells was detected in naïve Ac^{flox} CD4cre KO mice, however compared to WT littermates no difference was observed during *C. rodentium* infection (Fig. 18D).

5.2.2 Loss of acid ceramidase expression enhances CD4⁺ T cell activation

Overall, CD4⁺ and CD8⁺ T cells amounts were not altered due to Ac deficiency. Therefore, the activation status of CD4⁺ and CD8⁺ T cells dependent on their Ac expression was assessed. First, lamina propria lymphocytes (LPL) from the colon of naïve and *C. rodentium* infected Ac^{flox} CD4cre WT and KO mice were subjected to flow cytometry analysis. T cell activation was assessed by expression of the activation marker CD44 (Fig. 19A). CD44 is a transmembrane glycoprotein and adhesion receptor, which is upregulated on activated T cells and important for T cell migration to the site of infection [171].

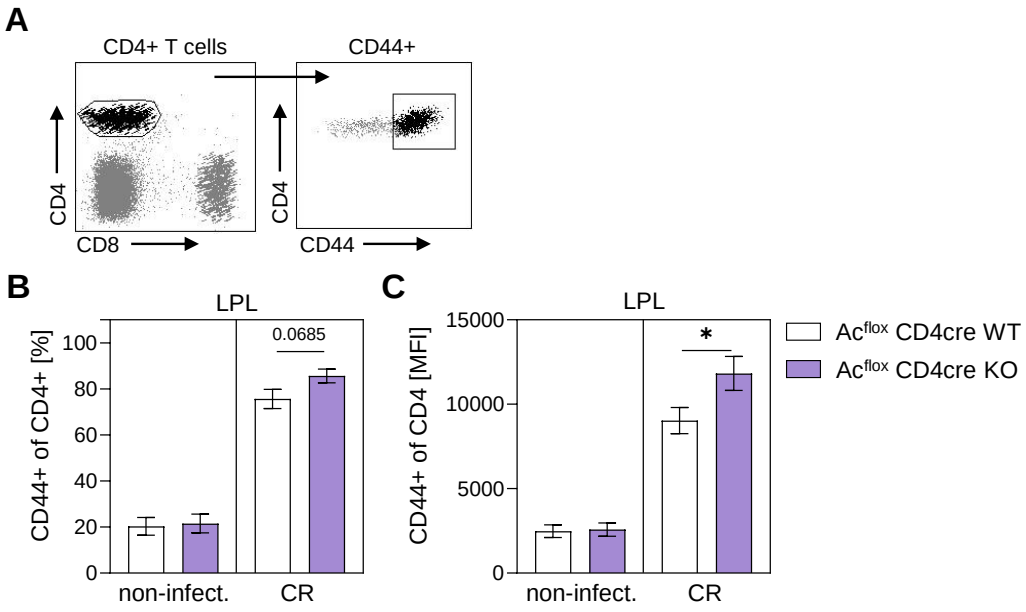

Fig. 19: Activation of Ac WT and KO CD4⁺ T cells in the colonic lamina propria.
(A-C) Ac^{flox} CD4cre WT and KO mice were left untreated or orally gavaged with ~2 x 10^9 CFU *C. rodentium* in 100 µL PBS and analyzed 10 days post infection. Colonic lamina propria lymphocytes were subjected to flow cytometry analysis. (**A**) Representative gating strategy to identify CD44 expression on CD4⁺ T cells. (**B**) CD4⁺ CD44⁺ frequencies (n = 3-10). (**C**) CD44 expression on CD4⁺ T cells determined by mean fluorescence intensity (MFI, n = 3-10). Data are presented as mean ± SEM. Statistical analyses were performed using Student's t-test (*$p < 0.05$).

The CD4⁺ T cell population showed low CD44 expression in the colon of naïve Ac^{flox} CD4cre WT and KO mice (Fig. 19B, C). During infection with *C. rodentium*, WT colonic CD4⁺ T cells were strongly activated with high frequencies of CD4⁺ CD44⁺ T cells (Fig. 19B). Activation was significantly more enhanced when CD4⁺ T lymphocytes were lacking Ac expression, as indicated by increased CD44 expression (Fig. 19C).

In the draining mLN, non-infected Ac^{flox} CD4cre KO mice exhibited similar CD4⁺ CD44⁺ T cell abundances and CD44 expression on CD4⁺ T cells compared to WT mice (Fig. 20A, B). Infection with *C. rodentium* did not induce further activation in mLN in both groups (Fig. 20A, B).

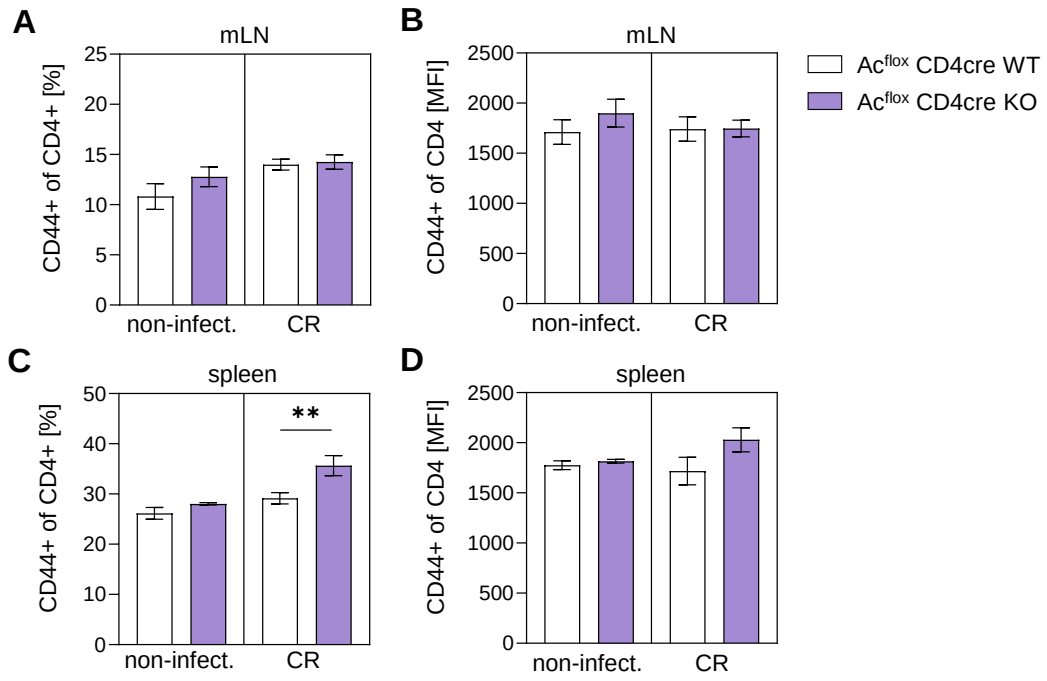

Fig. 20: Activation status of CD4⁺ T cells in the mLN and spleen upon Ac depletion and *C. rodentium* infection.
(A-D) Ac^{flox} CD4cre WT and KO mice were left untreated or orally gavaged with ~2 x 10^9 CFU *C. rodentium* in 100 µL PBS and sacrificed 10 dpi. Single cell suspensions from mesenteric lymph nodes and spleen were analyzed by flow cytometry. (**A**) $CD4^+$ $CD44^+$ frequencies and (**B**) CD44 expression on $CD4^+$ T cells determined by mean fluorescence intensity (MFI, n = 3-11) in mLN. (**C**) Splenic $CD4^+$ $CD44^+$ frequencies (n = 3-11) and (**D**) CD44 expression on splenic $CD4^+$ T cells determined using MFI (n = 3-8). Data are presented as mean ± SEM. Statistical analyses were performed using Student's t-test (**$p < 0.01$).

Similar to the situation in the mLN, the absence of Ac in splenic $CD4^+$ T lymphocytes of naïve mice did not alter their activation (Fig. 20C, D). $CD4^+$ T cells of WT mice were not further activated when challenged with *C. rodentium*, as indicated by similar CD44 expression and $CD44^+$ T cell abundances (Fig. 20C, D). However, when Ac was depleted in $CD4^+$ T cells during *C. rodentium* infection, the frequency of the $CD44^+$ T cell population was significantly increased compared to the infected WT (Fig. 20C).

Subsequently, it was investigated whether the activation of $CD8^+$ T lymphocytes was also influenced by Ac upon *C. rodentium* infection (Fig. 21). In general, the colonic lamina propria $CD8^+$ T cell population of both Ac^{flox} CD4cre WT and KO mice showed similar CD44 levels in the naïve status and a strong increase of the $CD44^+$ T cell subset and higher CD44 expression after *C. rodentium* infection (Fig. 21A, B). However, compared to WT mice depletion of Ac resulted in only slightly higher CD44 expression and $CD8^+$ $CD44^+$ T cell abundances in the colon of infected mice (Fig. 21B).

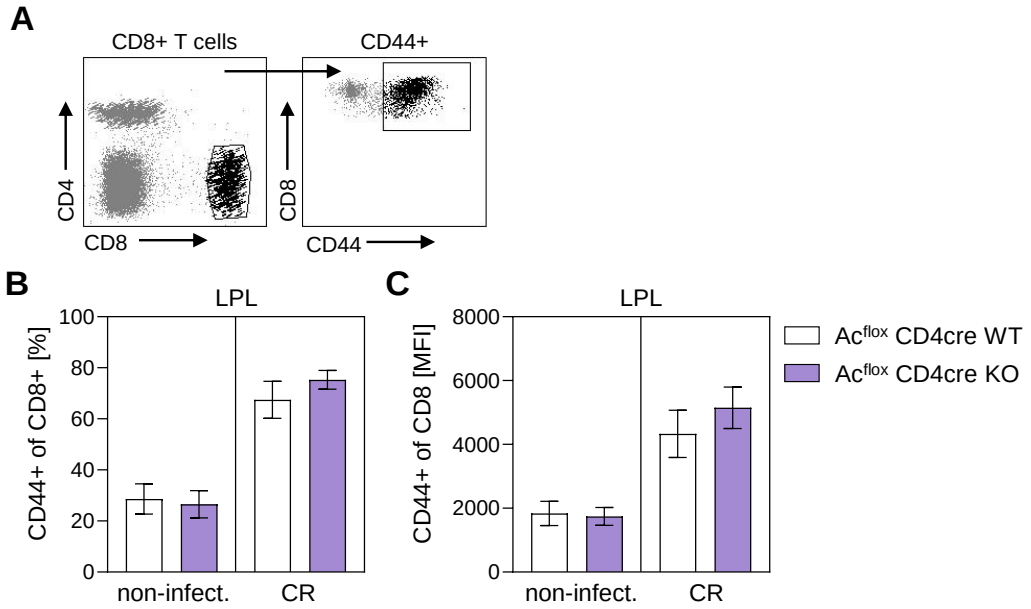

Fig. 21: Influence of Ac on the activation status of CD8⁺ lymphocytes in the colonic lamina propria.
(A-C) Ac^{flox} CD4cre WT and KO mice were left untreated or orally gavaged with ~2 x 10^9 CFU *C. rodentium* in 100 µL PBS and analyzed 10 days post infection. Colonic lamina propria lymphocytes were subjected to flow cytometry analysis. (**A**) Representative gating strategy to identify CD44 expressing $CD8^+$ cells. (**B**) $CD8^+$ $CD44^+$ frequencies (n = 3-8) and (**C**) CD44 expression on $CD8^+$ T lymphocytes determined by mean fluorescence intensity (MFI, n = 3-8). Data are presented as mean ± SEM.

Activation of $CD8^+$ T cells was further assessed in mLN and spleen of Ac^{flox} CD4cre WT and KO mice (Fig. 22).

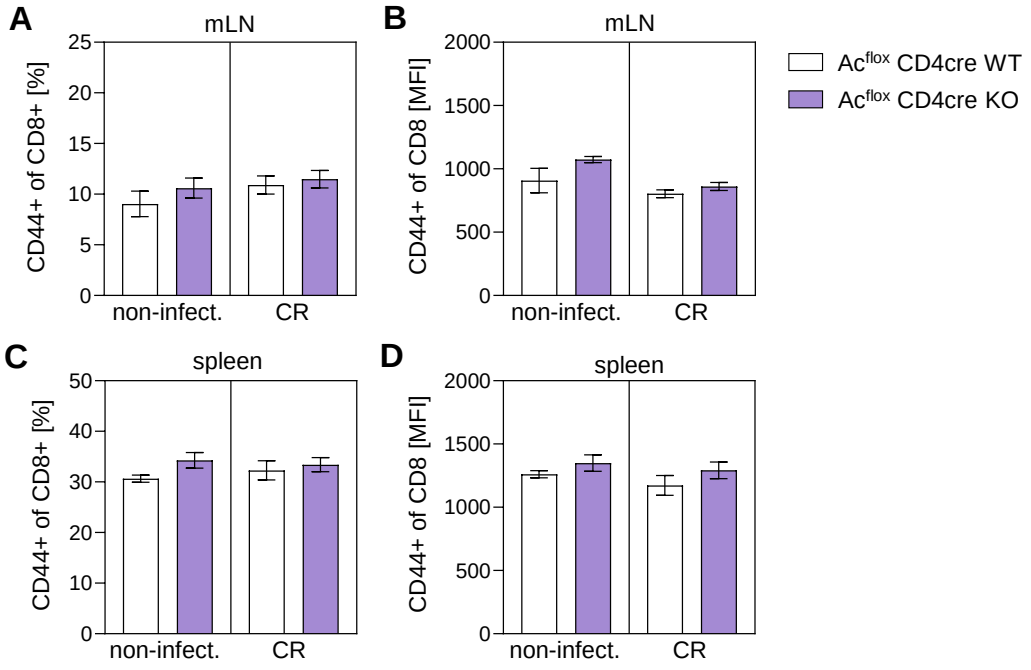

Fig. 22: Acid ceramidase deficiency does not alter $CD8^+$ T cell activation in mLN and spleen.
(A-D) Ac^{flox} CD4cre WT and KO mice were left untreated or orally gavaged with ~2 x 10^9 CFU *C. rodentium* in 100 µL PBS and sacrificed 10 dpi. Single cell suspensions from mLN and spleen subjected to flow cytometry analysis. (**A**) $CD8^+$ $CD44^+$ frequencies (n = 3-8) and (**B**) CD44 expression on $CD8^+$ T lymphocytes determined by mean fluorescence intensity (MFI, n = 3-8) in mLN. (**C**) $CD4^+$ $CD44^+$ frequencies (n = 3-8) and (**D**) CD44 MFI on $CD8^+$ T lymphocytes (n = 3-8) of the spleen. Data are presented as mean ± SEM.

C. rodentium infection boosted $CD8^+$ T cell activation in mLN and spleen measured by CD44 expression and $CD8^+$ $CD44^+$ frequencies (Fig. 22A-D). However, CD44 expression on $CD8^+$ T cells was not influenced by Ac depletion neither in mLN nor in the spleen (Fig. 22A-D).

Collectively, these findings show that Ac expression has an impact on $CD4^+$ T cell activation, which was particularly evident in the colon as the site of infection, but interestingly also in the spleen. In the context of $CD8^+$ T cell activation however, Ac seems to be only modestly involved.

5.3 Effect of acid ceramidase depletion on effector T cell populations

To investigate the role of Ac in the T cell response to enteric *C. rodentium* infection in depth, effector T cell subsets were studied under homeostasis and during *C. rodentium* infection of Ac^{flox} CD4cre WT and KO mice. Using flow cytometry, helper, regulatory and cytotoxic T cell populations were assessed.

5.3.1 Acid ceramidase modulates the T_h17 and T_h1 response in *C. rodentium* induced intestinal inflammation

The *C. rodentium* colitis model is known to elicit a strong IL-17 and IFNγ response by T_h17 and T_h1 cells, respectively, to combat the infection [86, 172]. Upon Ac deficiency IFNγ producing $CD4^+$ T cells were identified to be enhanced in the context of tumorigenesis [118]. Therefore, it was investigated whether Ac is influencing the T_h17 and T_h1 response during *C. rodentium* infectious colitis. Ac^{flox} CD4cre WT and KO mice were left uninfected or orally gavaged with ~2 x 10^9 CFU *C. rodentium* and first T_h17 cells were measured via flow cytometry.

The T_h17 response characterized by intracellular IL-17 expression in $CD4^+$ T cells was assessed in Ac^{flox} CD4cre WT and KO mice with and without *C. rodentium* infection (Fig. 23A-C). Under homeostasis, low levels of T_h17 cells were detected in the colonic lamina propria and the spleen of WT mice and this was also not altered by Ac depletion (Fig. 23B, C). During *C. rodentium* infection a massive influx of T_h17 cells into the colon was observed in both groups, with significantly higher T_h17 frequencies in Ac^{flox} CD4cre KO mice compared to WT littermates (Fig. 23B). The abundances of T_h17 cells was in general lower in the spleen compared to the colon (Fig. 23B, C). However, in the spleen T_h17 levels were also increased after *C. rodentium* challenge and showed a strong tendency of further enhanced T_h17 frequencies in infected Ac^{flox} CD4cre KO mice (Fig. 23C).

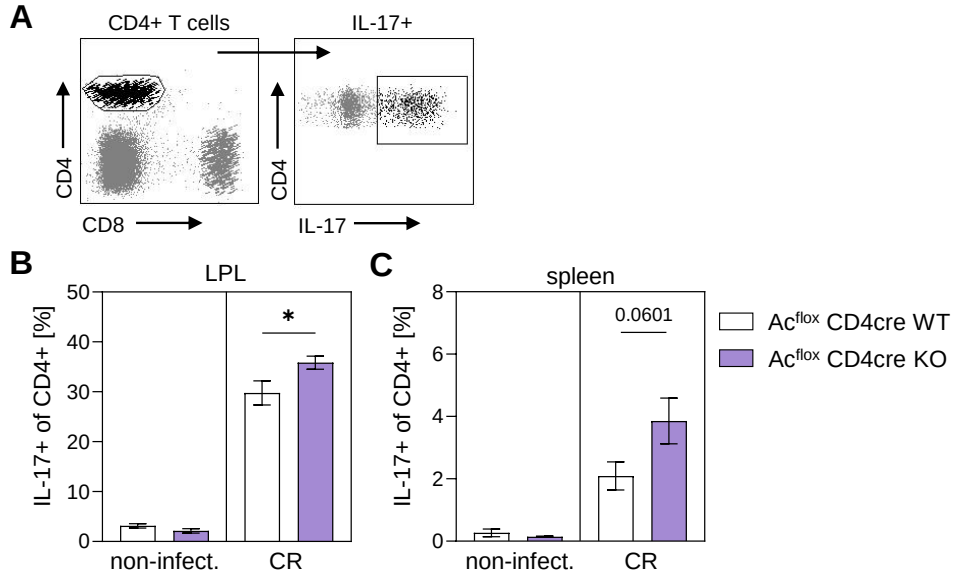

Fig. 23: Acid ceramidase depletion enhances colonic T_h17 cell frequencies during *C. rodentium* induced colitis.
(**A-D**) Ac^{flox} CD4cre WT and KO mice were left untreated or orally gavaged with ~2 x 10^9 CFU *C. rodentium* in 100 µL PBS and analyzed 10 days post infection. Colonic lamina propria lymphocytes (LPL) and single cell suspensions of the spleen were subjected to flow cytometry analysis. (**A**) Representative gating strategy to identify $CD4^+$ $IL\text{-}17^+$ producing T_h17 cells. T_h17 cell frequencies in (**B**) in colonic LPLs and (**C**) spleen (n = 3-8). Data are presented as mean ± SEM. Statistical analyses were performed using Student's t-test (*p < 0.05).

To determine whether the observed elevated T_h17 cell abundances upon Ac depletion resulted from altered T_h17 differentiation, a T_h17 differentiation assay was performed *in vitro*. Naïve $CD4^+$ $CD25^-$ T cells were incubated with IL-1β, IL-6, IL-21, IL-23, TGFβ and antibodies against CD3, CD28, IL-2, IL-4 and IFNγ to induce T_h17 differentiation (Fig. 24A). As negative control naïve $CD4^+$ $CD25^-$ T cells were cultured with antibodies against CD3 and CD28. After 5 days, cells were analyzed and equal frequencies of living $CD4^+$ T cells were detected in T_h0 and T_h17 cultures of Ac^{flox} CD4cre WT and KO mice (Fig. 24B). Interestingly, IL-17 production was similarly induced in both Ac WT and KO $CD4^+$ T cells showing comparable T_h17 differentiation *in vitro* (Fig. 24C).

Taken together, it was demonstrated that Ac is modulating the T_h17 response against *C. rodentium in vivo*, which could not be attributed to an altered *in vitro* differentiation capacity in absence of Ac.

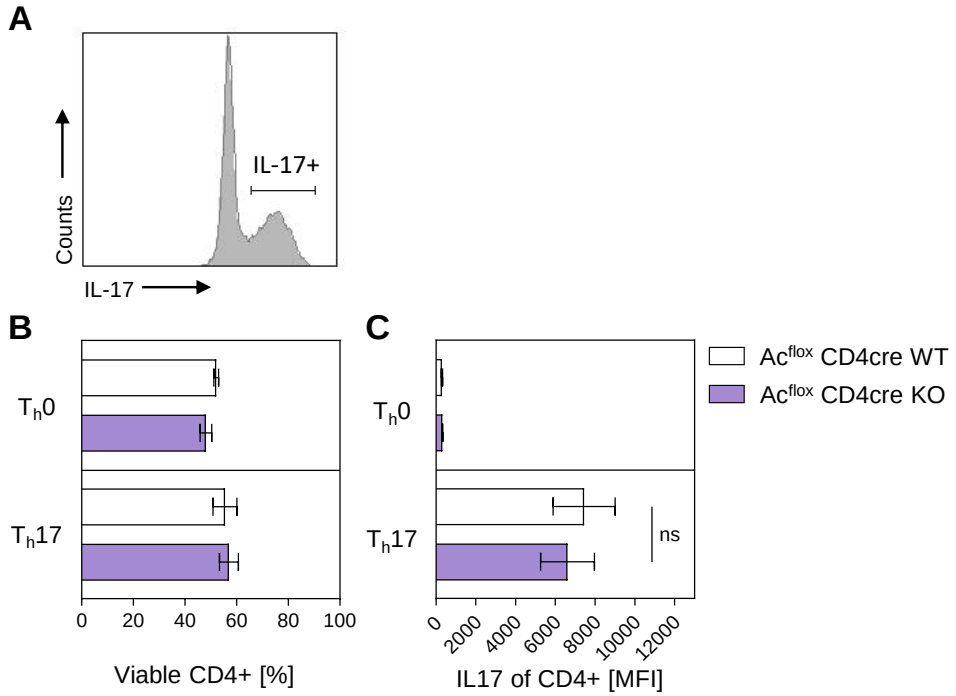

Fig. 24: T_h17 differentation assay of Ac WT and KO T cells.
(A-C) Splenic $CD4^+$ $CD25^-$ naïve T cells from Ac^{flox} CD4cre WT and KO mice were cultured in the presence of αCD3/αCD28 as negative control (T_h0 condition) and additional IL-1β, IL-6, IL-21, IL-23, TGFβ, αIL-2, αIL-4 and αIFNγ for T_h17 differentiation. After 5 days cells were harvested and analyzed via flow cytometry. (**A**) The histogram illustrates the gating of the $IL\text{-}17^+$ subset of $CD4^+$ T cells upon T_h17 differentiation. (**B**) Viable $CD4^+$ T cell frequencies and (**C**) mean fluorescence intensity (MFI) of IL-17 on $CD4^+$ T cells (n = 4). Data are presented as mean ± SEM. Statistical analyses were performed using Student's t-test (ns = not significant).

Next, the T_h1 response characterized by intracellular IFNγ and intranuclear T-bet expression in $CD4^+$ T cells was assessed in naïve and *C. rodentium* infected Ac^{flox} CD4cre WT and KO mice (Fig. 25A). Under homeostasis, the T_h1 transcription factor T-bet was expressed at similar levels in the colon of both Ac^{flox} CD4cre WT and KO mice (Fig. 25B). After *C. rodentium* infection $CD4^+$ $T\text{-}bet^+$ frequencies increased in the colon with a clear tendency of higher abundances in the infected Ac^{flox} CD4cre KO mice compared to WT littermates (Fig. 25B). In line with this, IFNγ producing $CD4^+$ T cells were also more abundant in the colon of infected mice compared to naïve mice (Fig. 25C). More importantly, Ac deficiency during *C. rodentium* infection was accompanied by significantly higher colonic $CD4^+$ $IFN\gamma^+$ T cell frequencies (Fig. 25C). In the spleen, T-bet and IFNγ expression among $CD4^+$ T cells were less pronounced than in the colon (Fig. 25D, E). Splenic $CD4^+$ $T\text{-}bet^+$ T cell frequencies were moderately elevated in the naïve Ac^{flox} CD4cre KO mice compared to WT mice (Fig. 25D). However, both uninfected groups showed identical $CD4^+$ $IFN\gamma^+$ frequencies in the spleen (Fig. 25D, E). In WT mice T-bet expression of splenic $CD4^+$ T cells was modestly induced after *C. rodentium* infection, whereas IFNγ remained on the same levels as in naïve mice (Fig. 25D, E). In the infected Ac^{flox} CD4cre KO mice however, significantly enhanced $CD4^+$ $T\text{-}bet^+$ and $IFN\gamma^+$ frequencies were observed in the spleen in comparison with infected WT mice (Fig. 25D, E).

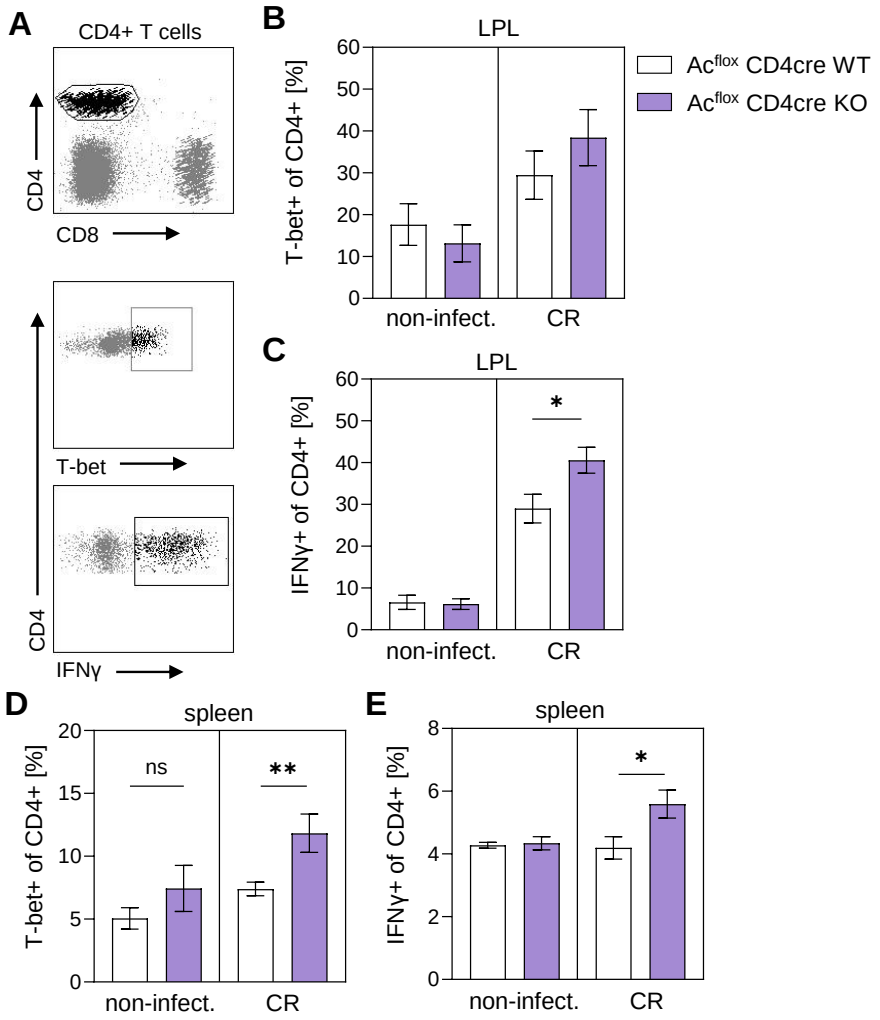

Fig. 25: Acid ceramidase modulates the T_h1 response to *C. rodentium* infection.
(**A-E**) Ac^{flox} CD4cre WT and KO mice were left untreated or orally gavaged with ~2 x 10^9 CFU *C. rodentium* in 100 µL PBS and analyzed 10 days post infection. Colonic lamina propria lymphocytes (LPL) and single cell suspension of the spleen were subjected to flow cytometry analysis. (**A**) Representative gating strategy to identify T-bet and IFNγ expressing $CD4^+$ T cells. (**B**) $CD4^+$ $T\text{-}bet^+$ T cells (n = 3-11) and (**C**) $CD4^+$ $IFN\gamma^+$ T cells (n = 6-16) of colonic LPLs. (**D**) $CD4^+$ $T\text{-}bet^+$ T cells (n = 3-11) and (**E**) $CD4^+$ $IFN\gamma^+$ T cells in the spleen. Data are presented as mean ± SEM. Statistical analyses were performed using Student's t-test (C, E) and Mann-Whitney test (D) (*$p < 0.05$, **$p < 0.01$).

Next, it was tested whether Ac is influencing the differentiation of $CD4^+$ T cells into T_h1 cells *in vitro*. Naïve $CD4^+$ $CD25^-$ T cells of Ac^{flox} CD4cre WT and KO mice were cultured with CD3 and CD28 antibodies (T_h0) and additional IL-12 and anti IL-4 antibodies to induce T_h1 differentiation (Fig. 26A). Ac^{flox} CD4cre WT and KO derived $CD4^+$ T cells showed a similar viability after 5 days of culture with T_h0 and T_h1 conditioning medium (Fig. 26B). A comparable IFNγ production was observed in WT and Ac deficient $CD4^+$ T cells, indicating that Ac is not influencing T_h1 differentiation *in vitro* (Fig. 26C).

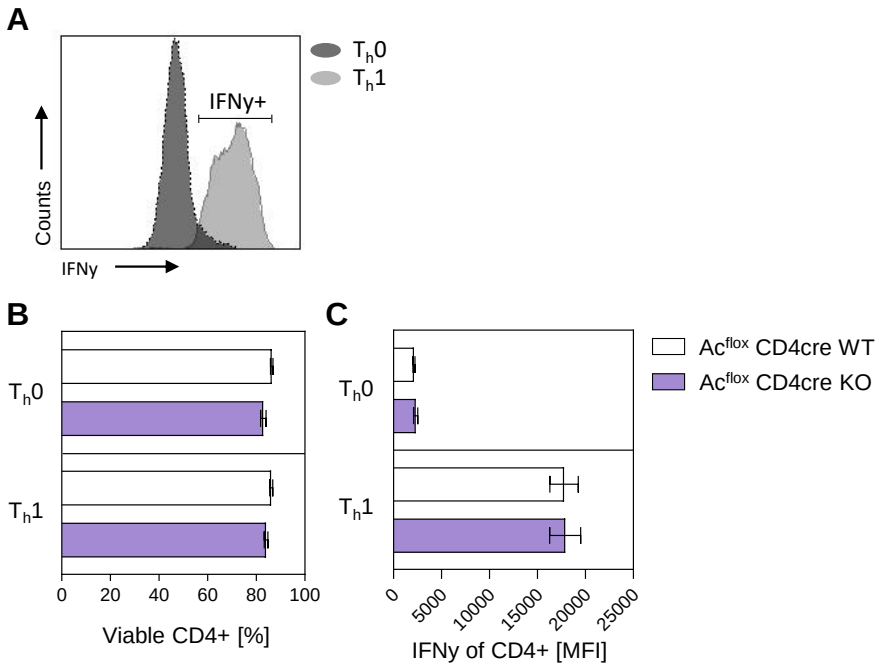

Fig. 26: Acid ceramidase depletion does not alter T_h1 differentiation *in vitro*.
(**A-C**) Splenic $CD4^+$ $CD25^-$ naïve T cells from Ac^{flox} CD4cre WT and KO mice were cultured in the presence of αCD3/αCD28 as negative control (T_h0 condition) and additional IL-12 and αIL-4 for T_h1 differentiation. After 5 days cells were harvested and analyzed via flow cytometry. (**A**) The histogram illustrates the gating of the $IFNγ^+$ subset of $CD4^+$ T cells and the induction of this T cell population in response to T_h1 conditioning medium. (**B**) Viable $CD4^+$ T cell frequencies, (**C**) mean fluorescence intensity (MFI) of IFNγ on $CD4^+$ T cells (n = 5). Data are pooled from two independent experiments and presented as mean ± SEM.

To sum up, although Ac deficiency does not impair T_h17 and T_h1 differentiation *in vitro*, Ac depletion in T cells modulates T_h17 and T_h1 responses against *C. rodentium* infection *in vivo.*

5.3.2 Cytotoxic T cells in absence and presence of acid ceramidase in *C. rodentium* induced intestinal infection

Cytotoxic T cells (CTL) are crucial cellular components producing granzymes and perforins in response to tumor or infections [48, 49]. Studies in the past years demonstrated that besides the classical $CD8^+$ cytotoxic T cells also $CD4^+$ T cell subsets express CTL factors including granzyme B (GrzB) and perforin [40]. Further, GrzB was shown recently to be an important mediator in *C. rodentium* infectious colitis [173]. Studies on the role of sphingolipids and Ac in cytotoxic T cells during intestinal infection are lacking. Hence, $CD4^+$ and $CD8^+$ cytotoxic T cells were analyzed in absence and presence of Ac and upon challenge with *C. rodentium* infection.

First, $CD8^+$ CTL frequencies in colon and spleen of naïve and *C. rodentium* infected Ac^{flox} CD4cre WT and KO mice were assessed by flow cytometry. Cytotoxic T cells were identified by intracellular GrzB production (Fig. 27A). Low levels of $CD8^+$ CTLs were detected in colons of naïve Ac^{flox} CD4cre WT and KO mice (Fig. 27B).

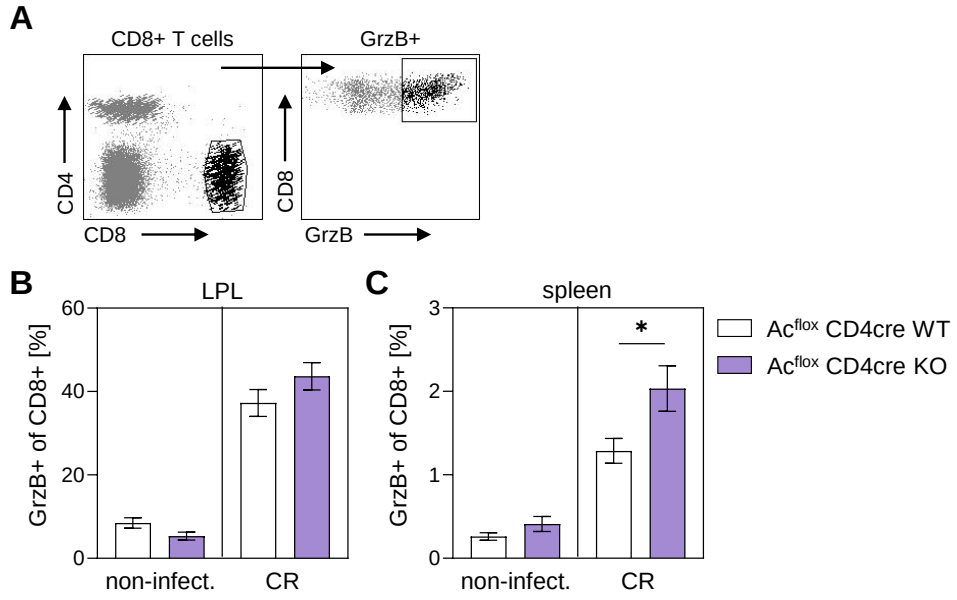

Fig. 27: CD8⁺ cytotoxic T cell abundances in colon and spleen of Ac^{flox} CD4cre WT and KO mice.
(**A-D**) Ac^{flox} CD4cre WT and KO mice were left untreated or orally gavaged with ~2 x 10^9 CFU *C. rodentium* in 100 µL PBS and analyzed 10 days post infection. Colonic lamina propria lymphocytes (LPL) and single cell suspensions of the spleen were subjected to flow cytometry analysis. (**A**) Representative gating strategy to identify CD8⁺ granzyme B producing (GrzB⁺) T cells. CD8⁺ GrzB⁺ T cell frequencies in (**B**) in colonic LPLs and (**C**) spleen (n = 6-23). Data are presented as mean ± SEM. Statistical analyses were performed using Mann-Whitney test (*p < 0.05).

During *C. rodentium* infection however, the frequency of CD8⁺ CTLs in the colonic tissue increased tremendously and T cell specific Ac deficient mice showed even higher CD8⁺ CTL levels (Fig. 27B). In the spleen, CD8⁺ CTL abundances were comparably low in non-infected Ac^{flox} CD4cre WT and KO mice (Fig. 27C). Similar to the situation in the colon, during *C. rodentium* infection higher frequencies of CD8⁺ CTLs were present in the spleen and CD8⁺ CTLs were significantly enriched in Ac^{flox} CD4cre KO mice (Fig. 27C).

Next, the impact of Ac deficiency on CD4⁺ GrzB producing T cells (CD4⁺ CTLs) was investigated (Fig. 28A). In non-infected Ac^{flox} CD4cre WT and KO mice, comparably low frequencies of CD4⁺ CTLs were detected in both, spleen and colon (Fig. 28B, C). During *C. rodentium* infectious colitis, levels of colonic CD4⁺ CTLs were strongly elevated compared to the naïve status, and importantly, Ac^{flox} CD4cre KO mice showed an even stronger elevation in the CD4⁺ GrzB⁺ population (Fig. 28B). While CD4⁺ CTL frequencies in the spleen generally did not increase as much between naïve and infected mice as it was observed in the colon, a significant increase of CD4⁺ CTLs was detected in the spleen of infected Ac^{flox} CD4cre KO mice compared to WT littermates (Fig. 28C).

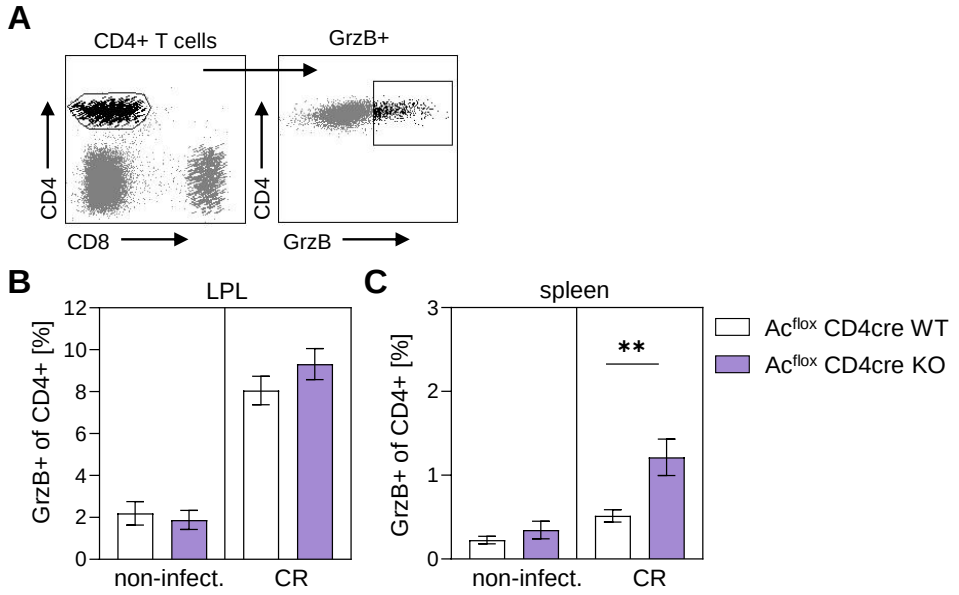

Fig. 28: CD4⁺ cytotoxic T cell abundances in colon and spleen of Ac^{flox} CD4cre WT and KO mice.
(**A-D**) Ac^{flox} CD4cre WT and KO mice were left untreated or orally gavaged with ~2 x 10^9 CFU *C. rodentium* in 100 µL PBS and analyzed 10 days post infection. Colonic lamina propria lymphocytes (LPL) and single cell suspensions of the spleen were subjected to flow cytometry analysis. (**A**) Representative gating strategy to identify CD4⁺ granzyme B producing (GrzB⁺) T cells. CD4⁺ GrzB⁺ T cell frequencies in (**B**) in colonic LPLs and (**C**) spleen (n = 6-23). Data are presented as mean ± SEM. Statistical analyses was performed using Mann-Whitney test (**p < 0.01).

To investigate the influence of Ac on the polarization of CD4⁺ T cells CTLs, the T_h1 assay was utilized since the IL-12 of the T_h1 condition triggers cytotoxic activity (Fig. 29) [50, 51].

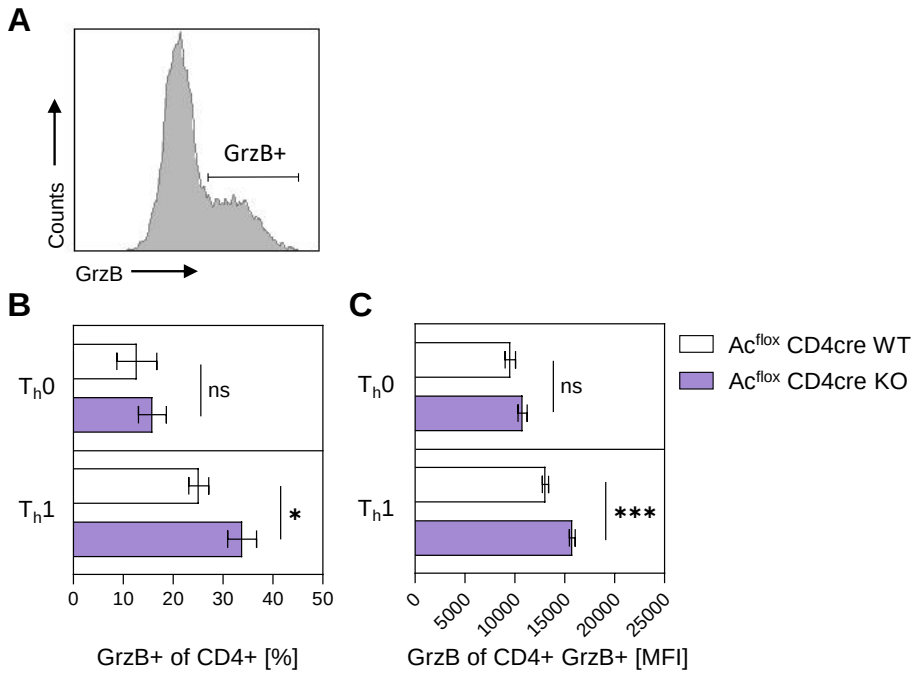

Fig. 29: Acid ceramidase deficiency leads to enhanced cytotoxicity in presence of IL-12.
(**A-C**) Splenic CD4⁺ CD25⁻ naïve T cells of Ac^{flox} CD4cre WT and KO mice were cultured in the presence of αCD3/αCD28 as negative control (T_h0) and additional IL-12 and αIL-4 triggering T_h1 differentiation cytotoxic properties. After 5 days cells were harvested and analyzed via flow cytometry. (**A**) The histogram illustrates the gating of the granzyme B (GrzB⁺) subset of CD4⁺ T cells exemplified by T_h1/cytotoxic condition. (**B**) Frequencies of GrzB expressing CD4⁺ T cells and (**C**) MFI of GrzB on GrzB⁺ CD4⁺ T cells (n = 5). Data are pooled from two independent experiments and presented as mean ± SEM. Statistical analyses were performed using Student's t-test (*p < 0.05, ***p < 0.001).

Interestingly, under T_h1 skewing conditions Ac depleted $CD4^+$ T cells exhibited significantly higher $GrzB^+$ frequencies and this $GrzB^+$ subset also expressed significantly more GrzB upon Ac deficiency (Fig. 29A, B). These findings are in accordance with the enhanced $CD4^+$ CTL frequencies observed in infected Ac^{flox} CD4cre KO mice during *C. rodentium* infection described above.

Collectively, $CD4^+$ and $CD8^+$ CTL abundances were elevated in the spleen and in tendency increased in the colon of *C. rodentium* infected Ac^{flox} CD4cre KO mice. Together with the enhanced polarization into $GrzB^+$ $CD4^+$ T cells upon Ac deficiency, this suggests that Ac is involved in cytotoxic GrzB production following T cell activation.

5.3.3 The regulatory T cell population remains unaffected by Ac deficiency

$CD4^+$ regulatory T cells (T_{reg}), classified by FoxP3 expression, are important for immune tolerance of non-pathogenic luminal antigens and the limitation of inflammatory immune reactions [53, 174, 175]. T_{regs} emerge in response to T helper, cytotoxic T cells and tissue damage to mediate recovery, enable memory formation and the return to homeostasis [54, 55]. In the context of gut infection, timing and extent of the T_{reg} response is critical, as immunosuppression also promotes bacterial expansion [54]. Hence, the T_{reg} proportions were assessed in absence and presence of Ac in T cells of naïve and *C. rodentium* infected mice (Fig. 30A-C).

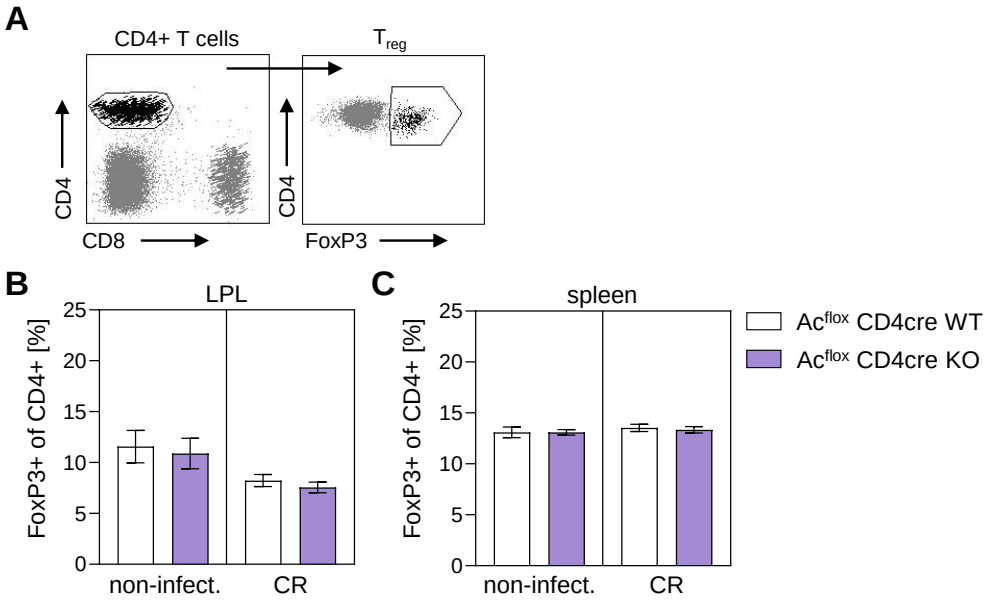

Fig. 30: Regulatory T cell abundances in the colonic lamina propria and spleen of Ac^{flox} CD4cre WT and KO mice.
(**A-D**) Ac^{flox} CD4cre WT and KO mice were left untreated or orally gavaged with ~2 x 10^9 CFU *C. rodentium* in 100 µL PBS and analyzed 10 days post infection. Colonic lamina propria lymphocytes (LPL) and splenic single cell suspension were subjected to flow cytometry analysis. (**A**) Representative gating strategy to identify $CD4^+$ $FoxP3^+$ regulatory T cells (T_{reg}). T_{reg} frequencies in (**B**) colonic LPLs and (**C**) the spleen (n = 6-23). Data are presented as mean ± SEM.

Regulatory T cells were detected in similar frequencies in Ac^{flox} CD4cre WT and KO in the colonic lamina propria and the spleen under homeostasis (Fig. 30B, C). During *C. rodentium* peak infection colonic T_{reg} proportions were decreased, and Ac^{flox} CD4cre WT and KO animals revealed similar T_{reg} levels (Fig. 30B). In the spleen, T_{reg} frequencies in both Ac^{flox} CD4cre WT and KO remained unchanged in response to *C. rodentium* infection compared to the naïve status (Fig. 30C). Collectively, these findings indicate that Ac is dispensable for the regulatory T cell response.

5.3.4 Differential gene expression upon acid ceramidase deficiency in CD4⁺ T cells of the colon during *C. rodentium* infection

Finally, to get further insight into the role of Ac in $CD4^+$ T cells in response to *C. rodentium* challenge, mRNA sequencing was performed on colonic $CD4^+$ T cells of *C. rodentium* infected Ac^{flox} CD4cre WT and KO mice. Differential gene expression analysis revealed 83 genes significantly different among WT and *Asah1* deprived $CD4^+$ T cells (Fig. 31A).

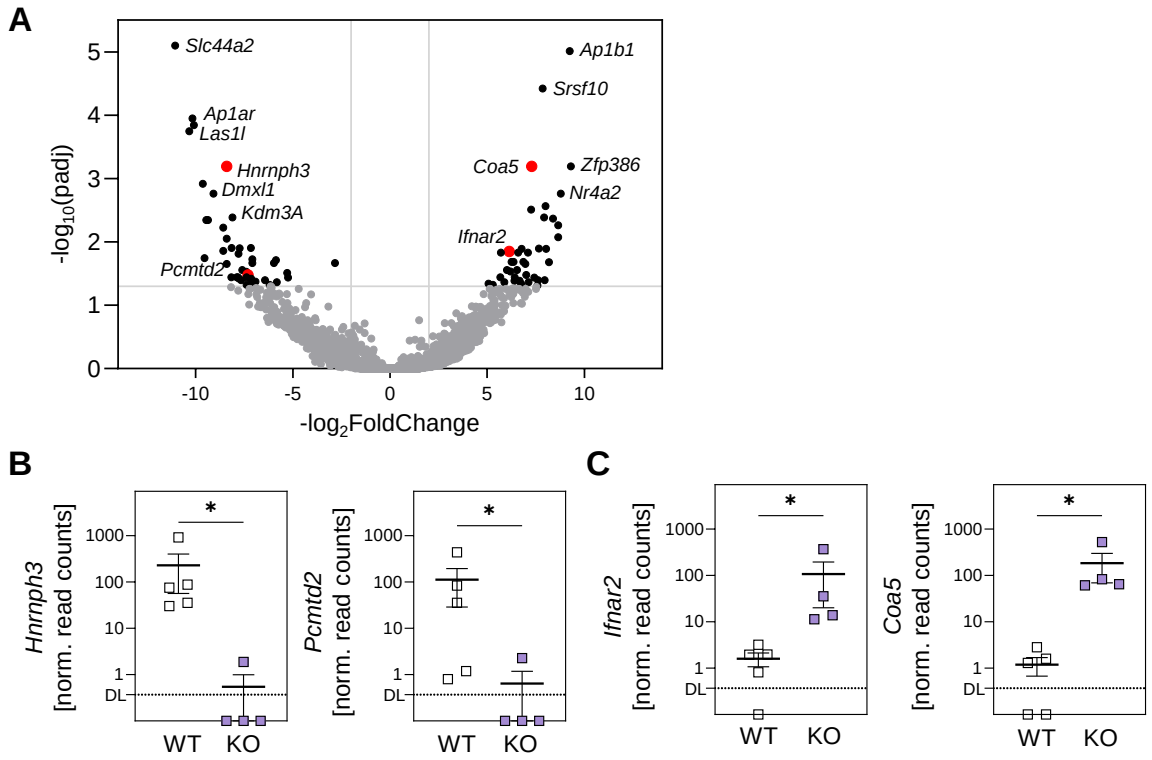

Fig. 31: mRNA sequencing reveals differential gene expression in Ac deficient $CD4^+$ T cells.
(**A-C**) Ac^{flox} CD4cre WT and KO mice were orally gavaged with ~2 x 10^9 CFU *C. rodentium* in 100 µL PBS and analyzed 10 days post infection. $CD4^+$ T cells were FACS-sorted from colonic lamina propria lymphocytes and subjected to mRNA sequencing analysis. (**A**) Volcano plot of the comparison WT versus Ac KO $CD4^+$ T cells (n=4-5). Significantly differentially expressed genes (DEGs) are depicted as black dots (adjusted p-value (padj) < 0.05 and correspondigly -$\log_{10}$(padj) < 1.3). Red dots highlight genes, which are further described in B and C. (**B**) Normalized read counts of DEGs downregulated in Ac deficient T cells including, *Hrnph3* and *Pcmtd2*, and (**C**) upregulated DEGs *Ifnar2, Srfs10 and Coa5* (n=4-5). (DL = detection limit; *Hrnph3* = Heterogeneous nuclear ribonucleoprotein H3, *Pcmtd2* = Protein-L-isoaspartate (D-aspartate) O-methyltransferase domain containing 2, *Ifnar2* = Interferon alpha/beta receptor 2, *Coa5* = Cytochrome c oxidase assembly factor 5). Data are presented as mean ± SEM. Differential gene expression analysis was performed using the R/Bioconductor software package DESeq2. Genes with an padj < 0.05 were defined as differentially expressed. DEGs with a negative log2 fold change (FC) greater 2 or less than -2 were considered as upregulated or downregulated, respectively.

The genes of the heterogeneous nuclear ribonucleoprotein H3 (*Hnrnph3*) and the protein-L-isoaspartate (D-aspartate) O-methyltransferase domain containing 2 (*Pcmtd2*) were found to be significantly downregulated in Ac deficient $CD4^+$ T cells (Fig. 31A, B). Hnrnph3 belongs to a family of splicing repressors, which can control T cell function via alternative splicing [176]. Pcmtd2 was characterized as a suppressor of cytokine signaling (SOCS) protein [177]. SOCS proteins negatively regulate cytokine signaling in T cells [178]. Among the 40 upregulated genes in Ac KO T cells the interferon alpha/beta receptor 2 (*Ifnar2*) and the cytochrome c oxidase assembly factor 5 (*Coa5*) were identified (Fig. 31A, C). Ifnar2 is part of the type I IFN receptor and is involved in antiviral and antibacterial T cell responses [179, 180]. Coa5 belongs to the mitochondrial respiratory chain, which is important for the energy metabolism upon T cell activation [181, 182].

In conclusion, mice deficient in Ac and concomitant accumulation of ceramide are more susceptible to *C. rodentium* induced colitis. Using cell type specific Ac KO mouse strains it was shown that Ac plays a minor role in epithelial cells, macrophages and granulocytes under homeostasis and in response to *C. rodentium* infection. T cell specific targeting of Ac revealed a protective role of the enzyme in the adaptive immune system. Acid ceramidase deficiency in T cells resulted in a pro-inflammatory cytokine milieu in the colon and significantly enhanced T_h1 and T_h17 responses along with elevated $CD4^+$ and $CD8^+$ CTL levels. Interestingly, *in vitro* T_h1 and T_h17 differentiation was not altered in Ac deficient T cells. However, T_h1 conditioning medium triggered an enhanced cytotoxic phenotype of Ac depleted $CD4^+$ T cells. Further, Ac might act via *Ifnar2* and *Pctmd2* signaling, alternative splicing and modulation of the mitochondrial respiratory chain on the function of $CD4^+$ T cells. Yet, further research is needed to test this hypothesis. Although the abundance of T_{regs}, which counteract T_h1/T_h17/CTL responses, was not affected by the absence of Ac, the increased frequencies of pro-inflammatory T cells favor an imbalance towards inflammation.

6 Discussion

The metabolism of sphingolipids is a complex network of pathways interconnected by the central nexus Cer [96]. Apart from their role as membrane components, sphingolipids are involved in diverse functions in many cellular processes and thus in immunity and disease [96, 123]. Another layer of complexity is added because sphingolipids and the corresponding enzymes may have divergent effects depending on the (pathological) stimulus. Acid ceramidase critically determines the levels of typical sphingolipid signaling molecules, Cer, Sph, S1P and C1P, as it generates Sph from Cer, thereby also enabling S1P production and modulating C1P levels [95]. The pathomechanisms of intestinal inflammation and infection are still not fully understood and although Ac has been linked to gut disorders, its role remains elusive [146]. Studies on the impact of Ac in intestinal infection are lacking. The present work, sheds light on the influence of Ac on gut infection and the function of the enzyme was dissected among the different cellular mediators in host defense, using the *C. rodentium* mouse model mimicking gut infection by pathogenic *E. coli* in humans.

First, global Ac deficiency and concomitant Cer accumulation in the colon resulted in an enhanced susceptibility to *C. rodentium* induced colitis (Fig. 7) with elevated *C. rodentium* load as described in previous work at this institute [168]. On the contrary, Cer synthase inhibition by the mycotoxin fumonisin B1, which is decreasing Cer levels, also enhances colonization of the gut by pathogenic *E. coli* in pigs [133]. These differences could be due to the possibility that fumonisin B1 might have other toxic influences via Cer independent mechanisms. Additionally, for the inoculation of the pigs extraintestinal pathogenic *E. coli* was used [133], while in the present study mice were infected with a natural enteropathogen. Extraintestinal *E. coli* might elicit different pathomechanisms compared to genuine intestinal bacteria, which could be the reason for the divergent results.

Interestingly, studies in IBD patients showed that intestinal inflammation was accompanied by elevated Ac expression in colonic tissue [146]. The severe colitis found here upon global Ac deficiency (Fig. 7), indicates that the expression of Ac is crucial to control inflammation. Thus, Ac may be upregulated in IBD as a countermeasure to inflammatory responses.

The intestinal epithelium, a layer of epithelial cells, intimately connected by tight junctions and constantly replenished by stem cells, provides an important barrier against invading pathogens [12, 21]. Sphingolipids, as components of the cell membrane and signaling molecules, have previously been studied with regard to their role in the epithelium. Treatment of Caco-2 cells, colon carcinoma derived epithelial monolayers, with exogenous

sphingomyelinase resulted in increased Cer levels and enhanced permeability [183]. In contrast to that, downregulation of Cer production by the knockout of Cer synthase 2 in naïve mice also mediated a leaky intestinal epithelium with ablation of tight junction protein expression [140]. However, Baduva *et al.* showed that treatment of a conjunctiva epithelial cell line with exogenous Ac, does not affect tight junction expression [184]. Thus, depending on the model and the targeted enzyme, a change in Cer levels has different effects on the epithelium. Furthermore, the role of intrinsic Ac activity in the epithelium of the intestine was not described.

In this work, Ac function in intestinal epithelial cells was determined by utilizing colonic organoids, an *ex vivo* 3D model of the gut epithelium (Fig. 8). Organoids and their morphology are a valuable tool, to assess the overall constitution of the epithelium. As an example, organoids derived from IBD patients exhibited an inflammatory phenotype, with reduced formation of crypt-like domains (budding), an increase of dead cells and reduced expression of tight junctions [185]. Comparing Ac deficient and competent organoids, identical formation of crypt-like domains (budding) and an unaltered cell death, as shown by comparable abundance of destroyed and partially intact organoids, were observed (Fig. 8). Additionally similar tight junction expression, indicated by Occludin, and equal $Lgr5^{+}$ stem cell expression was detected (Fig. 8). This is in line with the aforementioned study by Baduva and colleagues, where tight junction expression of conjunctiva epithelial cells was not altered with exogenous Ac treatment [184]. The different finding of an enhanced permeability in Caco-2 monolayers after addition of sphingomyelinase might be due to alterations in other sphingolipids than Cer. Sphingomyelinases degrade sphingomyelin to Cer, consequently exogenous sphingomyelinase treatment decreases sphingomyelin levels, which is also an important component of the cellular membrane [102, 183]. Furthermore, the decrease of sphingomyelin levels after sphingomyelinase treatment was also observed in glycosphingolipid enriched domains in the membrane of Caco-2 cells, in which tight junctions are located [183]. Therefore, the increased permeability of Caco-2 monolayers could possibly be attributed to deficiency of sphingomyelin. The disturbance of intestinal epithelial barrier function in Cer synthase 2 depleted mice might similarly be dependent on distinct sphingolipid species [140]. Ceramide synthase 2 synthesizes very long chain Cer, such as C22-, C24- and C24:1-Cer [142], while Ac preferentially catabolizes Cer species between a chain length of C12 and C16 [104, 186]. Accordingly, upon Cer synthase 2 deficiency colonic C24- and C24:1-Cer levels were reduced, while C14- and C16-Cer levels remained largely unaffected [140]. Thus, the impairment of epithelial barrier function observed in Cer synthase 2 KO mice might be a result of altered levels of very long chain Cer. Since the present study focused on Ac deficiency in epithelial cells, which would modulate the shorter C12 to C16 Cer, this might be the reason for the divergent findings.

To conclude, our work together with the findings of Baduva and colleagues indicates that Ac is unlike Cer synthase 2 or sphingomyelinase not significantly interfering with epithelial homeostasis.

Nevertheless, during *C. rodentium* induced colitis an enhanced epithelial damage was observed in mice with global Ac deficiency (Fig. 7). To investigate whether epithelial cell derived Ac is critical for epithelial barrier function in response to gut infection, mice with epithelial specific deletion of Ac were challenged with *C. rodentium*. Similar to the findings under homeostasis, the loss of Ac in epithelial cells did not alter course and outcome of the gut infection (Fig. 9). Potentially neutral ceramidase, another ceramidase located at the plasma membrane and also highly expressed in the epithelium, compensates for the loss of Ac [139, 187]. Taken together, Ac function in epithelial cells is dispensable for barrier function and host defense and is therefore less suitable as a target for therapeutic approaches with respect to the intestinal epithelium. In turn, the epithelial defects detected in Ac^{flox} creER KO mice upon *C. rodentium* infection might rather be a secondary effect due to pro-inflammatory immune reactions, especially since a tremendous influx of immune cells into the colonic tissue was detected (Fig. 7).

A variety of innate immune cells surveil the intestine, recruit adaptive immune cells by cytokine release or directly kill bacteria, which is associated with collateral tissue damage [5]. Innate immune cells including granulocytes, typically neutrophils, macrophages, dendritic cells (DCs) and innate lymphoid cells (ILCs), mediate the early response to incoming bacteria [5]. In this work, the role of Ac and accordingly Cer accumulation in innate immune cells was investigated, more specifically in macrophages and granulocytes (Fig. 11). In previous studies, where Cer enrichment in peritoneal macrophages was induced by fueling the *de novo* synthesis together with LPS stimulation *ex vivo*, TNFα and IL-1β production was elevated [188]. Accordingly, reduced IL-1β and TNFα production was observed in LPS stimulated macrophages after inhibition of the Cer producing enzyme acid sphingomyelinase (Asm) *in vitro* [138]. Additionally, using the same Asm inhibitor, the sphingomyelin analogue SMA-7, decreased levels of IL-1β and TNFα were detected in colonic tissue along with an attenuated pathology in DSS induced colitis [138]. In the present work, a mouse model was used in which specifically macrophages and granulocytes were deficient in the Cer degrading enzyme Ac (Fig. 11). During bacterial colitis, the lack of Ac in these cells did not affect colonic IL-1β and TNFα levels and was accompanied with moderately enhanced colon pathology (Fig. 12, Fig. 13). Stimulation of sphingolipid *de novo* synthesis together with LPS alters IL-1β and TNFα formation [188], which represents a difference from the data described here. *De novo* synthesis was fueled by addition of palmitate, needed for the first enzymatic step in sphingolipid synthesis [188].

By adding the precursor for the formation of sphingolipids, not only *de novo* synthesis but also downstream sphingolipid pathways are influenced [102]. In fact, not only Cer levels, but also S1P levels were enhanced after palmitate and LPS stimulation [188]. Consequently, the pro-inflammatory cytokine production by macrophages might be mediated by other sphingolipids, such as the signaling molecule S1P. Palmitate/LPS stimulation led to simultaneous Cer and S1P upregulation [188]. However, Ac acts in the sphingolipid pathway between Cer and S1P [102]. Thus, a different Cer/S1P ratio is probably present upon Ac deficiency compared with palmitate stimulation. This could be a reason for the different results in terms of macrophage function. Furthermore, Asm inhibition was linked to reduced pro-inflammatory cytokine production of LPS stimulated macrophages *in vitro* [138]. Since Asm is degrading sphingomyelin to Cer, this finding could also be attributed to sphingomyelin accumulation or an altered sphingomyelin/Cer ratio [138]. This sphingomyelin/Cer ratio is likely to be different from Ac deficiency, which may explain the differential effects on macrophage function. In summary, the macrophage response to bacterial infection is not dependent on Ac activity, but may be influenced by other sphingolipid mediators. Additionally, we investigated the function of Ac in macrophages *in vivo* with a more natural pathogen-macrophage interaction, in contrast to the LPS stimulation *in vitro* [138, 188].

With regard to the study where the Asm inhibitor is applied systemically *in vivo* [138], it cannot be excluded that secondary effects on macrophages or other cells cause the downregulation of pro-inflammatory cytokines. The advantage of the present study is that Ac function was investigated in a macrophage- and granulocyte-specific manner. Therefore, the observations can be linked to the function of Ac in these cells directly.

Interestingly, treatment of mice with amitriptyline, a potent Asm inhibitor, resulted apart from sphingomyelin also in the accumulation of Cer in colonic tissue during *C. rodentium* infection, probably due to the partial inhibition of Ac by amitriptyline [83]. Similar to our results, the macrophage response in the colon of amitriptyline treated mice was not altered in response to *C. rodentium* induced colitis [83]. This corroborates the finding that Ac activity in macrophages plays a minor role in host defense against bacterial infection of the gut. In line with that, Espaillat *et al.* showed in a similar mouse strain with Ac ablation under the control of the lysozyme 2 promoter, that Ac deletion in macrophages and granulocytes does not affect macrophage recruitment to the colon in chemically induced intestinal inflammation [146]. This allows to broaden the previous conclusion by stating that Ac generally appears to have little influence on macrophages in the context of intestinal inflammation.

Regarding the impact of Ac on neutrophil function, we demonstrated that *C. rodentium* induced colitis was only slightly altered upon Ac ablation in granulocytes and macrophages. In Ac^{flox} LysMcre KO mice an in tendency higher histopathological score including modestly

enhanced neutrophil infiltration into the colon was observed (Fig. 12). Another study demonstrated that exogenous synthetic C2-Cer treatment blocks phagocytic properties of human granulocytes [189]. In contrast to that, intrinsic Cer accumulation enhanced human neutrophil mediated killing of *E. coli in vitro* and Sitrin *et al.* found Cer was necessary for human neutrophil orientation towards the chemotactic agent fMLP (N-formylmethionine-leucyl-phenylalanine) [190, 191]. In the present work, Ac deficiency in macrophages and neutrophils resulted in a slightly enhanced influx of neutrophils into the colon (Fig. 12). This finding together with study of Sitrin and colleagues suggests that Ac deficiency and concomitant Cer accumulation might modulate neutrophilic chemotaxis. Killing ability of neutrophils and macrophages towards *C. rodentium* is putatively unaffected by Ac deficiency, since a comparable *C. rodentium* load was detected in Ac^{flox} LysMcre WT and KO animals (Fig. 11). These findings do not suggest a significant loss of phagocytic activity of Ac deficient neutrophils and macrophages, as is the case for neutrophils with exogenous C2 administration [189]. This could be the result of different properties between intrinsically produced, naturally occurring Cer in Ac^{flox} LysMcre KO animals compared with exogenous, synthetic C2-Cer. Nevertheless, intrinsic Cer enrichment promoted bacterial killing by neutrophils *in vitro* [190]. Naturally, other immune cells and the epithelial barrier are present alongside neutrophils in the colon [5]. Therefore, the contact between neutrophils and bacteria and consequently the killing might occur to a different extent *in vivo* than *in vitro*. Taken together, we demonstrated that the neutrophil response is to a limited extent dependent on Ac activity in bacterial infection.

As mentioned above, Espaillat and colleagues used a similar mouse strain with lysozyme 2 dependent Ac depletion in DSS induced colitis [146]. Absence of Ac in macrophages and neutrophils attenuated colon pathology during DSS colitis, along with reduced colonic infiltration of neutrophils [146]. However, in *C. rodentium* infection, colitis was moderately altered with an in tendency higher histopathological score and slightly elevated neutrophil infiltration in Ac^{flox} LysMcre KO mice (Fig. 12). In DSS colitis, the gut architecture is chemically destroyed and tissue damage leads to immune cell recruitment, while in the colitis model used here, intestinal inflammation is elicited by a genuine immune response targeted at the natural murine enteropathogen *C. rodentium* [81, 82, 192]. During *C. rodentium* infection, typically a T_h1/T_h17 response is initiated, while in DSS colitis commonly T_h1 cells are induced and regulatory IL-10 levels are enhanced [81, 82, 192]. T_h17 derived IL-17 is known for its neutrophil recruiting and activating properties, which may indicate one reason for a differential neutrophil reactivity between the two colitis models, and thus the disparity in the outcomes [88]. In fact, Espaillat *et al.* found reduced IL-17 levels in colonic tissue upon Ac deletion in macrophages and neutrophils [146], whereas in *C. rodentium* infection colonic IL-17 levels were not affected in Ac^{flox} LysMcre KO mice

(Fig. 13). How Ac depletion in macrophages and neutrophils relates to reduced IL-17 levels in DSS colitis remains to be fully elucidated. To conclude, Ac depletion in neutrophils and macrophages has a minor influence in bacterial gut infection. Consequently, Ac activity is dispensable for the host defense mediated by these innate immune cells and cannot be utilized for potential therapeutic interventions.

Other innate immune cells, such as DCs and ILCs, particularly the T_h17-like ILC3s, are additional cells that contribute to combating pathogenic bacterial colonization of the gut, through antigen presentation to T cells and cytokine secretion [5]. The role of Ac in ILC and DC mediated immunity was not addressed here and would be of interest for future studies.

Apart from the innate immunity, T cells as important players of the adaptive immunity mediate antigen specific protection against gut infection [5]. T cell specific Ac deficiency led to aggravated *C. rodentium* mediated colitis with enhanced tissue damage (Fig. 15). Although $CD4^+$ and $CD8^+$ T cell infiltration into the colonic lamina propria was not affected by the loss of Ac expression in T cells, the elevated IFNγ and IL-17 levels in the colonic tissue of Ac^{flox} CD4cre KO mice indicated an altered T cell response (Fig. 16, Fig. 17, Fig. 18). Consistent with that, enhanced T cell activation was observed with elevated IFNγ and IL-17 production by colonic $CD4^+$ T cells (Fig. 19, Fig. 23, Fig. 25). Nevertheless, this T cell response did not interfere with pathogen clearance, as *C. rodentium* loads were independent of Ac expression, and thus rather prompts to more collateral tissue damage in the host (Fig. 14).

These results are in line with previous work from our group, showing that systemic Asm inhibition by amitriptyline with accumulation of sphingomyelin and Cer increases the susceptibility to *C. rodentium* induced colitis with enhanced T_h1 and T_h17 reactivity in the colon [83]. Additionally, while amitriptyline treatment caused reduced colonic T_{reg} frequencies [83], the T_{reg} response was not dependent on Ac activity, as demonstrated by similar T_{reg} frequencies in gut infection (Fig. 30). Similar to the present study, Hose *et al.* did not detect significant differences in tumor infiltrating T_{regs} upon Ac deficiency in a mouse model using melanoma transplants [118]. In contrast to the amitriptyline-mediated reduction of colonic T_{regs} in gut infection, genetic Asm deficiency enhanced the T_{reg} response in the setting of melanoma [118]. However, it cannot be excluded that the tumor environment in contrast to the pro-inflammatory milieu in gut infection differentially acts on T_{reg} induction. Our work together with the findings in the melanoma study demonstrates that Ac deletion is independently of the environment not interfering with T_{reg} function. Therefore, Asm mediated alteration in the T_{reg} induction, might be dependent on Ac/Cer independent factors, such as sphingomyelin and might be further determined by the surrounding cytokine milieu.

The recent tumor study by Hose and colleagues revealed some features with regard to Ac function in T cells that corroborate our findings in intestinal infection. In the study, T cell specific Ac deficiency resulted in reduced tumor growth and elevated IFNγ and granzyme B (GrzB) production of $CD4^+$ and $CD8^+$ tumor infiltrating lymphocytes [118]. This is consistent with the enhanced T_h1 response as well as in tendency more frequent GrzB producing $CD4^+$ and $CD8^+$ CTLs in the colon identified in this work (Fig. 25, Fig. 27, Fig. 28). Consequently, Ac deficiency robustly induces inflammatory and cytotoxic properties in T cells regardless of the environment. On the one hand, this could be used to fight tumor progression, but on the other hand, it also indicates possible side effects caused by excessive T_h1, $CD4^+$ and $CD8^+$ CTL responses.

Work by Sofi and colleagues using a T cell transfer mediated colitis with Cer synthase 6 deletion in T cells found an attenuated intestinal pathology with a reduced T_h1 and T_h17 response in the colon [142]. This is in keeping with the enhanced colonic T_h1 and T_h17 response observed when the Cer degrading enzyme Ac is lacking (Fig. 23, Fig. 25). Ceramide synthase 6 deficient $CD4^+$ T cells show a reduced IFNγ production after alloantigen stimulation *in vitro*, albeit this was not observed in case of Cer synthase 4 deficiency [142]. There are six different Cer synthases, which have a differential preference to produce Cer of different chain lengths [142]. Ceramide synthase 6 synthesizes C16-Cer, while Cer synthase 4 primarily produces C18- and C20-Cer, which might account for the divergent T cell mediated phenotypes [142]. As stated earlier, Ac possesses a substrate preference for Cer species between a chain length of C12 and C16 [104, 186]. In line with that, C16-Cer was the most abundant Cer in stimulated Ac depleted $CD4^+$ and $CD8^+$ T cells [118]. This is in keeping with the consistencies in our work on Ac and the Cer synthase 6 study by Sofi *et al.*, and the differential findings with regard to Cer synthase 4. Thus, distinct Cer species might have divergent roles in T cell function, with C16-Cer promoting pro-inflammatory T cell differentiation. On the contrary, systemic Cer synthase 6 deficiency (and reduction in Cer) was detrimental in DSS induced colitis [141]. This is however likely not due to T cell mediated pathology, but enhanced immune cell migration, predominantly neutrophils, in response to the strong tissue damage and elevated S1P levels observed in this model [141]. To sum up, Ac mediated control of C16-Cer seems to be an important checkpoint to control T_h1 and T_h17 reactivity.

Enhanced $CD4^+$ and $CD8^+$ CTL responses upon Ac deficiency and Cer accumulation are further consistent with reduced ($CD8^+$) CTL cytotoxicity observed along with decreased Cer levels in Asm KO mice [193]. On the contrary, Hoek *et al.* found in a T cell transfer colitis model, that GrzB deficient $CD4^+$ T cells also exacerbated immunopathology in colonic tissue, accompanied by an enhanced T_h17 response [173]. Similarly, global GrzB knockout aggravated *C. rodentium* induced colitis with elevated T_h17 levels in spleen and colon [173].

Albeit we demonstrated elevated $CD4^+$ and $CD8^+$ $GrzB^+$ T cell activity along with a stronger intestinal pathology, the work by Hoek and colleagues indicates, that GrzB is important to control intestinal inflammation. This relationship is similar to the regulation of the T_h1 response, where a lack of IFNγ is detrimental in *C. rodentium* induced colitis, but an overshooting T_h1 reactivity is aggravating intestinal inflammation as well, highlighting the necessity of fine-tuned effector T cell reactions [81, 83]. In turn, both extremes, the lack of GrzB and overshooting GrzB responses mediate tissue damage.
In conclusion, Ac activity in T cells importantly keeps pro-inflammatory T_h1, T_h17 and $CD4^+/CD8^+$ CTL reactivity in check and prevents immunopathology in the intestine. Potentially, this protective role of Ac in T cells could be exploited by exogenous administration of Ac to counteract inflammation in intestinal diseases. However, this needs to be investigated in more detail in the future. Among other questions, it is necessary to clarify whether increased Ac activity can also mediate immunosuppression.

T cell function in presence and absence of Ac was further investigated in the spleen, which is often used as proxy in experimental colitis to assess systemic immune responses. In the present study a stronger $CD4^+$ CTL, $CD8^+$ CTL, T_h1 and T_h17 response was found to emerge in the spleen, demonstrating that Ac activity in T cells is important to control pro-inflammatory T cell reactivity not only in the intestine but also beyond, in peripheral organs (Fig. 23, Fig. 25, Fig. 27, Fig. 28). This highlights the systemic regulatory function of intrinsic Ac expression in T cells during intestinal inflammation. It further indicates that a reduction of Ac activity in T cells in putative therapeutic approaches may lead to side effects.

The loss of Ac resulting in abnormal T cell activity and inflammation suggests that Cer under the control of Ac is a critical rheostat in T cell activation and that a precise balance is required to drive appropriate T cell responses. Well in line, deletion of Cer synthase 6, led to disrupted T cell receptor (TCR) signaling with impaired zeta chain associated protein kinase 70 (ZAP-70) and protein kinase CΘ expression and consequently attenuated T cell transfer colitis and graft-versus host disease [142]. In keeping with that, Ac deletion in primary T cells and concomitant intrinsic Cer accumulation increased TCR signaling and T cell activation [118]. Ceramide enrichment and TCR clustering was detected at the immunological synapse along with phosphorylation of the TCR downstream molecules ZAP-70 and phospholipase Cγ [118]. On the contrary, in a leukemic T cell line, exogenous treatment with Ac was associated with increased activation of TCR downstream molecules [184]. These divergent results could stem from the use of a cancer cell line compared to primary cells. Enhanced TCR signaling in Ac deficient T cells is therefore likely to cause overreactive T_h1, T_h17 and $CD4^+/CD8^+$ CTL responses in *C. rodentium* infection as well.

Considering now the T_h1 and T_h17 differentiation of Ac depleted T cells, where Cer enrichment and also TCR engagement is given, there is nevertheless no increase in the *in vitro* differentiation of T_h1 or T_h17 cells compared to WT T cells. This, together with the similar $CD4^+$ T cell abundance in Ac^{flox} CD4cre WT and KO mice (Fig. 17, Fig. 18), suggests that Ac might control the development of T_h1 and T_h17 cells by additional factors. Hence, to shed light on the divergent regulation in absence and presence of Ac, colonic $CD4^+$ T cells were analyzed during *C. rodentium* infection on transcriptional level, revealing distinct differentially expressed genes.

Besides others, the splicing repressor heterogeneous nuclear ribonucleoprotein H3 (Hnrnph3) was found to be downregulated in Ac deficient $CD4^+$ T cells, suggesting an upregulation of alternative splicing (Fig. 31) [176]. Sphingolipids were shown to influence alternative splicing. Exogenous Cer treatment of lung cancer cells inhibited alternative splicing and mediated apoptosis, albeit in a pro-monocytic cell line blocking of Cer synthesis was accompanied with a downregulation in differential splicing of caspase 2 (with both pro- and anti-apoptotic effects) [194, 195]. However, the precise role of Cer and Ac in alternative splicing and the importance for cellular functions is poorly understood. In turn, the involvement of Ac/Cer regulated alternative splicing and its effects on T cell function is unknown, although alternative splicing in general has been investigated in T cells. As such, immunosuppressive functions of $FoxP3^+$ T_{regs} are repressed by overexpression of Hnrnpf and FoxP3 crosstalk [196]. Albeit, Hnrnph3 and Hnrnpf belong to the same family of splicing repressors, the same study demonstrated that Hnrnph3 in contrast to Hnrnpf is not interacting with FoxP3, suggesting a distinct regulation of this repressor in T cells [196]. In myeloid leukemia cells, binding of Hnrnph3 resulted in upregulation of heat shock protein 70 and in turn to pro-inflammatory responses [197]. This stands in contrast to downregulation of Hnrnph3 and the pro-inflammatory T cell responses observed here, which might be due to the different cell type and the discrepancy between a cancer cell line and primary cells. In another study, increased levels of Hnrnph3 have been associated with impaired T cell development, highlighting the importance of Hnrnph3 regulation and alternative splicing in T cells [176]. To conclude, Ac deficiency putatively modulates alternative splicing in $CD4^+$ T cells, but further studies are needed to understand how Hnrnph3 repression influences T cell function.

The gene of protein-L-isoaspartate (D-aspartate) O-methyltransferase domain containing 2 (Pcmtd2) was downregulated in Ac depleted $CD4^+$ T cells (Fig. 31). Pcmtd2 is a protein containing a suppressor of cytokine signaling (SOCS)-box, with which it binds cullin 5 ubiquitin ligase [177]. Crosstalk of SOCS proteins and cullin 5 is initiated upon cytokine sensing to exert regulatory responses, as such T_{regs} express high levels of another SOCS protein, SOCS1 [178]. Ablation of SOCS1 promotes induction of IFNγ producing $CD4^+$ and

$CD8^+$ T cells and enhanced anti-tumor responses [178]. Additionally SOCS1 deletion in T_{regs} induces polarization into a T_h1 or T_h17 like phenotype [178]. Studies on the role of the SOCS protein Pcmtd2 in T cells are lacking, albeit depletion of its binding partner cullin 5 led to T helper mediated lung inflammation involving IL-4, IL-5 and IL-9 cytokines [198]. Interestingly, in a very recent, not peer reviewed study by Liao and colleagues, Pcmtd2 deficiency in $CD8^+$ T cells increased GrzB and IFNγ production similar to cullin 5 knockout, which was linked to enhanced TCR and IL-2 signaling [199]. In conclusion, reduced *Pcmtd2* expression upon Ac deficiency might be similar to SOCS1 downregulation responsible for the enhanced pro-inflammatory T cell function in gut infection.

The cytochrome c oxidase assembly factor 5 (*Coa5*) was elevated in Ac depleted $CD4^+$ T cells (Fig. 31). Coa5 is involved in the formation of cytochrome c oxidase or complex IV, which is the rate-limiting enzyme of the mitochondrial respiratory chain [182]. Upon T cell activation, mitochondria translocate to the immune synapse and their respiratory chain exerts oxidative phosphorylation (OXPHOS) [181]. OXPHOS is important in initial T cell activation and T cell differentiation [181]. Little is known about Coa5 with regard to T cell function. Yet, another complex IV assembly factor, COX10 (cytochrome c oxidase assembly factor heme A:farnesyltransferase COX10), revealed critical functions of complex IV in T cells [181]. Interestingly, diminished OXPHOS due to COX10 deficiency and complex IV dysfunction decreased the ability of $CD4^+$ T cells to differentiate into T_h1 and T_h17 cells [181]. In our work, gene expression of complex IV subunits was unlike *Coa5* not found to be differentially expressed between Ac KO and WT $CD4^+$ T cells (data not shown). Yet, Tarasenko *et al.* also demonstrated that complex IV activity is upregulated in response to T cell activation without increasing its synthesis [181]. In turn, upregulation of *Coa5* in Ac deficient T cells might influence OXPHOS and subsequently T cell differentiation similar to COX10. Nevertheless, if ablation of Ac would (via TCR signaling or directly) enhance *Coa5* expression and Coa5 alters OXPHOS and T cell differentiation, one would expect an enhanced T_h1 and T_h17 differentiation *in vitro*. Thus, upregulation of *Coa5* expression *in vivo* might putatively be a downstream effect of another Ac/Cer dependent signal.
The relationship between Cer and complex IV has previously been investigated, showing that mitochondrial Cer can stimulate or inhibit complex IV activity and OXPHOS depending on its chain length [200]. However, these studies were mainly conducted in cells of liver or heart and not in immune cells. Therefore, further research is needed to clarify, whether Ac and Cer interfere with Coa5 and if this is truly triggering enhanced pro-inflammatory T cell differentiation [200].

Finally, *Ifnar2* the interferon alpha/beta receptor 2 gene was upregulated in Ac deficient $CD4^+$ T cells (Fig. 31) [179]. The Ifnar2 protein is part of the dimeric Ifnar [179, 201]. Usually Ifnar consists of both Ifnar1 and Ifnar2 subunits, which bind different parts of IFNα and β

[179, 201]. Although also antiviral activities of Ifnar2 homodimers have been demonstrated, with IFNβ being able to interact with Ifnar2 only [179, 201, 202]. Ifnar is known for its antiviral signaling, albeit it has also been linked to *C. rodentium* infection, where global Ifnar KO attenuated colitis [179, 180]. Interestingly, the Cer derived glycosphingolipid galabiosylceramide (Gb2) was reported to bind and mediate Ifnar signaling [203]. Conversely, Ac deficiency might modulate $CD4^+$ T cell function via Cer and Ifnar2 signaling. In turn, Ac activity in T cells potentially protects from intestinal inflammation after *C. rodentium* infection by regulating *Ifnar2* expression. Interestingly, another study revealed an association between *Ifnar2* expression and T_h17 cells, showing reduced IL-17 production by $CD4^+$ T cells in the gut mucosa of *Ifnar2*$^{-/-}$ mice in response to a model antigen [204]. The increased T_h17 proportions and concurrent increased *Ifnar2* expression of $CD4^+$ T cells in the absence of Ac observed here, possibly indicate that the T_h17 response is influenced by Ac via type I interferon signaling. Therefore, type I interferons could be the other important signal which is negatively associated with Ac expression influencing T cell differentiation.

Taken together, several mechanisms were highlighted, including alternative splicing, OXPHOS, Pcmtd2, and Ifnar2 signaling by which Ac could alter T cell function and in turn the host response to *C. rodentium* infection. However, further research is needed to accurately unravel how these pathways are modulated by Ac and Cer and how they may influence each other.

The present study demonstrated that cell-intrinsic Ac plays a minor role in epithelial cells, macrophages and granulocytes and thus Ac tends not to be a suitable therapeutic target in these cells. Additionally, Ac might have further functions in gut infection, as in the above-mentioned ILCs and DCs, but also in immune cell migration, thereby potentially further influencing the host defense. Acid ceramidase expression in T cells during infection with an A/E enteropathogen importantly protects from overreactive pro-inflammatory T_h1, T_h17 and CTL responses in the intestine and beyond. This might be mediated via Ifnar2 and TCR signaling. Further processes including OXPHOS, alternative splicing and Pcmtd2 signaling could be involved, which remains to be further elucidated. Overall, the loss of Ac in T cells led to increased inflammation without promoting bacterial clearance. Conversely, increased Ac activity in T cells could cause immunosuppression, which might be detrimental in intestinal infection. Additionally, in putative therapies targeting Ac in T cells systemically, side effects cannot be excluded. Yet, an increase in Ac activity in inflammatory diseases might be able to limit T cell mediated (intestinal) inflammation.

7 References

1. Treuting, P.M., Arends, M.J., Dintzis, S.M., *11 - Upper Gastrointestinal Tract & 12 - Lower Gastrointestinal Tract*, in *Comparative Anatomy and Histology*, P.M. Treuting, Dintzis, S.M., Montine, K.S., Editor. 2018, Mica Haley, Academic Press: London UK, Oxford UK, San Diego USA, Cambridge USA. p. 191-228.
2. Mowat, A.M. and W.W. Agace, *Regional specialization within the intestinal immune system.* Nat Rev Immunol, 2014. **14**(10): p. 667-85.
3. Brestoff, J.R. and D. Artis, *Commensal bacteria at the interface of host metabolism and the immune system.* Nat Immunol, 2013. **14**(7): p. 676-84.
4. Cummings, J.H. and G.T. Macfarlane, *The control and consequences of bacterial fermentation in the human colon.* J Appl Bacteriol, 1991. **70**(6): p. 443-59.
5. Perez-Lopez, A., et al., *Mucosal immunity to pathogenic intestinal bacteria.* Nat Rev Immunol, 2016. **16**(3): p. 135-48.
6. Zhou, H., L. Wang, and F. Liu, *Immunological Impact of Intestinal T Cells on Metabolic Diseases.* Front Immunol, 2021. **12**: p. 639902.
7. Peterson, L.W. and D. Artis, *Intestinal epithelial cells: regulators of barrier function and immune homeostasis.* Nat Rev Immunol, 2014. **14**(3): p. 141-53.
8. Chaplin, D.D., *Overview of the immune response.* J Allergy Clin Immunol, 2010. **125**(2 Suppl 2): p. S3-23.
9. Sakowska, J., et al., *Autoimmunity and Cancer-Two Sides of the Same Coin.* Front Immunol, 2022. **13**: p. 793234.
10. Elkoshi, Z., *Cancer and Autoimmune Diseases: A Tale of Two Immunological Opposites?* Front Immunol, 2022. **13**: p. 821598.
11. Holmes, R. and R.W. Lobley, *Intestinal brush border revisited.* Gut, 1989. **30**(12): p. 1667-78.
12. Barker, N., et al., *Identification of stem cells in small intestine and colon by marker gene Lgr5.* Nature, 2007. **449**(7165): p. 1003-7.
13. Noah, T.K., B. Donahue, and N.F. Shroyer, *Intestinal development and differentiation.* Exp Cell Res, 2011. **317**(19): p. 2702-10.
14. Johansson, M.E., et al., *The inner of the two Muc2 mucin-dependent mucus layers in colon is devoid of bacteria.* Proc Natl Acad Sci U S A, 2008. **105**(39): p. 15064-9.
15. Okumura, R. and K. Takeda, *Roles of intestinal epithelial cells in the maintenance of gut homeostasis.* Exp Mol Med, 2017. **49**(5): p. e338.
16. Tollin, M., et al., *Antimicrobial peptides in the first line defence of human colon mucosa.* Peptides, 2003. **24**(4): p. 523-30.
17. Mantis, N.J., N. Rol, and B. Corthesy, *Secretory IgA's complex roles in immunity and mucosal homeostasis in the gut.* Mucosal Immunol, 2011. **4**(6): p. 603-11.
18. Johansen, F.E. and C.S. Kaetzel, *Regulation of the polymeric immunoglobulin receptor and IgA transport: new advances in environmental factors that stimulate pIgR expression and its role in mucosal immunity.* Mucosal Immunol, 2011. **4**(6): p. 598-602.
19. Farquhar, M.G. and G.E. Palade, *Junctional complexes in various epithelia.* J Cell Biol, 1963. **17**(2): p. 375-412.
20. Buckley, A. and J.R. Turner, *Cell Biology of Tight Junction Barrier Regulation and Mucosal Disease.* Cold Spring Harb Perspect Biol, 2018. **10**(1).
21. Turner, J.R., *Intestinal mucosal barrier function in health and disease.* Nat Rev Immunol, 2009. **9**(11): p. 799-809.
22. Van Itallie, C.M., et al., *The density of small tight junction pores varies among cell types and is increased by expression of claudin-2.* J Cell Sci, 2008. **121**(Pt 3): p. 298-305.
23. Watson, C.J., et al., *Interferon-gamma selectively increases epithelial permeability to large molecules by activating different populations of paracellular pores.* J Cell Sci, 2005. **118**(Pt 22): p. 5221-30.

24. Wang, F., et al., *Interferon-gamma and tumor necrosis factor-alpha synergize to induce intestinal epithelial barrier dysfunction by up-regulating myosin light chain kinase expression.* Am J Pathol, 2005. **166**(2): p. 409-19.
25. Rieger, M.A. and T. Schroeder, *Hematopoiesis.* Cold Spring Harb Perspect Biol, 2012. **4**(12).
26. Trabanelli, S., et al., *Human innate lymphoid cells (ILCs): Toward a uniform immune-phenotyping.* Cytometry B Clin Cytom, 2018. **94**(3): p. 392-399.
27. Boyapati, R.K., et al., *Gut mucosal DAMPs in IBD: from mechanisms to therapeutic implications.* Mucosal Immunol, 2016. **9**(3): p. 567-82.
28. Akira, S., S. Uematsu, and O. Takeuchi, *Pathogen recognition and innate immunity.* Cell, 2006. **124**(4): p. 783-801.
29. Steimle, A., I.B. Autenrieth, and J.S. Frick, *Structure and function: Lipid A modifications in commensals and pathogens.* Int J Med Microbiol, 2016. **306**(5): p. 290-301.
30. Steinbach, E.C. and S.E. Plevy, *The role of macrophages and dendritic cells in the initiation of inflammation in IBD.* Inflamm Bowel Dis, 2014. **20**(1): p. 166-75.
31. Parkin, J. and B. Cohen, *An overview of the immune system.* Lancet, 2001. **357**(9270): p. 1777-89.
32. Mantovani, A., et al., *Neutrophils in the activation and regulation of innate and adaptive immunity.* Nat Rev Immunol, 2011. **11**(8): p. 519-31.
33. Mantovani, A., et al., *The chemokine system in diverse forms of macrophage activation and polarization.* Trends Immunol, 2004. **25**(12): p. 677-86.
34. Najafi, M., B. Farhood, and K. Mortezaee, *Contribution of regulatory T cells to cancer: A review.* J Cell Physiol, 2019. **234**(6): p. 7983-7993.
35. Curtsinger, J.M. and M.F. Mescher, *Inflammatory cytokines as a third signal for T cell activation.* Curr Opin Immunol, 2010. **22**(3): p. 333-40.
36. Wesa, A.K. and A. Galy, *IL-1 beta induces dendritic cells to produce IL-12.* Int Immunol, 2001. **13**(8): p. 1053-61.
37. Panda, S.K. and M. Colonna, *Innate Lymphoid Cells in Mucosal Immunity.* Front Immunol, 2019. **10**: p. 861.
38. Murphy, K.P., and C. Janeway, *Janeway's immunobiology (8. edition)*. 2012, Garland Science: NY, USA and Abingdon, UK. p. 294-316.
39. Luckheeram, R.V., et al., *CD4(+)T cells: differentiation and functions.* Clin Dev Immunol, 2012. **2012**: p. 925135.
40. Takeuchi, A., et al., *CRTAM determines the CD4+ cytotoxic T lymphocyte lineage.* J Exp Med, 2016. **213**(1): p. 123-38.
41. Macatonia, S.E., et al., *Dendritic cells produce IL-12 and direct the development of Th1 cells from naive CD4+ T cells.* J Immunol, 1995. **154**(10): p. 5071-9.
42. Neurath, M.F., S. Finotto, and L.H. Glimcher, *The role of Th1/Th2 polarization in mucosal immunity.* Nat Med, 2002. **8**(6): p. 567-73.
43. Nava, P., et al., *Interferon-gamma regulates intestinal epithelial homeostasis through converging beta-catenin signaling pathways.* Immunity, 2010. **32**(3): p. 392-402.
44. Romagnani, S., *Human TH1 and TH2 subsets: regulation of differentiation and role in protection and immunopathology.* Int Arch Allergy Immunol, 1992. **98**(4): p. 279-85.
45. Reynolds, L.A., K.J. Filbey, and R.M. Maizels, *Immunity to the model intestinal helminth parasite Heligmosomoides polygyrus.* Semin Immunopathol, 2012. **34**(6): p. 829-46.
46. Okumura, R. and K. Takeda, *Maintenance of gut homeostasis by the mucosal immune system.* Proc Jpn Acad Ser B Phys Biol Sci, 2016. **92**(9): p. 423-435.
47. Tian, Y., A. Sette, and D. Weiskopf, *Cytotoxic CD4 T Cells: Differentiation, Function, and Application to Dengue Virus Infection.* Front Immunol, 2016. **7**: p. 531.
48. Mittrucker, H.W., A. Visekruna, and M. Huber, *Heterogeneity in the differentiation and function of CD8(+) T cells.* Arch Immunol Ther Exp (Warsz), 2014. **62**(6): p. 449-58.

49. Mucida, D., et al., *Transcriptional reprogramming of mature CD4(+) helper T cells generates distinct MHC class II-restricted cytotoxic T lymphocytes.* Nat Immunol, 2013. **14**(3): p. 281-9.
50. Marshall, N.B. and S.L. Swain, *Cytotoxic CD4 T cells in antiviral immunity.* J Biomed Biotechnol, 2011. **2011**: p. 954602.
51. Barbosa, C.D., et al., *Cytotoxic CD4(+) T cells driven by T-cell intrinsic IL-18R/MyD88 signaling predominantly infiltrate Trypanosoma cruzi-infected hearts.* Elife, 2022. **11**.
52. Workman, C.J., et al., *The development and function of regulatory T cells.* Cell Mol Life Sci, 2009. **66**(16): p. 2603-22.
53. Barnes, M.J. and F. Powrie, *Regulatory T cells reinforce intestinal homeostasis.* Immunity, 2009. **31**(3): p. 401-11.
54. Belkaid, Y., *Regulatory T cells and infection: a dangerous necessity.* Nat Rev Immunol, 2007. **7**(11): p. 875-88.
55. Mills, K.H., *Regulatory T cells: friend or foe in immunity to infection?* Nat Rev Immunol, 2004. **4**(11): p. 841-55.
56. Petri, W.A., Jr., et al., *Enteric infections, diarrhea, and their impact on function and development.* J Clin Invest, 2008. **118**(4): p. 1277-90.
57. Guan, Q., *A Comprehensive Review and Update on the Pathogenesis of Inflammatory Bowel Disease.* J Immunol Res, 2019. **2019**: p. 7247238.
58. Laass, M.W., D. Roggenbuck, and K. Conrad, *Diagnosis and classification of Crohn's disease.* Autoimmun Rev, 2014. **13**(4-5): p. 467-71.
59. Conrad, K., D. Roggenbuck, and M.W. Laass, *Diagnosis and classification of ulcerative colitis.* Autoimmun Rev, 2014. **13**(4-5): p. 463-6.
60. Ananthakrishnan, A.N., *Epidemiology and risk factors for IBD.* Nat Rev Gastroenterol Hepatol, 2015. **12**(4): p. 205-17.
61. Ng, S.C., et al., *Worldwide incidence and prevalence of inflammatory bowel disease in the 21st century: a systematic review of population-based studies.* Lancet, 2017. **390**(10114): p. 2769-2778.
62. Windsor, J.W. and G.G. Kaplan, *Evolving Epidemiology of IBD.* Curr Gastroenterol Rep, 2019. **21**(8): p. 40.
63. Gomes, T.A., et al., *Diarrheagenic Escherichia coli.* Braz J Microbiol, 2016. **47 Suppl 1**(Suppl 1): p. 3-30.
64. Rojas-Lopez, M., et al., *Intestinal Pathogenic Escherichia coli: Insights for Vaccine Development.* Front Microbiol, 2018. **9**: p. 440.
65. Kaper, J.B., J.P. Nataro, and H.L. Mobley, *Pathogenic Escherichia coli.* Nat Rev Microbiol, 2004. **2**(2): p. 123-40.
66. Woodward, S.E., Z. Krekhno, and B.B. Finlay, *Here, there, and everywhere: How pathogenic Escherichia coli sense and respond to gastrointestinal biogeography.* Cell Microbiol, 2019. **21**(11): p. e13107.
67. Mundy, R., et al., *Citrobacter rodentium of mice and man.* Cell Microbiol, 2005. **7**(12): p. 1697-706.
68. Croxen, M.A. and B.B. Finlay, *Molecular mechanisms of Escherichia coli pathogenicity.* Nat Rev Microbiol, 2010. **8**(1): p. 26-38.
69. Khan, M.A., et al., *Toll-like receptor 4 contributes to colitis development but not to host defense during Citrobacter rodentium infection in mice.* Infect Immun, 2006. **74**(5): p. 2522-36.
70. Simmons, C.P., et al., *Impaired resistance and enhanced pathology during infection with a noninvasive, attaching-effacing enteric bacterial pathogen, Citrobacter rodentium, in mice lacking IL-12 or IFN-gamma.* J Immunol, 2002. **168**(4): p. 1804-12.
71. Wiles, S., et al., *Organ specificity, colonization and clearance dynamics in vivo following oral challenges with the murine pathogen Citrobacter rodentium.* Cell Microbiol, 2004. **6**(10): p. 963-72.

72. Wiles, S., et al., *Corrigendum: Organ ‐ specificity, colonization and clearance dynamics in vivo following oral challenges with the murine pathogen Citrobacter rodentium.* Cellular Microbiology, 2005. **7**(3): p. 459-459.
73. Eckmann, L., *Animal models of inflammatory bowel disease: lessons from enteric infections.* Ann N Y Acad Sci, 2006. **1072**: p. 28-38.
74. Mullineaux-Sanders, C., et al., *Citrobacter rodentium-host-microbiota interactions: immunity, bioenergetics and metabolism.* Nat Rev Microbiol, 2019. **17**(11): p. 701-715.
75. Luperchio, S.A. and D.B. Schauer, *Molecular pathogenesis of Citrobacter rodentium and transmissible murine colonic hyperplasia.* Microbes Infect, 2001. **3**(4): p. 333-40.
76. Collins, J.W., et al., *Citrobacter rodentium: infection, inflammation and the microbiota.* Nat Rev Microbiol, 2014. **12**(9): p. 612-23.
77. Zhang, Y., et al., *Glycine Attenuates Citrobacter rodentium-Induced Colitis by Regulating ATF6-Mediated Endoplasmic Reticulum Stress in Mice.* Mol Nutr Food Res, 2021. **65**(15): p. e2001065.
78. Barthold, S.W. and A.M. Jonas, *Morphogenesis of early 1, 2-dimethylhydrazine-induced lesions and latent period reduction of colon carcinogenesis in mice by a variant of Citrobacter freundii.* Cancer Res, 1977. **37**(12): p. 4352-60.
79. Gibson, D.L., et al., *MyD88 signalling plays a critical role in host defence by controlling pathogen burden and promoting epithelial cell homeostasis during Citrobacter rodentium-induced colitis.* Cell Microbiol, 2008. **10**(3): p. 618-31.
80. Gibson, D.L., et al., *Toll-like receptor 2 plays a critical role in maintaining mucosal integrity during Citrobacter rodentium-induced colitis.* Cell Microbiol, 2008. **10**(2): p. 388-403.
81. Higgins, L.M., et al., *Citrobacter rodentium infection in mice elicits a mucosal Th1 cytokine response and lesions similar to those in murine inflammatory bowel disease.* Infect Immun, 1999. **67**(6): p. 3031-9.
82. Mangan, P.R., et al., *Transforming growth factor-beta induces development of the T(H)17 lineage.* Nature, 2006. **441**(7090): p. 231-4.
83. Meiners, J., et al., *Intestinal Acid Sphingomyelinase Protects From Severe Pathogen-Driven Colitis.* Front Immunol, 2019. **10**: p. 1386.
84. Goncalves, N.S., et al., *Critical role for tumor necrosis factor alpha in controlling the number of lumenal pathogenic bacteria and immunopathology in infectious colitis.* Infect Immun, 2001. **69**(11): p. 6651-9.
85. Schreiber, H.A., et al., *Intestinal monocytes and macrophages are required for T cell polarization in response to Citrobacter rodentium.* J Exp Med, 2013. **210**(10): p. 2025-39.
86. Atarashi, K., et al., *Th17 Cell Induction by Adhesion of Microbes to Intestinal Epithelial Cells.* Cell, 2015. **163**(2): p. 367-80.
87. Stockinger, B., *T cell subsets and environmental factors in Citrobacter rodentium infection.* Curr Opin Microbiol, 2021. **63**: p. 92-97.
88. Rubino, S.J., K. Geddes, and S.E. Girardin, *Innate IL-17 and IL-22 responses to enteric bacterial pathogens.* Trends Immunol, 2012. **33**(3): p. 112-8.
89. Wang, Z., et al., *Regulatory T cells promote a protective Th17-associated immune response to intestinal bacterial infection with C. rodentium.* Mucosal Immunol, 2014. **7**(6): p. 1290-301.
90. Ota, N., et al., *IL-22 bridges the lymphotoxin pathway with the maintenance of colonic lymphoid structures during infection with Citrobacter rodentium.* Nat Immunol, 2011. **12**(10): p. 941-8.
91. Maaser, C., et al., *Clearance of Citrobacter rodentium requires B cells but not secretory immunoglobulin A (IgA) or IgM antibodies.* Infect Immun, 2004. **72**(6): p. 3315-24.

92. Poysti, S., et al., *Plasmacytoid dendritic cells regulate host immune response to Citrobacter rodentium induced colitis in colon-draining lymph nodes.* Eur J Immunol, 2021. **51**(3): p. 620-625.
93. Silberger, D.J., C.L. Zindl, and C.T. Weaver, *Citrobacter rodentium: a model enteropathogen for understanding the interplay of innate and adaptive components of type 3 immunity.* Mucosal Immunol, 2017. **10**(5): p. 1108-1117.
94. Li, L., et al., *Cytokine IL-6 is required in Citrobacter rodentium infection-induced intestinal Th17 responses and promotes IL-22 expression in inflammatory bowel disease.* Mol Med Rep, 2014. **9**(3): p. 831-6.
95. Futerman, A.H. and Y.A. Hannun, *The complex life of simple sphingolipids.* EMBO Rep, 2004. **5**(8): p. 777-82.
96. Bartke, N. and Y.A. Hannun, *Bioactive sphingolipids: metabolism and function.* J Lipid Res, 2009. **50 Suppl**(Suppl): p. S91-6.
97. Hannun, Y.A. and L.M. Obeid, *Sphingolipids and their metabolism in physiology and disease.* Nat Rev Mol Cell Biol, 2018. **19**(3): p. 175-191.
98. Mallela, S.K., S. Merscher, and A. Fornoni, *Implications of Sphingolipid Metabolites in Kidney Diseases.* Int J Mol Sci, 2022. **23**(8).
99. Gulbins, E., et al., *Ceramide, membrane rafts and infections.* J Mol Med (Berl), 2004. **82**(6): p. 357-63.
100. Espaillat, M.P., et al., *Ceramide and sphingosine-1-phosphate in cancer, two faces of the sphinx.* Translational Cancer Research, 2015. **4**(5): p. 484-499.
101. Romero-Guevara, R., et al., *Sphingosine 1-phosphate signaling pathway in inner ear biology. New therapeutic strategies for hearing loss?* Front Aging Neurosci, 2015. **7**: p. 60.
102. Gault, C.R., L.M. Obeid, and Y.A. Hannun, *An overview of sphingolipid metabolism: from synthesis to breakdown.* Adv Exp Med Biol, 2010. **688**: p. 1-23.
103. Li, C.M., et al., *The human acid ceramidase gene (ASAH): structure, chromosomal location, mutation analysis, and expression.* Genomics, 1999. **62**(2): p. 223-31.
104. Ferlinz, K., et al., *Human acid ceramidase: processing, glycosylation, and lysosomal targeting.* J Biol Chem, 2001. **276**(38): p. 35352-60.
105. Li, C.M., et al., *Cloning and characterization of the full-length cDNA and genomic sequences encoding murine acid ceramidase.* Genomics, 1998. **50**(2): p. 267-74.
106. Bernardo, K., et al., *Purification, characterization, and biosynthesis of human acid ceramidase.* J Biol Chem, 1995. **270**(19): p. 11098-102.
107. Gatt, S., *Enzymic Hydrolysis and Synthesis of Ceramides.* J Biol Chem, 1963. **238**: p. 3131-3.
108. Gatt, S., *Enzymatic hydrolysis of sphingolipids. I. Hydrolysis and synthesis of ceramides by an enzyme from rat brain.* J Biol Chem, 1966. **241**(16): p. 3724-30.
109. Azuma, N., et al., *Stimulation of acid ceramidase activity by saposin D.* Arch Biochem Biophys, 1994. **311**(2): p. 354-7.
110. Linke, T., et al., *Interfacial regulation of acid ceramidase activity. Stimulation of ceramide degradation by lysosomal lipids and sphingolipid activator proteins.* J Biol Chem, 2001. **276**(8): p. 5760-8.
111. Sugita, M., J.T. Dulaney, and H.W. Moser, *Ceramidase deficiency in Farber's disease (lipogranulomatosis).* Science, 1972. **178**(4065): p. 1100-2.
112. Yu, F.P.S., et al., *Acid ceramidase deficiency: Farber disease and SMA-PME.* Orphanet J Rare Dis, 2018. **13**(1): p. 121.
113. Zhou, J., et al., *Spinal muscular atrophy associated with progressive myoclonic epilepsy is caused by mutations in ASAH1.* Am J Hum Genet, 2012. **91**(1): p. 5-14.
114. Farina, F., et al., *Involvement of caspase-3 and GD3 ganglioside in ceramide-induced apoptosis in Farber disease.* J Histochem Cytochem, 2000. **48**(1): p. 57-62.
115. Park, J.H. and E.H. Schuchman, *Acid ceramidase and human disease.* Biochim Biophys Acta, 2006. **1758**(12): p. 2133-8.
116. Lang, J., et al., *Acid ceramidase of macrophages traps herpes simplex virus in multivesicular bodies and protects from severe disease.* Nat Commun, 2020. **11**(1): p. 1338.

117. Grafen, A., et al., *Use of Acid Ceramidase and Sphingosine Kinase Inhibitors as Antiviral Compounds Against Measles Virus Infection of Lymphocytes in vitro.* Front Cell Dev Biol, 2019. **7**: p. 218.
118. Hose, M., et al., *Cell-intrinsic ceramides determine T cell function during melanoma progression.* Elife, 2022. **11**.
119. Kanto, T., et al., *Ceramide mediates tumor-induced dendritic cell apoptosis.* J Immunol, 2001. **167**(7): p. 3773-84.
120. Duan, R.D. and A. Nilsson, *Metabolism of sphingolipids in the gut and its relation to inflammation and cancer development.* Prog Lipid Res, 2009. **48**(1): p. 62-72.
121. Jenkins, R.W., et al., *Regulation of CC ligand 5/RANTES by acid sphingomyelinase and acid ceramidase.* J Biol Chem, 2011. **286**(15): p. 13292-303.
122. Lapteva, N. and X.F. Huang, *CCL5 as an adjuvant for cancer immunotherapy.* Expert Opin Biol Ther, 2010. **10**(5): p. 725-33.
123. Albeituni, S. and J. Stiban, *Roles of Ceramides and Other Sphingolipids in Immune Cell Function and Inflammation.* Adv Exp Med Biol, 2019. **1161**: p. 169-191.
124. Franchi, L., et al., *Ceramide catabolism critically controls survival of human dendritic cells.* J Leukoc Biol, 2006. **79**(1): p. 166-72.
125. Grassme, H., et al., *Ceramide in bacterial infections and cystic fibrosis.* Biol Chem, 2008. **389**(11): p. 1371-9.
126. Kunz, T.C. and V. Kozjak-Pavlovic, *Diverse Facets of Sphingolipid Involvement in Bacterial Infections.* Front Cell Dev Biol, 2019. **7**: p. 203.
127. Becker, K.A., et al., *Acid Ceramidase Rescues Cystic Fibrosis Mice from Pulmonary Infections.* Infect Immun, 2021. **89**(2).
128. Gardner, A.I., et al., *Recombinant Acid Ceramidase Reduces Inflammation and Infection in Cystic Fibrosis.* Am J Respir Crit Care Med, 2020. **202**(8): p. 1133-1145.
129. Monick, M.M., et al., *Cooperative prosurvival activity by ERK and Akt in human alveolar macrophages is dependent on high levels of acid ceramidase activity.* J Immunol, 2004. **173**(1): p. 123-35.
130. Zhao, D., et al., *Inhibition of acid ceramidase regulates MHC class II antigen presentation and suppression of autoimmune arthritis.* Cytokine, 2020. **135**: p. 155219.
131. Holmgren, J., et al., *Interaction of cholera toxin and membrane GM1 ganglioside of small intestine.* Proc Natl Acad Sci U S A, 1975. **72**(7): p. 2520-4.
132. Bouhet, S., et al., *Mycotoxin fumonisin B1 selectively down-regulates the basal IL-8 expression in pig intestine: in vivo and in vitro studies.* Food Chem Toxicol, 2006. **44**(10): p. 1768-73.
133. Oswald, I.P., et al., *Mycotoxin fumonisin B1 increases intestinal colonization by pathogenic Escherichia coli in pigs.* Appl Environ Microbiol, 2003. **69**(10): p. 5870-4.
134. Cuschieri, J., J. Billgren, and R.V. Maier, *Phosphatidylcholine-specific phospholipase C (PC-PLC) is required for LPS-mediated macrophage activation through CD14.* J Leukoc Biol, 2006. **80**(2): p. 407-14.
135. Fischer, H., et al., *Ceramide as a TLR4 agonist; a putative signalling intermediate between sphingolipid receptors for microbial ligands and TLR4.* Cell Microbiol, 2007. **9**(5): p. 1239-51.
136. Abdel Hadi, L., C. Di Vito, and L. Riboni, *Fostering Inflammatory Bowel Disease: Sphingolipid Strategies to Join Forces.* Mediators Inflamm, 2016. **2016**: p. 3827684.
137. Xiong, Y., et al., *Inhibition of ASM activity ameliorates DSS-induced colitis in mice.* Prostaglandins Other Lipid Mediat, 2019. **140**: p. 26-30.
138. Sakata, A., et al., *Acid sphingomyelinase inhibition suppresses lipopolysaccharide-mediated release of inflammatory cytokines from macrophages and protects against disease pathology in dextran sulphate sodium-induced colitis in mice.* Immunology, 2007. **122**(1): p. 54-64.
139. Snider, A.J., et al., *Loss of neutral ceramidase increases inflammation in a mouse model of inflammatory bowel disease.* Prostaglandins Other Lipid Mediat, 2012. **99**(3-4): p. 124-30.

140. Oertel, S., et al., *Ceramide synthase 2 deficiency aggravates AOM-DSS-induced colitis in mice: role of colon barrier integrity.* Cell Mol Life Sci, 2017. **74**(16): p. 3039-3055.
141. Helke, K., et al., *Ceramide Synthase 6 Deficiency Enhances Inflammation in the DSS model of Colitis.* Sci Rep, 2018. **8**(1): p. 1627.
142. Sofi, M.H., et al., *Ceramide synthesis regulates T cell activity and GVHD development.* JCI Insight, 2017. **2**(10).
143. Scheffel, M.J., et al., *Adoptive Transfer of Ceramide Synthase 6 Deficient Splenocytes Reduces the Development of Colitis.* Sci Rep, 2017. **7**(1): p. 15552.
144. Zeidan, Y.H., et al., *Acid ceramidase but not acid sphingomyelinase is required for tumor necrosis factor-alpha-induced PGE2 production.* J Biol Chem, 2006. **281**(34): p. 24695-703.
145. Maines, L.W., et al., *Suppression of ulcerative colitis in mice by orally available inhibitors of sphingosine kinase.* Dig Dis Sci, 2008. **53**(4): p. 997-1012.
146. Espaillat, M.P., et al., *Loss of acid ceramidase in myeloid cells suppresses intestinal neutrophil recruitment.* FASEB J, 2018. **32**(5): p. 2339-2353.
147. Love, M.I., W. Huber, and S. Anders, *Moderated estimation of fold change and dispersion for RNA-seq data with DESeq2.* Genome Biol, 2014. **15**(12): p. 550.
148. Lawrence, M., et al., *Software for computing and annotating genomic ranges.* PLoS Comput Biol, 2013. **9**(8): p. e1003118.
149. Kim, D., B. Langmead, and S.L. Salzberg, *HISAT: a fast spliced aligner with low memory requirements.* Nat Methods, 2015. **12**(4): p. 357-60.
150. Kim, D., et al., *Graph-based genome alignment and genotyping with HISAT2 and HISAT-genotype.* Nat Biotechnol, 2019. **37**(8): p. 907-915.
151. Seibler, J., et al., *Rapid generation of inducible mouse mutants.* Nucleic Acids Res, 2003. **31**(4): p. e12.
152. Hayashi, S. and A.P. McMahon, *Efficient recombination in diverse tissues by a tamoxifen-inducible form of Cre: a tool for temporally regulated gene activation/inactivation in the mouse.* Dev Biol, 2002. **244**(2): p. 305-18.
153. Mattioni, T., J.F. Louvion, and D. Picard, *Regulation of protein activities by fusion to steroid binding domains.* Methods Cell Biol, 1994. **43 Pt A**: p. 335-52.
154. Picard, D., *Regulation of protein function through expression of chimaeric proteins.* Curr Opin Biotechnol, 1994. **5**(5): p. 511-5.
155. el Marjou, F., et al., *Tissue-specific and inducible Cre-mediated recombination in the gut epithelium.* Genesis, 2004. **39**(3): p. 186-93.
156. Clausen, B.E., et al., *Conditional gene targeting in macrophages and granulocytes using LysMcre mice.* Transgenic Res, 1999. **8**(4): p. 265-77.
157. Gunther, A., et al., *The acid ceramidase/ceramide axis controls parasitemia in Plasmodium yoelii-infected mice by regulating erythropoiesis.* Elife, 2022. **11**.
158. Lee, P.P., et al., *A critical role for Dnmt1 and DNA methylation in T cell development, function, and survival.* Immunity, 2001. **15**(5): p. 763-74.
159. Barthold, S.W., *The microbiology of transmissible murine colonic hyperplasia.* Lab Anim Sci, 1980. **30**(2 Pt 1): p. 167-73.
160. Barthold, S.W., G.W. Osbaldiston, and A.M. Jonas, *Dietary, bacterial, and host genetic interactions in the pathogenesis of transmissible murine colonic hyperplasia.* Lab Anim Sci, 1977. **27**(6): p. 938-45.
161. Schauer, D.B., et al., *Genetic and biochemical characterization of Citrobacter rodentium sp. nov.* J Clin Microbiol, 1995. **33**(8): p. 2064-8.
162. Gulbins, A., et al., *Antidepressants act by inducing autophagy controlled by sphingomyelin-ceramide.* Mol Psychiatry, 2018. **23**(12): p. 2324-2346.
163. Naser, E., et al., *Characterization of the small molecule ARC39, a direct and specific inhibitor of acid sphingomyelinase in vitro.* J Lipid Res, 2020. **61**(6): p. 896-910.
164. Li, Y., R.J. Nicholson, and S.A. Summers, *Ceramide signaling in the gut.* Mol Cell Endocrinol, 2022. **544**: p. 111554.
165. Koroleva, E.P., et al., *Citrobacter rodentium-induced colitis: A robust model to study mucosal immune responses in the gut.* J Immunol Methods, 2015. **421**: p. 61-72.

166. Li, C.M., et al., *Insertional mutagenesis of the mouse acid ceramidase gene leads to early embryonic lethality in homozygotes and progressive lipid storage disease in heterozygotes.* Genomics, 2002. **79**(2): p. 218-24.
167. Günther, A., *The Role of Acid Ceramidase during Plasmodium Infection and Tumorigenesis,* doctoral dissertation (Dr. rer. nat), 2022. University of Duisburg-Essen, Faculty of Biology
168. Meiners, J., *The effect of the acid sphingomyelinase/ceramidase system on bacterial induced colitis,* doctoral dissertation (Dr. rer. nat), 2019. University of Duisburg-Essen, Faculty of Biology
169. Sato, T., et al., *Long-term expansion of epithelial organoids from human colon, adenoma, adenocarcinoma, and Barrett's epithelium.* Gastroenterology, 2011. **141**(5): p. 1762-72.
170. Rallabandi, H.R., et al., *Evaluation of Intestinal Epithelial Barrier Function in Inflammatory Bowel Diseases Using Murine Intestinal Organoids.* Tissue Eng Regen Med, 2020. **17**(5): p. 641-650.
171. Baaten, B.J., C.R. Li, and L.M. Bradley, *Multifaceted regulation of T cells by CD44.* Commun Integr Biol, 2010. **3**(6): p. 508-12.
172. Shiomi, H., et al., *Gamma interferon produced by antigen-specific CD4+ T cells regulates the mucosal immune responses to Citrobacter rodentium infection.* Infect Immun, 2010. **78**(6): p. 2653-66.
173. Hoek, K.L., et al., *Granzyme B prevents aberrant IL-17 production and intestinal pathogenicity in CD4(+) T cells.* Mucosal Immunol, 2021. **14**(5): p. 1088-1099.
174. Rubtsov, Y.P., et al., *Regulatory T cell-derived interleukin-10 limits inflammation at environmental interfaces.* Immunity, 2008. **28**(4): p. 546-58.
175. Zenewicz, L.A., A. Antov, and R.A. Flavell, *CD4 T-cell differentiation and inflammatory bowel disease.* Trends Mol Med, 2009. **15**(5): p. 199-207.
176. Lawir, D.F., et al., *Pervasive changes of mRNA splicing in upf1-deficient zebrafish identify rpl10a as a regulator of T cell development.* Proc Natl Acad Sci U S A, 2020. **117**(27): p. 15799-15808.
177. Mahrour, N., et al., *Characterization of Cullin-box sequences that direct recruitment of Cul2-Rbx1 and Cul5-Rbx2 modules to Elongin BC-based ubiquitin ligases.* J Biol Chem, 2008. **283**(12): p. 8005-13.
178. Yoshimura, A., et al., *SOCS: negative regulators of cytokine signaling for immune tolerance.* Int Immunol, 2021. **33**(12): p. 711-716.
179. Platis, D. and G.R. Foster, *Activity of hybrid type I interferons in cells lacking Tyk2: a common region of IFN-alpha 8 induces a response, but IFN-alpha2/8 hybrids can behave like IFN-beta.* J Interferon Cytokine Res, 2003. **23**(11): p. 655-66.
180. Martin, P.K., et al., *Autophagy proteins suppress protective type I interferon signalling in response to the murine gut microbiota.* Nat Microbiol, 2018. **3**(10): p. 1131-1141.
181. Tarasenko, T.N., et al., *Cytochrome c Oxidase Activity Is a Metabolic Checkpoint that Regulates Cell Fate Decisions During T Cell Activation and Differentiation.* Cell Metab, 2017. **25**(6): p. 1254-1268 e7.
182. Watson, S.A. and G.P. McStay, *Functions of Cytochrome c oxidase Assembly Factors.* Int J Mol Sci, 2020. **21**(19).
183. Bock, J., et al., *Exogenous sphingomyelinase causes impaired intestinal epithelial barrier function.* World J Gastroenterol, 2007. **13**(39): p. 5217-25.
184. Baduva, K., et al., *Signalling Effects Induced by Acid Ceramidase in Human Epithelial Or Leukemic Cell Lines.* Cell Physiol Biochem, 2019. **52**(5): p. 1092-1102.
185. d'Aldebert, E., et al., *Characterization of Human Colon Organoids From Inflammatory Bowel Disease Patients.* Front Cell Dev Biol, 2020. **8**: p. 363.
186. Momoi, T., Y. Ben-Yoseph, and H.L. Nadler, *Substrate-specificities of acid and alkaline ceramidases in fibroblasts from patients with Farber disease and controls.* Biochem J, 1982. **205**(2): p. 419-25.
187. Kono, M., et al., *Neutral ceramidase encoded by the Asah2 gene is essential for the intestinal degradation of sphingolipids.* J Biol Chem, 2006. **281**(11): p. 7324-31.

188. Schilling, J.D., et al., *Palmitate and lipopolysaccharide trigger synergistic ceramide production in primary macrophages.* J Biol Chem, 2013. **288**(5): p. 2923-32.
189. Suchard, S.J., et al., *Mitogen-activated protein kinase activation during IgG-dependent phagocytosis in human neutrophils: inhibition by ceramide.* J Immunol, 1997. **158**(10): p. 4961-7.
190. Corriden, R., et al., *Tamoxifen augments the innate immune function of neutrophils through modulation of intracellular ceramide.* Nat Commun, 2015. **6**: p. 8369.
191. Sitrin, R.G., T.M. Sassanella, and H.R. Petty, *An obligate role for membrane-associated neutral sphingomyelinase activity in orienting chemotactic migration of human neutrophils.* Am J Respir Cell Mol Biol, 2011. **44**(2): p. 205-12.
192. Yan, Y., et al., *Temporal and spatial analysis of clinical and molecular parameters in dextran sodium sulfate induced colitis.* PLoS One, 2009. **4**(6): p. e6073.
193. Herz, J., et al., *Acid sphingomyelinase is a key regulator of cytotoxic granule secretion by primary T lymphocytes.* Nat Immunol, 2009. **10**(7): p. 761-8.
194. Hagiwara, M., *Alternative splicing: a new drug target of the post-genome era.* Biochim Biophys Acta, 2005. **1754**(1-2): p. 324-31.
195. Iwanaga, N., et al., *Regulation of alternative splicing of caspase-2 through an intracellular signaling pathway in response to pro-apoptotic stimuli.* J Lab Clin Med, 2005. **145**(2): p. 105-10.
196. Du, J., et al., *FOXP3 interacts with hnRNPF to modulate pre-mRNA alternative splicing.* J Biol Chem, 2018. **293**(26): p. 10235-10244.
197. Liu, M., et al., *Long Noncoding RNA RP11-115N4.1 Promotes Inflammatory Responses by Interacting With HNRNPH3 and Enhancing the Transcription of HSP70 in Unexplained Recurrent Spontaneous Abortion.* Front Immunol, 2021. **12**: p. 717785.
198. Kumar, B., et al., *The ubiquitin ligase Cul5 regulates CD4(+) T cell fate choice and allergic inflammation.* Nat Commun, 2022. **13**(1): p. 2786.
199. Liao, X., et al., *The Cul5 E3 Ligase Complex Is a Key Negative Feedback Regulator of TCR/IL2 Signaling and Anti-Tumor Activity in CD8+ T Cells.* bioRxiv, 2022: p. 2022.11.16.516824.
200. Kogot-Levin, A. and A. Saada, *Ceramide and the mitochondrial respiratory chain.* Biochimie, 2014. **100**: p. 88-94.
201. Lewerenz, M., K.E. Mogensen, and G. Uze, *Shared receptor components but distinct complexes for alpha and beta interferons.* J Mol Biol, 1998. **282**(3): p. 585-99.
202. Pattyn, E., et al., *Dimerization of the interferon type I receptor IFNaR2-2 is sufficient for induction of interferon effector genes but not for full antiviral activity.* J Biol Chem, 1999. **274**(49): p. 34838-45.
203. Ghislain, J., C.A. Lingwood, and E.N. Fish, *Evidence for glycosphingolipid modification of the type 1 IFN receptor.* J Immunol, 1994. **153**(8): p. 3655-63.
204. Hemmi, M., et al., *T Helper 17 Promotes Induction of Antigen-Specific Gut-Mucosal Cytotoxic T Lymphocytes following Adenovirus Vector Vaccination.* Front Immunol, 2017. **8**: p. 1456.

8 Appendix

8.1 Abbreviations

A/E	Attaching and effacing
Ac	Acid ceramidase
Ac^{flox}	*Asah1*$^{flox/flox}$
ACK	Ammonium chloride potassium
AKT	Protein kinase B
AMP	Antimicrobial peptide
APC	Allophycocyanine
APCs	Antigen presenting cells
ARP2/3	Actin-related protein 2/3 complex
Asah1	N-acylsphingosine amidohydrolase 1
Asm	Acid sphingomyelinase
BCR	B cell receptor
BFA	Brefeldin A
BSA	Bovine serum albumin
BV	Brilliant violet
C. rodentium	*Citrobacter rodentium*
C1P	Ceramide-1-phosphate
CCL5	CC-chemokine ligand 5
CD	Crohn's disease
CD(number)	Cluster of differentiation (number) e.g. CD4
CDase	Ceramidase
cDNA	Complementary deoxyribonucleic acid
Cer	Ceramide
CerS	Ceramide synthase
CERT	Ceramide transfer protein
CFU	Colony forming units
CK	Ceramide kinase
CO_2	Carbon dioxide
Coa5	Cytochrome c oxidase assembly factor 5
COX10	Cytochrome c oxidase assembly factor heme A:farnesyltransferase COX10
COX2	Cyclooxygenase 2
CR	*Citrobacter rodentium* (abbreviation in figures)
creER	Cre recombinase estrogen receptor fusion protein

CTL	Cytotoxic T lymphocyte
CTLA4	Cytotoxic T-Lymphocyte-associated protein 4
DAMP	Damage-associated molecular pattern
DC	Dendritic cell
DEG	Differentially expressed gene
DES	Dihydroceramide desaturase
dhCer	Dihydroceramide
DMEM	Dulbecco's modified eagle medium
DMSO	Dimethyl sulfoxide
DNA	Deoxyribonucleic acid
dNTP	Deoxynucleotide Triphosphate
d.p.	Days post
dpi	Day(s) post infection
DSS	Dextran sodium sulfate
E. coli	*Escherichia coli*
EDTA	Ethylene diamine tetraacetic acid
EGTA	Ethylene glycol tetraacetic acid
EHEC	Enterohaemorraghic E. coli
EPEC	Enteropathogenic E. coli
ER	Endoplasmic reticulum
ERK	Extracellular signal-regulated kinase
Esp	E. coli secreted protein
FACS	Fluorescence-activated cell sorting
FAPP2	Four-phosphate adaptor protein
FC	Fold change
FCS	Fetal calf serum
FCS	Fetal calf serum
FD	Farber disease
FITC	Fluorescein isothiocynate
fMLP	N-formylmethionine-leucyl-phenylalanine
FoxP3	Forkhead box P3
FSC	Forward scatter
FvD	Fixable viability dye
GALT	Gut associated lymphoid tissue
GATA3	GATA binding protein 3
Gb2	Galabiosylceramide
GFR	Growth factor reduced

GMP	Granulocyte-macrophage progenitor
Gran	Granulocytes
GrzB	Granzyme B
H&E	Hematoxylin and eosin
HEPES	4-(2-hydroxyethyl)-1-piperazineethanesulfonic acid
HLA	Human leukocyte antigen
HPLC-MS/MS	High performance liquid chromatography mass spectrometry/mass spectrometry
Hrnph3	Heterogeneous nuclear ribonucleoprotein H3
Hsp	Heat shock protein
i.p.	Intraperitoneal
IBD	Inflammatory bowel disease
ICV2	Individual ventilation
Id2	Inhibitor of DNA binding
IEC	Intestinal epithelial cell
IEL	Intraepithelial lymphocyte
IFN	Interferon
Ifnar2	Interferon alpha/beta receptor 2
Ig	Immunoglobulin
IL-	Interleukin
ILC	Innate lymphoid cell
IMDM	Iscove’s odified Dulbecco’s medium
iNOS	Inducible nitric oxide synthase
InPEC	Intestinal pathogenic E. coli
IRF	Interferon regulatory factor
ISC	Intestinal stem cell
iT_{reg}	Induced regulatory T cell
ki	Knockin
KO	Knockout
KSR	3-ketosphinganine reductase
LAG-3	Lymphocyte-activation gene 3
LANUV	State Agency for Nature, Environment and Consumer Protection
LB	Lysogeny broth
LBD	Ligand binding domain
LEE	Locus of enterocyte effacement
Lgr5	Leucine-rich repeat-containing G-protein-coupled receptor 5
LI	Large intestine

LP	Lamina Propria
LPL	Lamina Propria lymphocytes
LPS	Lipopolysaccharide
Ly-6G	Lymphocyte antigen 6 complex, locus G
LysMcre	Cre recombinase under control of lysozyme 2 promoter/enhancer elements
Macro	Macrophages
MACS	Magnetic-activated cell sorting
Map	Mitochondrial-associated protein
MDP	Monocyte-dendritic precursor
MHC	Major histocompatibility complex
mLN	Mesenteric lymph node
mRNA	Messenger ribonucleic acid
MyD88	Myeloid differentiation primary response protein 88
NET	Neutrophil extracellular trap
NK cell	Natural killer cell
NLR	Nucleotide-binding oligomerisation domain (NOD)-like leucine-rich repeat receptors
NO	Nitric oxide
NOD	Nucleotide-binding oligomerisation domain
nT_{reg}	Natural regulatory T cell
OGM	Organoid growth medium
OXPHOS	Oxidative phosphorylation
P. aeruginosa	*Pseudomonas aeruginosa*
PAMP	Pathogen-associated molecular patterns
PB	Pacific blue
PBS	Phosphate buffered saline
Pcmtd2	Protein-L-isoaspartate (D-aspartate) O-methyltransferase domain containing 2
PCR	Polymerase chain reaction
PE	R-Phycoerythrin
PE-Cy7	R-Phycoerythrin-Cyanine dye 7
PEG_2	Prostaglandin E2
PerCP	Peridinin-Chlorophyll-Protein
PFA	Paraformaldehyde
PLA2	Phospholipase A2
PMA	Phorbol 12-myristate 13-acetate

pMacro	Peritoneal Macrophages
PRR	Pattern recognition receptors
PSG	Penicillin-Streptomycin-Gentamycin
RA	Retinoic acid
Reg3γ	Regenerating islet-derived protein 3γ
RIG	Retinoic acid (RA)-inducible gene
RNA	Ribonucleic acid
RORγt	Retinoic acid receptor-related orphan γt
ROS	Reactive oxygen species
RPMI	Roswell Park Memorial Institute
Rps9	Ribosomal protein 9
RT-qPCR	Real-time quantitative polymerase chain reaction
S1P	Sphingosine-1-phosphate
S1PPase	Sphingosine-1-phosphate phosphatase
SCFA	Short chain fatty acid
SDS	Sodium dodecyl sulfate
SEM	Standard error of the mean
SI	Small intestine
SK	Sphingosine kinase
SMA-PME	Spinal muscular atrophy with progressive myoclonic epilepsy
SMase	Sphingomyelinase
SMS	Sphingomyelin synthase
SOCS	Suppressor of cytokine signaling
SPF	Specific pathogen-free
Sph	Sphingosine
SPT	Serine palmitoyl transferase
SSC	Side scatter
T3SS	Type III secretion system
TA cells	Transit-amplifying cells
TBE	TRIS-borate-EDTA
T-bet	T-box transcription factor
TCR	T cell receptor
TE	TRIS-EDTA
TGFβ	Transforming growth factor β
T_h	T helper
Tir	Translocated intimin receptor
TLR	Toll-like receptor

TS	Tela submucosa
TNFα	Tumor necrosis factor α
T_{reg}	Regulatory T cell classified by CD4 and FoxP3 expression
TRIS	Tris(hydroxymethyl)aminomethane
u.d.	Under detection limit
UC	Ulcerative colitis
Vilcre	Villin cre
WT	Wild type
ZAP-70	Zeta chain associated protein kinase 70
ZO-1	Zonula occludens 1

8.2 List of figures

8.3 List of tables

8.4 List of formulae

8.5 Acknowledgements

The Acknowledgements are not included in the published version.

8.6 Curriculum Vitae

The curriculum vitae is not included in the published version due to data protection reasons.

8.7 Declarations

Erklärung:
Hiermit erkläre ich, gem. § 6 Abs. (2) g) der Promotionsordnung der Fakultät für Biologie zur Erlangung des Dr. rer. nat., dass ich das Arbeitsgebiet, dem das Thema „The role of acid ceramidase in host defense against enteropathogenic bacterial infection“ zuzuordnen ist, in Forschung und Lehre vertrete und den Antrag von Jana-Fabienne Ebel befürworte und die Betreuung auch im Falle eines Weggangs, wenn nicht wichtige Gründe dem entgegenstehen, weiterführen werde.

Essen, den_____ _____

Prof. Dr. Astrid Westendorf

Erklärung:
Hiermit erkläre ich, gem. § 7 Abs. (2) d) + f) der Promotionsordnung der Fakultät für Biologie zur Erlangung des Dr. rer. nat., dass ich die vorliegende Dissertation selbständig verfasst und mich keiner anderen als der angegebenen Hilfsmittel bedient, bei der Abfassung der Dissertation nur die angegebenen Hilfsmittel benutzt und alle wörtlichen oder inhaltlich übernommen Stellen als solche gekennzeichnet habe.

Essen, den_____ _____

Jana-Fabienne Ebel

Erklärung:
Hiermit erkläre ich, gem. § 7 Abs. (2) e) + g) der Promotionsordnung der Fakultät für Biologie zur Erlangung des Dr. rer. nat., dass ich keine anderen Promotionen bzw. Promotionsversuche in der Vergangenheit durchgeführt habe und dass diese Arbeit von keiner anderen Fakultät/Fachbereich abgelehnt worden ist.

Essen, den_____ _____

Jana-Fabienne Ebel